A Study of the Structure and Internal Dynamics of

Calcitonin Gene-Related Peptide

by

Sara Sizemore

A Dissertation Presented in Partial Fulfillment
of the Requirements for the Degree
Doctor of Philosophy

Approved March 2015 by the
Graduate Supervisory Committee:

Sara Vaiana, Chair
Giovanna Ghirlanda
Robert Ros
Stuart Lindsay
Sefika Ozkan

ARIZONA STATE UNIVERSITY

May 2015

ABSTRACT

Calcitonin Gene-Related Peptide (CGRP) is an intrinsically disordered protein that has no regular secondary structure, but plays an important role in vasodilation and pain transmission in migraine. Little is known about the structure and dynamics of the monomeric state of CGRP or how CGRP is able to function in the cell, despite the lack of regular secondary structure. This work focuses characterizing the non-local structural and dynamical properties of the CGRP monomer in solution, and understanding how these are affected by the sequence and the solution environment. The unbound, free state of CGRP is measured using a nanosecond laser-pump spectrophotometer, which allows measuring the end-to-end distance (a non-local structural property) and the rate of end-to-end contact formation (intra-chain diffusional dynamics). The data presented in this work show that electrostatic interactions strongly modulate the structure of CGRP, and that peptide-solvent interactions are sequence and charge dependent and can have a significant effect on the internal dynamics of the peptide. In the last few years migraine research has shifted focus to disrupting the CGRP-receptor pathway through the design of pharmacological drugs that bind to either CGRP or its receptor, inhibiting receptor activation and therefore preventing or reducing the frequency of migraine attacks. Understanding what types of intra- and inter-chain interactions dominate in CGRP can help better design drugs that disrupt the binding of CGRP to its receptor.

ACKNOWLEDGMENTS

None of this would have been possible without the advice, support and guidance of my advisor, Dr. Sara Vaiana. I am extremely grateful that she entrusted such an interesting and demanding project to me, and her careful supervision and guidance was essential for the completion of this dissertation. The many valuable, critical discussions I have had with her over the years have taught me how to become a better scientist.

I want to thank all my labmates over the years, including Dr. Stephanie Cope, Alejandro Solis and Danmei Bian, who trained me on the techniques used in this work. I am particularly indebted to Stephanie as her intrinsic curiosity meant that I could always rely on her help me reason through any problem.

I am also extremely grateful for the collaborations I have had an opportunity to be a part of these past few years. I especially want to thank Dr. Giovanna Ghirlanda who, by making her chemistry laboratory available to me, made this project possible. Her graduate students and post-docs, including Dr. Sandip Shinde, Dr. Matthieu Walther, and Dr. Anindya Roy, trained me in the synthesis and purification of proteins. Anindya always readily answered any chemistry related question I had, and I am extremely grateful for all of his and Dr. Ghirlanda's advice over the years. I also want to thank Dr. Andrea Soranno for providing a model for the structure of CGRP in solution. Dr. Frank Tsen, thank you for letting me be a part of your fibrinogen project.

I am thankful to my supervisory committee for all their advice and guidance over the years, their feedback has made this work stronger.

I am indebted to all the employees of ASU that have assisted me with any technical, academic or administrative questions I've had over the years. Deanna Clark and Jill Kolp have especially always been quick to help me with anything I need, and I also particularly want to thank Dr. Zach Laughrey and Dr. John Lopez for their training and assistance in MALDI-TOF and CD.

I am extremely grateful for all the financial support I have received, including: ASU Department of Physics, ASU Graduate College, the Graduate and Professional Student Association, the US Department of Education, and the Biophysical Society.

Last but not least, I am indebted to my family and friends for their support and encouragement over the years.

TABLE OF CONTENTS

Page

CHAPTER Page

LIST OF TABLES

LIST OF FIGURES

Figure Page

LIST OF SYMBOLS

Symbol Page

Symbol Page

CHAPTER 1

INTRINSICALLY DISORDERED PROTEINS

1.1. INTRODUCTION TO INTRINSICALLY DISORDERED PROTEINS

The focus of this work is on elucidating the structure and dynamics of calcitonin gene-related peptide, or CGRP. CGRP has very little secondary structure in solution[1-3] and is part of a class of proteins that are intrinsically disordered, referred to as IDPs. Unlike enzymes that have a regular secondary structure and bind to specific binding partners, IDPs have no regular three dimensional structure and can be more promiscuous, with multiple binding partners.[4-7] However, despite this lack of regular structure, IDPs are still able perform biological functions in the cell. About one third to one half of all eukaryotic proteins have extensive disordered regions,[7-8] suggesting an evolutionary advantage for protein disorder. The exact mechanism for how the structure and dynamics of the unbound state of disordered proteins increase receptor promiscuity and affect the binding rates is unclear. It has been proposed that the presence of disordered states helps increase protein efficacy.[9] Some studies suggest that IDPs operate a fly-casting mechanism where the intrinsic disorder of IDPs allow them to bind weakly to their partners from long distances, thereby increasing the on-rate of binding.[10] However, other studies show that for at least some IDPs, the rate of binding is not diffusion limited and the on-rate of binding depends on the structure of the monomer.[11] As IDPs perform signaling and regulatory functions in the cell, it is important to elucidate the structure and dynamics of

IDPs to understand how IDPs bind to their partners and perform biological functions in the cell.

1.2. WHAT DETERMINES THE STRUCTURE OF IDPS

Interestingly, research has shown that despite the fact that IDPs have no regular three dimensional structure, IDPs can occupy a range of "structures" ranging from extended coils with little structure to collapsed states with extensive secondary structure, as shown in Figure 1.1 below.[12] This suggests that while IDPs have no characteristic three dimensional "structure," there are long range interactions present which occur on the same length scale of the protein that affect the structure and dynamics, and therefore the thermodynamics and kinetics of binding, in IDPs.

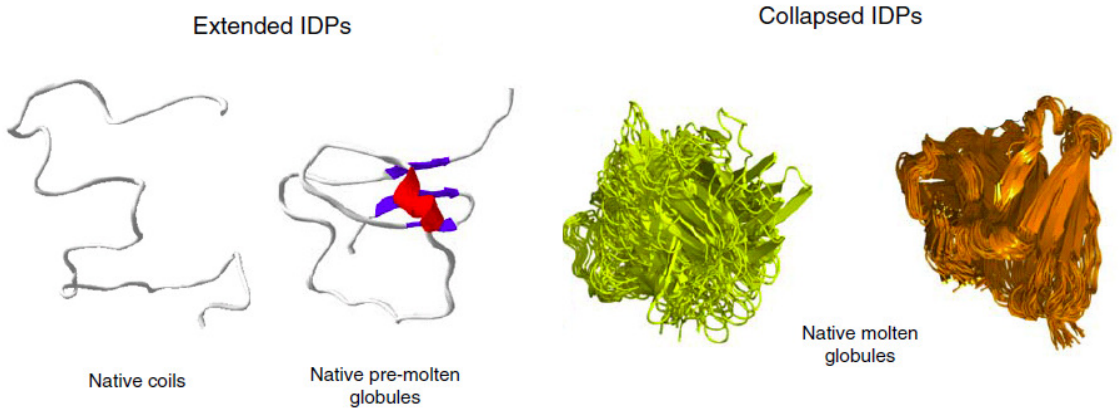

Figure 1.1. Representative structures of IDPs. The structure of IDPs can range from extended coils with no secondary structure to native molten globules with extensive secondary structure (Uversky, *Protein J* 2009).[12]

Despite the fact that IDPs occupy a wide variety of structures, they are still more expanded than natively folded proteins (NFPs). Marsh and Forman-Kay analyzed small-angle x-ray scattering (SAXS) and dynamic light scattering (DLS) data from folded proteins, chemically denatured proteins, and disordered proteins and found that although disordered proteins are more expanded than NFPs in aqueous solvent, they are more compact than unfolded proteins in denaturant (Figure 1.2).[13] This suggests the presence of attractive intra-chain interactions in IDPs in aqueous solvent, despite the lack of regular three dimensional structure.[14]

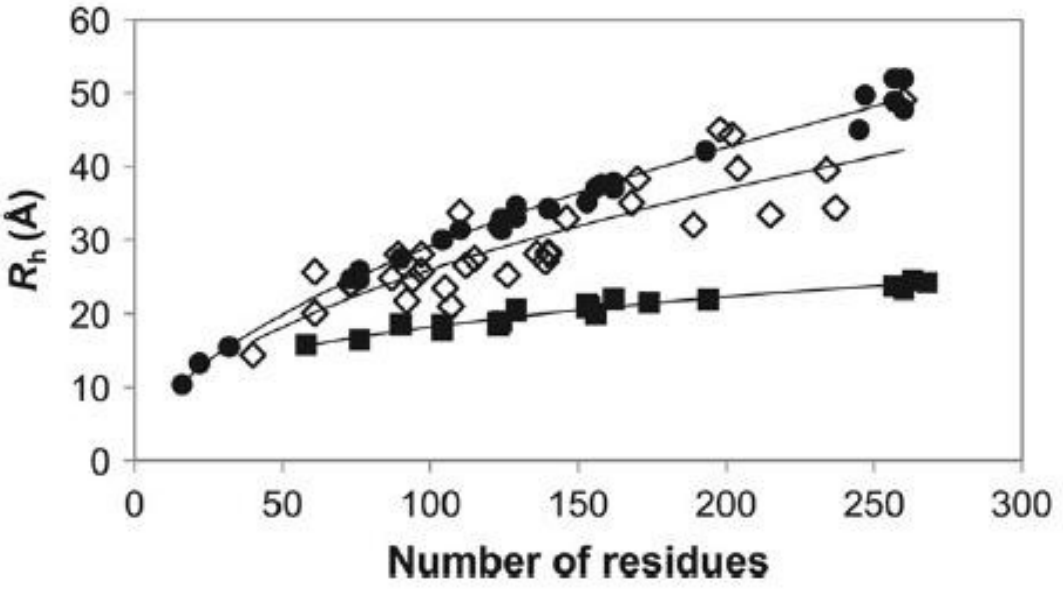

Figure 1.2. Compaction of IDPs in water. Plot of hydrodynamic radius R_h as a function of the number of residues for a selected sample of folded proteins (filled squares), unfolded proteins (filled circles) and IDPs (open diamonds). Despite being disordered, IDPs have a smaller R_h than unfolded proteins (Marsh and Forman-Kay *Biophysical J*, 2010).

To understand how IDPs can have attractive intra-chain interactions yet still be disordered, Uversky, et al plotted the net charge versus the average side chain hydrophobicity of various IDPs and NFPs, and found that on average IDPs have a higher net charge and lower net hydrophobicity than NFPs (Figure 1.3).[15]

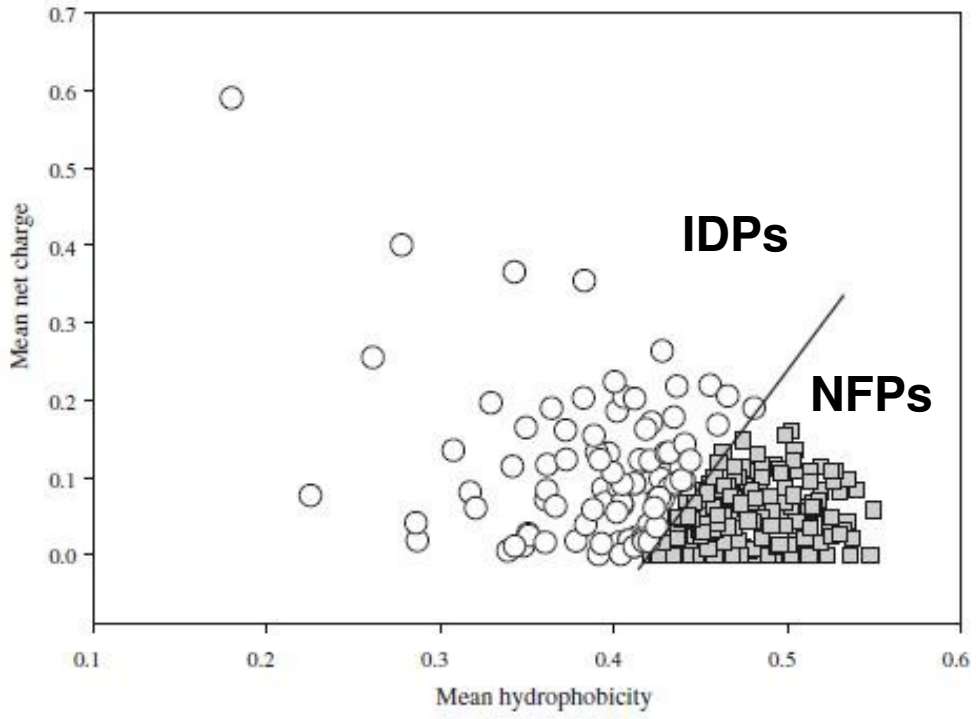

Figure 1.3. Uversky Plot. Plot of the mean net charge versus hydrophobicity of a selection of intrinsically disordered (open circles) and folded proteins (grey squares). (Uversky *Proteins*, 2000).

This is intuitive in that charge repulsion will create expanded states, especially if there are few hydrophobic residues to promote collapsed, folded states. However, this is only a generalization and most IDPs, with few exceptions, are not *that* significantly different in net charge or hydrophobicity than NFPs, but still remain disordered. Other studies have shown that IDPs have slightly different sequence composition, with IDPs having a higher

composition of “low-complexity” or “disorder promoting” amino acids such as prolines compared to folded proteins.[13,16] Further analysis of the sequence of various IDPs found that the amount of compaction seen in IDPs does not seem to correlate with secondary structure content, but instead on their net charge and amino acid content.[13]

Therefore it is an open question in the field as to what causes IDPs to adopt expanded, disordered conformations but still have long range attractive intra-chain interactions that cause IDPs to be more collapsed than unfolded proteins. As IDPs generally have a higher net charge than natively folded proteins,[15] electrostatic interactions appear to be an important factor in the structural propensities of IDPs. It is well known from polymer theories that chain stiffness can depend on Coulomb repulsion and the fraction of positive and negative charges (including how they are spaced along the linear sequence).[17-19] It has been suggested that the polymeric properties of IDPs can be explained by such models,[20-22] with variations in the environmental pH and the presence of ions in the extra-cellular region where CGRP (and other IDPs) are secreted playing an important role in their structure and dynamics.

As excluded volume interactions are the most basic interactions that give rise to the polymeric properties of IDPs, steric interactions might play a role in the expansion of IDPs in water. Even in small non-proline, non-hydrophobic side chain peptides, it was seen that restrictions in phi-psi angle extend beyond nearest neighbors, disproving the isolated-pair hypothesis and suggesting that steric clashes can have a significant effect on the structure of proteins.[23] IDPs also tend to have a higher proportion of disorder

promoting residues such as prolines which might play an important role in the structure of IDPs. Similar to the simulations of steric clashes, simulations have also showed that the presence of prolines can cause expansion in short peptides (but the effect is smaller in longer proteins).[24]

Other models suggest that it is not side chain-side chain interactions, but rather backbone-backbone interactions that cause compaction in disordered proteins. Measurements of the intra-chain diffusion times in polyglycine, a protein with no residues, and other peptides of varying hydrophobicity all saw faster diffusion than expected, suggesting that it is backbone interactions that drive collapse.[25] Modeling of polyglutamine (polyQ) which lacks hydrophobic residues showed that PolyQ populates collapsed states, further evidence of backbone-backbone interactions modulating the structure of disordered proteins.[26]

There are currently many models attempting to explain why, despite being disordered, IDPs are more compact than unfolded proteins, with the amount of compaction being sequence dependent. However, due to fast reconfiguration times, there is relatively few experimental data to verify these models and help understand the conformations IDPs adopt. As we will see in the next section, the study and characterization of long range interactions are important to discover how IDPs function in the cell.

1.3. HOW THE STRUCTURE AND INTERNAL DYNAMICS OF IDPS AFFECT THEIR BIOLOGICAL FUNCTION

The disordered structure of IDPs has been proposed to play an important role in biological function through a number of mechanisms. It has been suggested that intrinsic disorder increases receptor promiscuity, with one protein recorded as having over 80 binding partners.[7] Disorder also appears to play a role in binding kinetics with the rate of association "enhanced" by disorder, including a proposed fly-casting mechanism where IDPs weakly bind to their partners from long distances and then adopt the folded, functional conformations, thereby increasing the on-rate of binding.[10] Other experiments have shown that the kinetics of binding is not diffusion limited, suggesting that at least some IDPs might not bind through induced fit.[11] In fact, experiments have shown that IDPs, while unstructured, are still more compact than unfolded proteins, indicating the presence of attractive intra-chain interactions in water[13] and suggests that IDPs have the ability to favorably bind to its receptors through attractive inter-chain interactions.

Other theories focus on the role that the dynamics of conformational sampling plays in the function of IDPs. Some focus on how electrostatic interactions might drive binding thermodynamics and kinetics. For example, fast reconfiguration of a charged IDP will create an average electric field that favorably interacts with a charged receptor site.[27] Modeling shows that inter-residue contacts formed due to electrostatics can determine the polymeric properties of proteins, and might provide a mechanism for receptor specificity.[17] Some experiments have shown that some IDPs have large electrostatic

energies, which suggests that electrostatic interactions with the receptor might play a significant role in the binding affinity and receptor specificity of IDPs.[22] Other models suggest that internal friction is important in IDPs, slowing down dynamics in solution and affecting the binding rate. Prolines slow down the dynamics of short peptides but not longer ones[24] while more expanded proteins have lower internal friction and therefore faster dynamics[28] with faster chain dynamics tending to correlate with high internal friction.[29] Other studies show that chain dynamics can speed up upon binding[30]: this is called the induced fit mechanism where the IDP folds upon binding, with non-native interactions with binding partners increasing the binding rate.[4]

There are many proposed mechanisms to explain how the structure and dynamics of disordered proteins allow these proteins to carry out their biological function despite the lack of regular three dimensional structure. However, there is limited experimental information to support these proposed mechanisms due to fast reconfiguration on short timescales making the measurement of these global properties difficult. As it appears that the structure and dynamics of IDPs are important to the thermodynamics and kinetics of binding,[9,10] to understand how disordered proteins function in the cell experimental measurements of these non-local properties are needed. The goal of this work is to study the fundamental aspects of CGRP that are relevant to the biology of CGRP, including drug and receptor binding and activation.

REFERENCES

[1]Manning, M. C. (1989). Conformation of the alpha form of human calcitonin gene-related peptide (CGRP) in aqueous solution as determined by circular dichroism spectroscopy. *Biochemical and biophysical research communications*, *160*(1), 388-392.

[2]Hubbard, J. A., Martin, S. R., Chaplin, L. C., Bose, C., Kelly, S. M., & Price, N. C. (1991). Solution structures of calcitonin-gene-related-peptide analogues of calcitonin-gene-related peptide and amylin. *Biochem. J*, *275*, 785-788.

[3]Breeze, A. L., Harvey, T. S., Bazzo, R., & Campbell, I. D. (1991). Solution structure of human calcitonin gene-related peptide by proton NMR and distance geometry with restrained molecular dynamics. *Biochemistry*, *30*(2), 575-582.

[4]Wright, P. E., & Dyson, H. J. (2009). Linking folding and binding. *Current opinion in structural biology*, *19*(1), 31-38.

[5]Dunker, A. K., Brown, C. J., Lawson, J. D., Iakoucheva, L. M., & Obradovic, Z. (2002). Intrinsic disorder and protein function. *Biochemistry*, *41*(21), 6573-6582.

[6]Uversky, V. N., Oldfield, C. J., & Dunker, A. K. (2005). Showing your ID: intrinsic disorder as an ID for recognition, regulation and cell signaling. *Journal of Molecular Recognition*, *18*(5), 343-384.

[7]Dunker, A. K., Silman, I., Uversky, V. N., & Sussman, J. L. (2008). Function and structure of inherently disordered proteins. *Current opinion in structural biology*, *18*(6), 756-764.

[8]Dunker, A. K., Romero, P., Obradovic, Z., Garner, E. C., & Brown, C. J. (2000). Intrinsic protein disorder in complete genomes. *Genome Informatics*, *11*, 161-171.

[9]Tompa, P. (2005). The interplay between structure and function in intrinsically unstructured proteins. *FEBS letters*, *579*(15), 3346-3354.

[10]Shoemaker, B. A., Portman, J. J., & Wolynes, P. G. (2000). Speeding molecular recognition by using the folding funnel: the fly-casting mechanism. *Proceedings of the National Academy of Sciences*, *97*(16), 8868-8873.

[11]Rogers, J. M., Steward, A., & Clarke, J. (2013). Folding and binding of an intrinsically disordered protein: fast, but not 'diffusion-limited'. *Journal of the American Chemical Society*, *135*(4), 1415-1422.

[12]Uversky, V. N. (2009). Intrinsically disordered proteins and their environment: effects of strong denaturants, temperature, pH, counter ions, membranes, binding partners, osmolytes, and macromolecular crowding. *The protein journal*, *28*(7-8), 305-325.

[13]Marsh, J. A., & Forman-Kay, J. D. (2010). Sequence determinants of compaction in intrinsically disordered proteins. *Biophysical journal*, *98*(10), 2383-2390.

[14]Uversky, V. N. (2002). Natively unfolded proteins: a point where biology waits for physics. *Protein science*, *11*(4), 739-756.

[15]Uversky, V. N., Gillespie, J. R., & Fink, A. L. (2000). Why are "natively unfolded" proteins unstructured under physiologic conditions?. *Proteins: Structure, Function, and Bioinformatics*, *41*(3), 415-427.

[16]Romero, P., Obradovic, Z., Li, X., Garner, E. C., Brown, C. J., & Dunker, A. K. (2001). Sequence complexity of disordered protein. *Proteins: Structure, Function, and Bioinformatics*, *42*(1), 38-48.

[17]Higgs, P. G., & Joanny, J. F. (1991). Theory of polyampholyte solutions. The Journal of chemical physics, 94(2), 1543-1554.

[18]Zhou, H. X. (2002). A Gaussian-chain model for treating residual charge-charge interactions in the unfolded state of proteins. *Proceedings of the National Academy of Sciences*, *99*(6), 3569-3574.

[19]Ha, B. Y., & Thirumalai, D. (1992). Conformations of a polyelectrolyte chain. *Physical Review A*, *46*(6), R3012.

[20]Mao, A. H., Crick, S. L., Vitalis, A., Chicoine, C. L., & Pappu, R. V. (2010). Net charge per residue modulates conformational ensembles of intrinsically disordered proteins. *Proceedings of the National Academy of Sciences*, *107*(18), 8183-8188.

[21]Das, R. K., & Pappu, R. V. (2013). Conformations of intrinsically disordered proteins are influenced by linear sequence distributions of oppositely charged residues. *Proceedings of the National Academy of Sciences*, *110*(33), 13392-13397.

[22]Müller-Späth, S., Soranno, A., Hirschfeld, V., Hofmann, H., Rüegger, S., Reymond, L., Nettels, D., & Schuler, B. (2010). Charge interactions can dominate the dimensions of intrinsically disordered proteins. *Proceedings of the National Academy of Sciences*, *107*(33), 14609-14614.

[23]Pappu, R. V., Srinivasan, R., & Rose, G. D. (2000). The Flory isolated-pair hypothesis is not valid for polypeptide chains: implications for protein folding. *Proceedings of the National Academy of Sciences*, *97*(23), 12565-12570.

[24]Krieger, F., Möglich, A., & Kiefhaber, T. (2005). Effect of proline and glycine residues on dynamics and barriers of loop formation in polypeptide chains. *Journal of the American Chemical Society*, *127*(10), 3346-3352.

[25]Teufel, D. P., Johnson, C. M., Lum, J. K., & Neuweiler, H. (2011). Backbone-driven collapse in unfolded protein chains. *Journal of molecular biology*, *409*(2), 250-262.

[26]Crick, S. L., Jayaraman, M., Frieden, C., Wetzel, R., & Pappu, R. V. (2006). Fluorescence correlation spectroscopy shows that monomeric polyglutamine molecules form collapsed structures in aqueous solutions. *Proceedings of the National Academy of Sciences*, *103*(45), 16764-16769.

[27]Borg, M., Mittag, T., Pawson, T., Tyers, M., Forman-Kay, J. D., & Chan, H. S. (2007). Polyelectrostatic interactions of disordered ligands suggest a physical basis for ultrasensitivity. *Proceedings of the National Academy of Sciences*, *104*(23), 9650-9655.

[28]Soranno, A., Buchli, B., Nettels, D., Cheng, R. R., Müller-Späth, S., Pfeil, S. H., Hoffmann, A., Lipman, E.A., Makarov, D.E., & Schuler, B. (2012). Quantifying internal friction in unfolded and intrinsically disordered proteins with single-molecule spectroscopy. *Proceedings of the National Academy of Sciences*, *109*(44), 17800-17806.

[29]Cheng, R.R., Hawk, A.E., & Makarov (2013). Concerted dihedral rotations give rise to internal friction in unfolded proteins. *The Journal of Chemical Physics*, *138*(7), 074112.

[30]Narayanan, R., Ganesh, O. K., Edison, A. S., & Hagen, S. J. (2008). Kinetics of folding and binding of an intrinsically disordered protein: the inhibitor of yeast aspartic proteinase YPrA. *Journal of the American Chemical Society*, *130*(34), 11477-11485.

CHAPTER 2

CGRP AND THE CALCITONIN PEPTIDE FAMILY

2.1 CALCITONIN GENE-RELATED PEPTIDE

2.1.1 THE BIOLOGICAL FUNCTION OF CALCITONIN GENE-RELATED PEPTIDE

The focus of this work is on the structure and dynamics of CGRP, a short 37-residue intrinsically disordered hormone peptide that is primarily produced in both central and peripheral neurons.[1,2] CGRP is present in the cardiovascular, nervous and gastrointestinal systems, and has been strongly implicated in migraine pathophysiology. CGRP is one of the most potent vasodilators in the body and is involved in the transmission of pain signals.[1-5]

In the last few years, there has been a significant focus on CGRP and its role in migraine headache. In migraine, one of the primary signs of an attack is increased concentrations of CGRP in the brain, with a migraine attack corresponding to the release of CGRP from the trigeminal neurons in the brain, which densely enervate cerebral blood vessels.[6-8] As Figure 2.1 shows, CGRP is released from trigeminal neurons into the extracellular space, where it then binds to CGRP receptors on the exterior of cebrebral vascular smooth muscles, causing vasodilation.[9] Because of this and due to CGRP's role as a potent vasodilator and in pain transmission, it is thought that CGRP plays a significant role in migraine. One of the current focuses of research on migraine is on inhibiting the binding

of CGRP to its receptor through receptor antagonists that bind to, but do not activate the receptor.[7,8] It is thought that when CGRP binds and activates the CGRP receptors in the brain during migraine, in addition to increased blood flow that is a hallmark of migraine, elevated levels of CGRP can lead to pain signals, halos and other migraine symptoms.[7,6,10]

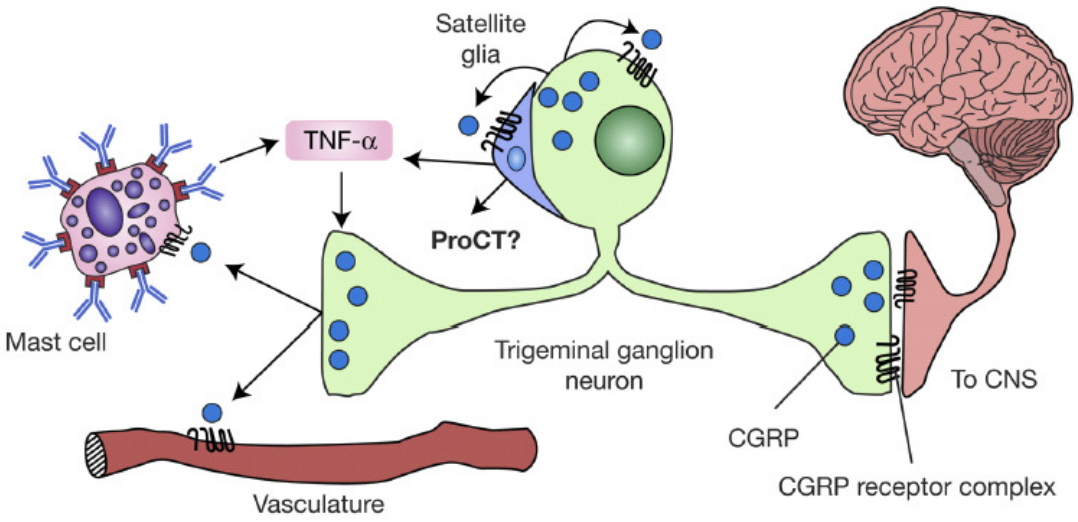

Figure 2.1. CGRP and its receptors in migraine. CGRP is released from trigeminal neurons and binds to CGRP receptors located on vasculature or on mast cells, which cause vasodilation and inflammation respectively (Raddant & Russo, *Expt. Rev. Mol. Med.,* 2011).[9]

Clinical studies are focusing on monoclonal antibodies that bind to CGRP itself, thereby preventing activation of the receptor and either preventing migraine or reducing the severity of pain during migraine attacks.[11-13] Other pharmacological studies are focusing on chemical and synthetic inhibitors that preferentially bind to CGRP receptors, with some currently in Phase II clinical trials.[7,12-14]

As a potent vasodilator, CGRP not only has an important role in increased blood flow during migraine, but also regulates blood flow and vasoconstriction elsewhere in the body. CGRP is such a strong vasodilator that the application of pico- or femtomolar quantities of CGRP to the human skin is enough to cause reddening of the skin.[3] In the circulatory system, CGRP plays an important role in reducing the effects of ischemia and myocardial infarction,[15] where the local release of CGRP due to tissue acidosis is thought to provide a cardiac protective effect and promote healing.[6,16,17] Other pathways in which CGRP's vasodilatory effect plays a role includes Reynaud's disease, where CGRP levels are lower than normal in the hands and feet, with vasoconstriction a major symptom of this disease; the intravenous application of CGRP causes vasodilation and promotes healing in Reynaud's.[18,19] CGRP plays a role in pulmonary vascular resistance by regulating vasoconstriction in the lungs, and a deficiency of CGRP in the lungs lead to an increase in pulmonary hypertension.[5,20] Through its vasodilatory effect, CGRP also plays a role in the immune response of the body through an increase in blood flow to the affected area, allowing the immune system better access and thereby modulating inflammation.[3,6,21]

Similarly, CGRP plays a role in the transmission of pain in the body. Studies in mice show that in inflamed areas of the body, the release of CGRP also plays a role in expression of pain.[22,23] Metastatic cancer cells have been found to stimulate the production of CGRP producing neurons in the bone, suggesting that CGRP plays a role in bone pain in cancer patients.[24] In addition, patients with lower back pain also have a measured increase in CGRP production near the affected areas of the vertebrae.[25,26] In

migraine, clinical trials report that migraine sufferers experience a reduction in pain shortly after the administration of the pharmacological CGRP antagonists that inhibit the activation of the CGRP receptor.[5,7,14]

All of this suggests that CGRP is a versatile neuropeptide that plays an important role in modulating many functions in the body through vasodilation, and is involved in the transmission of pain and migraine pathology. The current pharmacological focus on CGRP is on the interplay between CGRP and its receptor in order to design a better antagonist for migraine medication. As the release of CGRP has been associated with variations in extracellular conditions, such as tissue acidosis and high concentrations of ions, such environmental changes could potentially affect the structure and dynamics of CGRP. It is therefore important to study the structure and dynamics of the unbound state of CGRP, which can help understand how CGRP interacts with its receptor.

2.1.2 THE STRUCTURE OF CALCITONIN GENE-RELATED PEPTIDE

We present a brief review of the structural properties of the monomer state of CGRP, known prior to our current study. In the human body, CGRP has two variants which vary by only three amino acids, αCGRP and βCGRP, with αCGRP more widely studied.[2,4] The focus of this work is on αCGRP only.

Figure 2.2. Sequence composition of CGRP. CGRP has 37 amino acids and is constrained by a disulfide bond between residues 2 and 7. The positively charged amino acids (red) and negatively charged amino acids (green) at pH 4.9 are highlighted.

In its functional form, CGRP is amidated at the C terminus and contains a disulfide bond between the cysteines at residues 2 and 7, which confines residues 1-7 into a rigid structure.[27-29] CGRP has a lower net charge and more hydrophobic residues compared to most IDPs, but is still highly disordered with very little regular secondary structure as evidenced by prior circular dichroism (CD) and nuclear magnetic resonance (NMR) studies on CGRP.

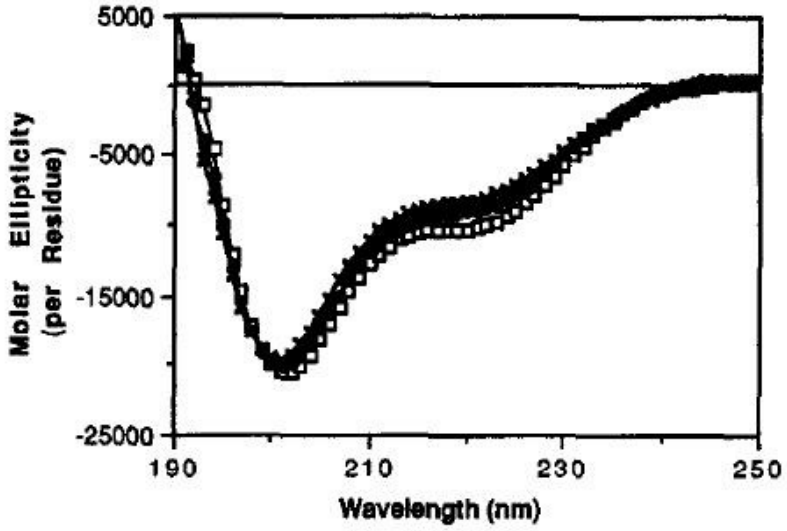

Figure 2.3. Temperature dependence of CD spectra of CGRP. The CD spectra of CGRP was measured as a function of temperature- 4°C (□), 15°C (◊), 30°C (x). (Manning, *Biochem. and Biophy. Res. Com.,* 1989)[31]

CD studies, which report on the bulk secondary structure of peptides in solution, showed that in aqueous solution CGRP is primarily disordered with a small percentage (~20%) of apparent alpha helical content (Figure 2.3), which increases in the presence of trifluoroethanol (TFE), a helix-inducing solvent.[30-31] As Figure 2.3 also shows, the apparent helical content of CGRP also exhibits a slight temperature dependence, decreasing with increasing temperature.[31,32] According to 2D ^{1}H NMR which reports on local contacts, the N-terminal disulfide loop of CGRP is followed by a stretch of residues from 8-18 with a somewhat higher propensity to sample helical states in solution, with the remaining residues 18-37 being highly disordered.[27,28] In aqueous solution, 2D NMR of CGRP has been unable to resolve sequential NOEs, indicating a lack of well-defined three-dimensional structure.[27] However, in helix stabilizing solutions, 2D NMR data reveal that residues 8-18 assume a well defined helical structure while residues thereafter remain largely disordered, with a few turn-type structures at the C-terminus.[27,28,33] Due to the fast reconfiguration of CGRP, NMR has been unable to resolve secondary structure without the aid of helix stabilizing solvents. Moreover, there have been no studies on the long range structural and dynamical properties of CGRP. The aim of this work is to use a novel characterization technique to measure the structure and dynamics of the monomeric state of CGRP. Such long-range (non-local) properties are expected to have a major influence on the affinity and kinetics of binding of IDPs to their receptors, as discussed in Chapter One. In order to study the long-range properties of CGRP in aqueous solvent in the absence of structure inducing solvents such as TFE, we use tryptophan triplet quenching (TTQ). This will also allow comparing such properties to those of a similar

peptide previously studied by the Vaiana research group, IAPP, both of which are members of the Calcitonin (Ct) peptide family.

2.2. THE CALCITONIN PEPTIDE FAMILY

As there are relatively few studies on the structure of CGRP, comparison of CGRP with similar, peptides for which more data is available can help understand the types of interactions that determine the structure and dynamics of CGRP. CGRP is a member of the Calcitonin peptide family, members of which also include calcitonin, adrenomedullin, and amylin (IAPP), among others.[4] These peptides are structurally and genetically related intrinsically disordered hormone peptides that share a sequence homology ranging from about 20 to 50%.[4,6] CGRP derives from alternative splicing of the calcitonin gene on chromosome 11,[1,34] while IAPP, which shares high sequence homology with CGRP, comes from chromosome 12, which is thought to be an evolutionary copy of chromosome 11.[4,34] Ct family members, and CGRP and IAPP in particular, share the highest sequence homology at the N and C terminal regions.[4,35-37] CGRP specifically shares a high sequence homology with IAPP, with both 37 aa peptides having 47% of their amino acids in common. Figure 2.4 is Uversky plot with CGRP and hIAPP labeled as shown below, with both Ct family peptides having a lower net charge and higher hydrophobicity than most disordered proteins, despite the lack of regular secondary structure. The structure of IAPP has previously been studied using the same technique as in this work by other members of the Vaiana research group,[38,39] and this work is a continuation of these

studies, exploring how variations in the sequence can affect the structure and dynamics of these peptides.

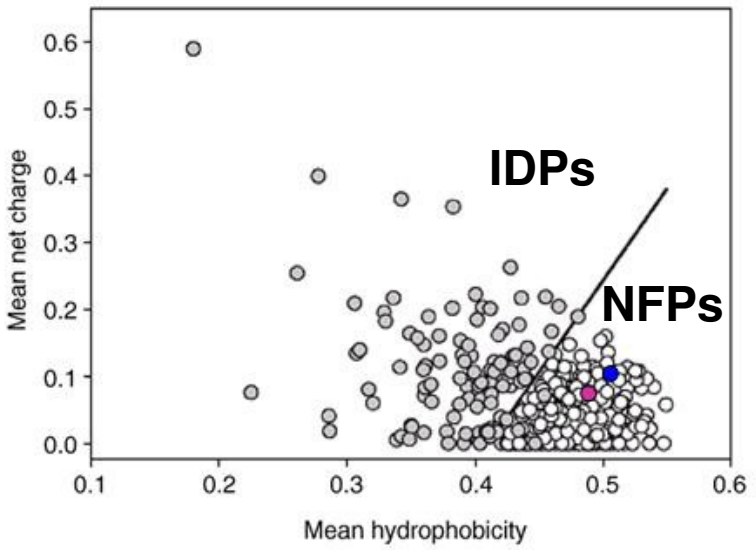

Figure 2.4. Uversky plot of CGRP and hIAPP. Plot of the mean net charge versus mean hydrophobicity of a selection of IDPs and NFPs, with CGRP (blue) and hIAPP (maroon) highlighted.

Like CGRP, all members of the Ct family contain a highly conserved disulfide bond at the N-terminus of the peptide, which forms a loop that increases binding affinity and is required for activation of cell response.[4,5,40-42] Previous studies by the Vaiana research group found that the N_loop, the loop in IAPP is rigid and found that the structure of the N_loop is conducive to aggregation.[43] The sequence of the N_loop in CGRP and IAPP are very similar and despite having a model for the structure of the N_loop in IAPP, there is no direct comparison of the structure of the two peptides in aqueous solvent (under near-native conditions). In addition to the N_loop, the C-terminal region in Ct family peptides are also always amidated, with the amidation required for receptor binding.[4,7,44]

Receptor	Composition	Rank order of agonist potency
CGRP	CLR + RAMP1	αCGRP > AM ≥ AMY ≥ CT
AM_1	CLR + RAMP2	AM > αCGRP > AMY > CT
AM_2	CLR + RAMP3	AM > αCGRP > AMY > CT
CTR	CTR alone	CT > AMY, αCGRP > AM
AMY_1	CTR + RAMP1	AMY ≥ αCGRP > CT > AM
AMY_2	CTR + RAMP2	Poorly defined
AMY_3	CTR + RAMP3	AMY > αCGRP > AM

Figure 2.5. Receptor cross-reactivity in Ct family peptides. For each receptor, the receptor composition and the order of binding affinity are listed (Moore & Salvatore, *Brit. J. of Pharm.*, 2011).[7]

Interestingly, these peptides which share many similar structural features have very different aggregation propensities: some members of the Ct family are prone to aggregate while others are remarkably soluble. Calcitonin and IAPP in particular are known to form amyloid fibrils in disease; fibrilization of calcitonin is implicated in some thyroid cancer[45] and IAPP aggregates into fibrils in the pancreas of people with Type II diabetes mellitus.[35-37] CGRP on the other hand, has never been found in amyloid.[35] This suggests that while the N and C terminal regions are similar in Ct family peptides, it is the differences in the rest of the peptide sequence that must account for the variation in receptor binding affinities and aggregation propensity observed in the Ct family.

In addition to being structurally similar, some Ct peptides can bind to the same receptors, although with varying affinities.[6,7,46] CGRP and its receptors are primarily found in the nervous system, while other peptides and receptors of the Ct family are found elsewhere

in the body.[4,6] Some Ct family members have been shown to bind to the CGRP receptor and are able to activate cell response, though with varying efficiency, as shown in Figure 2.5.[4,7,47] Though it is not yet known precisely how receptor binding and activation occurs, cross-reactivity between Ct peptides and their receptors is likely due to their sequence homology and possible structural similarities. The receptors of the calcitonin family are heterodimers composed of two parts: a trans-membrane protein composed of seven trans-membrane helices, which is a class B G-protein-coupled receptor (GPCR), and a receptor activity modifying protein (RAMP) with a single trans-membrane helix.[48] The Ct family has two GPCRs, the calcitonin receptor (CR) and calcitonin receptor like receptor (CLR) that are modified by three receptor modifying proteins: RAMP1, RAMP2, and RAMP3.[7] The combination of the two GPCRs and three receptor modifying proteins allow for several possible receptors, each of which Ct family peptides binds to with varying potency (Figure 2.5).[7]

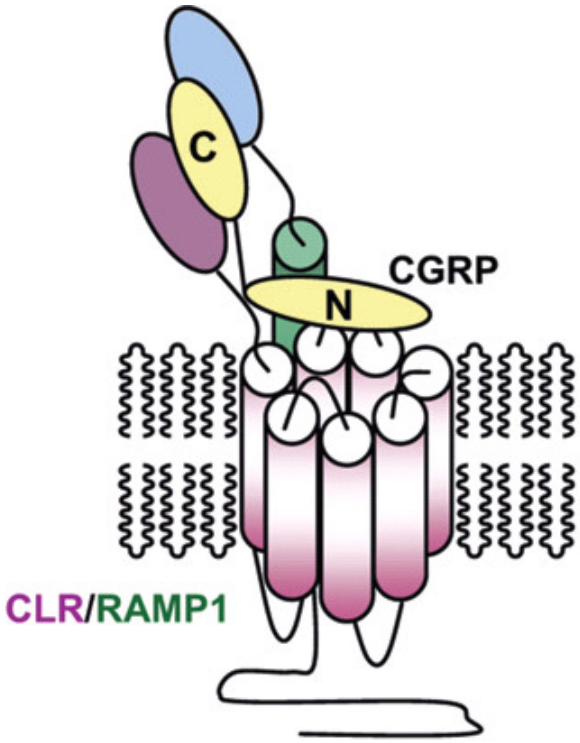

Figure 2.6. CGRP and its receptor. CGRP's receptor is composed of CLR with seven trans-membrane helicies and a single helix trans-membrane receptor modifying protein RAMP1. CGRP's C terminal binds to CLR & RAMP1 while the N terminal region activates the receptor upon binding to CLR (Moore & Salvatore *Brit. J. of Pharm*., 2011).

In the case of CGRP, CGRP's primary receptor is composed of the Calcitonin receptor like receptor, CLR and receptor modifying protein, RAMP1, as shown in Figure 2.6 above.[7,48] Similar to other Ct family peptides, CGRP's C-terminal region binds to the N-terminal regions of CLR and RAMP1 forming an affinity trap, allowing the N-terminal region to activate the receptor through interaction with CLR.[7] This method of receptor activation combined with receptor cross-reactivity likely explains why the N and C terminal regions are highly conserved in Ct family peptides. Understanding this receptor cross-reactivity in Ct family peptides is important as this cross-reactivity is thought to be due to the structural similarities among Ct peptides, and a comparison of the structure and

dynamics can help us understand how they carry out their biological function, despite being disordered. As there have been no studies of the long-range properties of the CGRP monomer and IAPP, which shares receptor cross-reactivity with CGRP, has previously been studied by the Vaiana research group, this work studies the CGRP monomer under near-native conditions (in the absence of structure inducing solvents), in the same solution conditions as IAPP.

REFERENCES

[1]Rosenfeld, M. G., Mermod, J. J., Amara, S. G., Swanson, L. W., Sawchenko, P. E., Rivier, J., Vale, W.W., & Evans, R. M. (1983). Production of a novel neuropeptide encoded by the calcitonin gene via tissue-specific RNA processing. *Nature,* 304 (129-135).

[2]Russo, A. F., & Dickerson, I. M. (2006). CGRP: A multifunctional neuropeptide. In *Handbook of neurochemistry and molecular neurobiology* (pp. 391-426). Springer US.

[3]Brain, S. D., Williams, T. J., Tippins, J. R., Morris, H. R., & MacIntyre, I. (1985). Calcitonin gene-related peptide is a potent vasodilator. *Nature,* 308 (653-655).

[4]Wimalawansa, S. J. (1997). Amylin, calcitonin gene-related peptide, calcitonin, and adrenomedullin: a peptide superfamily. *Critical Reviews™ in Neurobiology*, *11*(2-3).

[5]Brain, S. D., & Grant, A. D. (2004). Vascular actions of calcitonin gene-related peptide and adrenomedullin. *Physiological Reviews*, *84*(3), 903-934.

[6]Van Rossum, D., Hanisch, U. K., & Quirion, R. (1997). Neuroanatomical localization, pharmacological characterization and functions of CGRP, related peptides and their receptors. *Neuroscience & Biobehavioral Reviews*, *21*(5), 649-678.

[7]Moore, E. L., & Salvatore, C. A. (2012). Targeting a family B GPCR/RAMP receptor complex: CGRP receptor antagonists and migraine. *British journal of pharmacology*, *166*(1), 66-78.

[8]Doods, H., Arndt, K., Rudolf, K., & Just, S. (2007). CGRP antagonists: unravelling the role of CGRP in migraine. *Trends in pharmacological sciences*, *28*(11), 580-587.

[9]Ho, T. W., Edvinsson, L., & Goadsby, P. J. (2010). CGRP and its receptors provide new insights into migraine pathophysiology. *Nature Reviews Neurology*, *6*(10), 573-582.

[10]Raddant, A. C., & Russo, A. F. (2011). Calcitonin gene-related peptide in migraine: intersection of peripheral inflammation and central modulation. *Expert reviews in molecular medicine*, *13*, e36.

[11]Reuter, U. (2014). Anti-CGRP antibodies: a new approach to migraine prevention. *The Lancet Neurology*, *13*(9), 857-859.

[12]Tso, A. R., & Goadsby, P. J. (2014). New targets for migraine therapy. *Current treatment options in neurology*, *16*(11), 1-11.

[13]Hoffmann, J., & Goadsby, P. J. (2014). Emerging targets in migraine. *CNS drugs*, *28*(1), 11-17.

[14]Olesen, J., Diener, H. C., Husstedt, I. W., Goadsby, P. J., Hall, D., Meier, U., ... & Lesko, L. M. (2004). Calcitonin gene–related peptide receptor antagonist BIBN 4096 BS for the acute treatment of migraine. *New England Journal of Medicine*, *350*(11), 1104-1110.

[15]Lechleitner, P., Genser, N., Mair, J., Dienstl, A., Haring, C., Wiedermann, C. J., Puschendorf, B., Saria, A., & Dienstl, F. (1992). Calcitonin gene-related peptide in patients with and without early reperfusion after acute myocardial infarction. *American heart journal*, *124*(6), 1433-1439.

[16]Mair, J., Lechleitner, P., Längle, T., Wiedermann, C., Dienstl, F., & Saria, A. (1990). Plasma CGRP in acute myocardial infarction. *The Lancet*, *335*(8682), 168.

[17]Gennari, C., Nami, R., Agnusdei, D., & Fischer, J. A. (1990). Improved cardiac performance with human calcitonin gene related peptide in patients with congestive heart failure. *Cardiovascular research*, *24*(3), 239-241.

[18]Bunker, C. B., Dowd, P. M., Terenghi, G., Springall, D. R., & Polak, J. M. (1990). Deficiency of calcitonin gene-related peptide in Raynaud's phenomenon. *The Lancet*, *336*(8730), 1530-1533.

[19]Bunker, C. B., Reavley, C., Dowd, P. M., & O'Shaughnessy, D. J. (1993). Calcitonin gene-related peptide in treatment of severe peripheral vascular insufficiency in Raynaud's phenomenon. *The Lancet*, *342*(8863), 80-83.

[20]Tjen-A-Looi, S., Ekman, R., Lippton, H., Cary, J., & Keith, I. (1992). CGRP and somatostatin modulate chronic hypoxic pulmonary hypertension. *American Journal of Physiology-Heart and Circulatory Physiology*, *263*(3), H681-H690.

[21]Cruwys, S. C., Kidd, B. L., Mapp, P. I., Walsh, D. A., & Blake, D. R. (1992). The effects of calcitonin gene-related peptide on formation of intra-articular oedema by inflammatory mediators. *British journal of pharmacology*, *107*(1), 116-119.

[22]Salmon, A. M., Damaj, I., Sekine, S., Picciotto, M. R., Marubio, L., & Changeux, J. P. (1999). Modulation of morphine analgesia in αCGRP mutant mice. *Neuroreport*, *10*(4), 849-854.

[23]Salmon, A. M., Damaj, M. I., Marubio, L. M., Epping-Jordan, M. P., Merlo-Pich, E., & Changeux, J. P. (2001). Altered neuroadaptation in opiate dependence and neurogenic inflammatory nociception in αCGRP-deficient mice. *Nature neuroscience*, *4*(4), 357-358.

[24]Lozano-Ondoua, A. N., Symons-Liguori, A. M., & Vanderah, T. W. (2013). Cancer-induced bone pain: Mechanisms and models. *Neuroscience letters*, *557*, 52-59.

[25]Liang, C., Li, H., Tao, Y., Shen, C., Li, F., Shi, Z., Han, B., & Chen, Q. (2013). New hypothesis of chronic back pain: low pH promotes nerve ingrowth into damaged intervertebral disks. *Acta Anaesthesiologica Scandinavica*, *57*(3), 271-277.

[26]Ashton, I. K., Roberts, S., Jaffray, D. C., Polak, J. M., & Eisenstein, S. M. (1994). Neuropeptides in the human intervertebral disc. *Journal of orthopaedic research*, *12*(2), 186-192.

[27]Breeze, A. L., Harvey, T. S., Bazzo, R., & Campbell, I. D. (1991). Solution structure of human calcitonin gene-related peptide by proton NMR and distance geometry with restrained molecular dynamics. *Biochemistry*, *30*(2), 575-582.

[28]Boulanger, Y., Khiat, A., Chen, Y., Senecal, L., Tu, Y., St-Pierre, S., & Fournier, A. (1994). Structure of human calcitonin gene-related peptide (hCGRP) and of its antagonist hCGRP 8-37 as determined by NMR and molecular modeling. *Peptide research*, *8*(4), 206-213.

[29]Cope, S. M., Shinde, S., Best, R. B., Ghirlanda, G., & Vaiana, S. M. (2013). Cyclic N-terminal loop of amylin forms non amyloid fibers. *Biophysical journal*, *105*(7), 1661-1669.

[30]Lynch, B., & Kaiser, E. T. (1988). Biological properties of two models of calcitonin gene related peptide with idealized amphiphilic alpha-helices of different lengths. *Biochemistry*, *27*(20), 7600-7607.

[31]Manning, M. C. (1989). Conformation of the alpha form of human calcitonin gene-related peptide (CGRP) in aqueous solution as determined by circular dichroism spectroscopy. *Biochemical and biophysical research communications*, *160*(1), 388-392.

[32]Hubbard, J. A., Martin, S. R., Chaplin, L. C., Bose, C., Kelly, S. M., & Price, N. C. (1991). Solution structures of calcitonin-gene-related-peptide analogues of calcitonin-gene-related peptide and amylin. *Biochem. J*, *275*, 785-788.

[33]Watkins, H. A., Rathbone, D. L., Barwell, J., Hay, D. L., & Poyner, D. R. (2013). Structure–activity relationships for α-calcitonin gene-related peptide. *British journal of pharmacology*, *170*(7), 1308-1322.

[34]Amara, S. G., Jonas, V., Rosenfeld, M. G., Ong, E. S., & Evans, R. M. (1982). Alternative RNA processing in calcitonin gene expression generates mRNAs encoding different polypeptide products. *Nature,* 298 (240-244).

[35]Westermark, P., Wernstedt, C., Wilander, E., & Sletten, K. (1986). A novel peptide in the calcitonin gene related peptide family as an amyloid fibril protein in the endocrine pancreas. *Biochemical and biophysical research communications*, *140*(3), 827-831.

[36]Westermark, P., Engström, U., Johnson, K. H., Westermark, G. T., & Betsholtz, C. (1990). Islet amyloid polypeptide: pinpointing amino acid residues linked to amyloid fibril formation. *Proceedings of the National Academy of Sciences*, *87*(13), 5036-5040.

[37]Cooper, G. J., Willis, A. C., Clark, A., Turner, R. C., Sim, R. B., & Reid, K. B. (1987). Purification and characterization of a peptide from amyloid-rich pancreases of type 2 diabetic patients. *Proceedings of the National Academy of Sciences*, *84*(23), 8628-8632.

[38]Vaiana, S. M., Best, R. B., Yau, W. M., Eaton, W. A., & Hofrichter, J. (2009). Evidence for a partially structured state of the amylin monomer. Biophysical journal, 97(11), 2948-2957.

[39]Cope, S.M. (2013). Interactions driving the collapse of islet amyloid polypeptide: implications for amyloid aggregation (Doctoral Dissertation).

[40]Dennis, T., Fournier, A., St Pierre, S., & Quirion, R. (1989). Structure-activity profile of calcitonin gene-related peptide in peripheral and brain tissues. Evidence for receptor multiplicity. *Journal of Pharmacology and Experimental Therapeutics*, *251*(2), 718-725.

[41]Tippins, J. R., Di Marzo, V., Panico, M., Morris, H. R., & MacIntyre, I. (1986). Investigation of the structure/activity relationship of human calcitonin gene-related peptide (CGRP). *Biochemical and biophysical research communications*, *134*(3), 1306-1311.

[42]Saha, S., Waugh, D. J. J., Zhao, P., Abel, P. W., & Smith, D. D. (1998). Role of conformational constraints of position 7 of the disulphide bridge of h-α-CGRP derivatives in their agonist versus antagonist properties. *The journal of peptide research*, *52*(2), 112-120.

[43]Cope, S. M., Shinde, S., Best, R. B., Ghirlanda, G., & Vaiana, S. M. (2013). Cyclic N-Terminal Loop of Amylin Forms Non Amyloid Fibers. Biophysical journal, 105(7), 1661-1669.

[44]O'Connell, J. P., Kelly, S. M., Raleigh, D. P., Hubbard, J. A., Price, N. C., Dobson, C. M., & Smith, B. J. (1993). On the role of the C-terminus of alpha-calcitonin-gene-related peptide (alpha CGRP). The structure of des-phenylalaninamide37-alpha CGRP and its interaction with the CGRP receptor. *Biochem. J*, *291*, 205-210.

[45]Arvinte, T., Cudd, A., & Drake, A. F. (1993). The structure and mechanism of formation of human calcitonin fibrils. *Journal of Biological Chemistry*, *268*(9), 6415-6422.

[46]Galeazza, M. T., O'Brien, T. D., Johnson, K. H., & Seybold, V. S. (1991). Islet amyloid polypeptide (IAPP) competes for two binding sites of CGRP. *Peptides*, *12*(3), 585-591.

[47]Chantry, A., Leighton, B., & Day, A. J. (1991). Cross-reactivity of amylin with calcitonin-gene-related peptide binding sites in rat liver and skeletal muscle membranes. *Biochem. J*, *277*, 139-143.

[48]McLatchie, L. M., Fraser, N. J., Main, M. J., Wise, A., Brown, J., Thompson, N., Solari, R., Lee, M.G., & Foord, S. M. (1998). RAMPs regulate the transport and ligand specificity

CHAPTER 3

CHARACTERIZING INTRINSICALLY DISORDERED PROTEINS

3.1 SUMMARY OF EXPERIMENTAL TECHNIQUES

Intrinsically disordered proteins can be difficult to characterize experimentally, due to fast reconfiguration of the protein over short time scales. As IDPs also occupy a wide variety of structures, with some IDPs having more secondary structure than others, some techniques can used to characterize the protein secondary structure or local contacts (contacts between amino acids that are next to each other in sequence). To characterize the disordered states of IDPs, other techniques must be used to elucidate non-local contact formation (contacts between amino acids that are far apart in the sequence), which reports on the tertiary structure and the intra-chain protein dynamics, or the global properties, of IDPs. As discussed in Chapter One, non-local and long-range properties are expected to have the biggest effect on binding; therefore this work focuses on detecting such properties. In this chapter, I discuss various techniques used to characterize IDPs, with a focus on the primary technique used in this work to study the structure and dynamics of CGRP, tryptophan triplet quenching (TTQ).

3.1.1 CHARACTERIZING LOCAL CONTACTS

The characterization of local contacts such as the secondary structure of the protein will give information on the strength and types of intra-molecular bonds present. However,

IDPs do not contain large proportions of secondary structure promoting amino acids, and any secondary structure they have is likely transient.[1,2] In addition, the binding rates and tertiary structure of IDPs have not been found to correlate with secondary structure content.[1,3] The techniques used to measure the secondary structure present in IDPs look at the conformation of the backbone of the peptide; such techniques include CD, NMR, and Fourier Transform infrared spectroscopy (FTIR).

Circular dichroism is a good method for determining the bulk structure of IDPs in solution. CD has been used to measure secondary structure in CGRP[4-6] where it was found that CGRP has about 20% alpha helical content (as in Figure 2.3). NMR is another powerful characterization technique for IDPs, able to resolve the bonds between neighboring hydrogen molecules via nuclear Overhauser effect spectroscopy (NOESY), and is also able to detect the local structural propensity (alpha helix vs random coil) of the backbone via secondary chemical shifts. However, due to CGRP's rapid fluctuations, 2-D NMR measurements on CGRP was not able to resolve many sequential NOEs without the use of stabilizing solvents.[7-9] For more disordered peptides like CGRP, the structure stabilizing solvents like TFE and dimethyl sulfoxide (DMSO), while very useful in measurements to show structural preferences, are not representative of the structure of IDPs in aqueous solution which more closely mimic the environment prior to binding to the receptor.

Despite the fact that IDPs usually fluctuate on fast timescales, these methods are still extremely important in characterizing the structural preferences of disordered proteins through local contacts.

3.1.2 CHARACTERIZING NON-LOCAL CONTACTS

Due to fast chain reconfiguration times combined with relatively little secondary structure in IDPs, it is important to focus on characterizing non-local contact formation or the global structure of IDPs. The formation of non-local contacts, which are contacts between residues that are far away in sequence, will significantly restrict the ensemble of conformations of an IDP and the dynamics of conformational sampling within the ensemble, more so than the formation of a local contact. It is these large changes in the ensemble of conformations and in the dynamics of sampling that are expected to affect binding affinity and kinetics, as discussed in Chapter One. Recent studies have found prior evidence of non-local contacts in IDPs playing an important role in their structure.[10-12] Measurements on the global properties of IDPs can reveal information on the overall structural preferences, such as a preference for compact states (which can affect the rate of receptor binding, or conversely, promote aggregation of the protein through misfolding). Measurements of the global structure are typically done by determining the compactness of the protein through measurements of r_h or r_G.

Techniques like DLS and pulse field gradient NMR can be used to characterize the global structure of IDPs because they give information on the hydrodynamic radius r_H, through

the measurement of the diffusion of the protein in solution. The size of the protein affects the diffusion time and size of the signal, as smaller particles diffuse away more quickly and vice versa. However, since these are low resolution techniques, they do not give information on the intra-chain dynamics (or the dynamics of conformational sampling). In addition, for small IDPS, these techniques require higher concentrations of small proteins for good signal quality, thus will not work well for small, insoluble IDPs.

Other techniques measure the radius of gyration, rG, of disordered proteins to determine tertiary structural information. SAXS can be used to determine the overall compactness of disordered proteins, while paramagnetic relaxation enhancement (PRE) NMR measures long-range tertiary contacts between 1-3.5 nm. One of the most powerful characterization techniques for IDPs, single molecule Förster resonance energy transfer (smFRET) measures tertiary contact formation of disordered proteins. The drawback of PRE and smFRET is the use of large bulky dyes that are often very large compared to the size of the protein itself. As these dyes have a distance dependence of $1/r^6$, this technique works well for large, extended proteins but not for short, compact proteins like CGRP.[13] In addition, the dyes can also be highly charged, introducing electrostatic interactions that can affect reconfiguration rates and make probing electrostatic effects due to the sequence itself difficult.

Despite a few limitations, these techniques that measure the global structural properties of IDPs are a powerful way to measure the non-local contacts and structure of disordered proteins.

3.1.3 CHARACTERIZING DYNAMICAL PROPERTIES

Some techniques measure the dynamical properties of disordered proteins, which in conjunction with measurements of the tertiary structural properties can give an full picture of the disordered protein. One such technique is NMR relaxation times, which gives information on the overall dynamics of the system, where the overall time it takes to relax back to the ground state depends on solvent. Fluorescence correlation spectroscopy (FCS) is a time resolved technique that measures the diffusion coefficient, and is typically used in conjunction with smFRET to give information on both the structure and the inter-dye distance fluctuation correlation time for disordered proteins. As both of these techniques require the use of large prosthetic dyes that have a $1/r^6$ dependence, they have limitations for small proteins. In addition, for small peptides like CGRP, the R_o of FRET is large compared to the size of the protein and the highly insoluble nature of IAPP makes it very difficult to label with prosthetic dyes, therefore this technique cannot be used to compare CGRP with IAPP.

3.2 TECHNIQUES EMPLOYED IN THIS WORK

For a small, highly disordered protein like CGRP, characterization is extremely difficult due to the high concentrations or large prosthetic dyes most techniques require. In this work, CGRP was characterized using two spectroscopic methods: circular dichroism to give information on CGRP's secondary structural preferences, and tryptophan triplet quenching (TTQ) to determine end-to-end contact formation rates for CGRP, which give

information on both the structure and dynamics of CGRP. Since this work also builds upon previous work on IAPP measured by TTQ,[10,14] TTQ was chosen to allow direct comparison of CGRP and IAPP. These techniques do not require the use of large prosthetic dyes and can be used at low peptide concentrations, ideal for characterizing CGRP. They are described in detail below.

3.2.1 CIRCULAR DICHROISM

Circular dichroism is used to determine the secondary structural content of proteins by measuring the chirality of the molecule through the difference in absorption between right circularly polarized and left circularly polarized light. The instrument sends both right circularly polarized light and left circularly polarized light and measures the intensity of light that passes through the sample relative to the incident intensity. The difference in absorption is the CD signal in millidegrees, denoted by

$$\theta = A_L - A_R \qquad \text{Eq 1}$$

As the signal θ is dependent on the concentration *c*, optical pathlength *l*, and the molar extinction coefficient of the protein, the effect of the concentration and pathlength on the CD signal is eliminated to get the characteristic molar ellipticity [θ] of the protein.

$$[\theta] = \frac{\theta}{10 \cdot l \cdot c} \qquad \text{Eq 2}$$

To compare the CD signal across various peptides, each amino acid's individual contribution needs to be taken into account by dividing by the number of amino acid residues to get the molar ellipticity per residue or MRE.

$$MRE = \frac{[\theta]}{\#\,residues} \qquad \text{Eq 3}$$

Each protein will have a characteristic CD spectrum that is dependent on the amount and type of secondary structure present. There are known CD spectrums for random coil, alpha helix, beta sheet, polyproline II, and other structures, and the CD signal will be a convolution of these spectra, with each component of the signal in proportion to the proportion of the secondary structure content.

Circular dichroism experiments to determine secondary structure content are done in the near UV (260 to 190 nm). Small sample volumes of only 200uL and low sample concentrations of less than 0.2 mg/mL make circular dichroism a powerful way to determine secondary structural preferences of disordered proteins. Despite a few drawbacks, CD is a powerful way to characterize the secondary structural content of small, insoluble proteins and is used in this work to characterize CGRP's secondary structure content.

3.2.2 TRYPTOPHAN TRIPLET QUENCHING

3.2.2.1 EXPERIMENTAL BACKGROUND

The primary experimental technique utilized in this paper allows us to simultaneously probe the end-to-end distance and the dynamics of contact formation between the two ends of the peptide without some of the limitations present in other experimental techniques. TTQ uses the natural phosphorescence of tryptophan, the triplet state of which is quenched by cysteine or cystine. As cystine is not an efficient quencher of the triplet state of tryptophan,[15,16] the quenching reaction is not diffusion limited and the disordered protein can reconfigure many times before quenching occurs. The peptide therefore explores the ensemble of conformations before quenching and the quenching rate yields information on the structure through the equilibrium end-to-end distance P(r) and the internal dynamics of the peptide chain through the intra-chain diffusion coefficient, D. As TTQ can be used at low millimolar concentrations,[17] it is an effective technique for insoluble proteins. As TTQ uses the naturally occurring amino acids tryptophan and cystine as probes, TTQ does not require large, highly charged prosthetic dyes that can significantly perturb small peptides like CGRP. The technique has previously been described in detail[10,17,18] and a description of how the technique works is described as follows.

3.2.2.2 THEORY OF OPERATION

Tryptophan is optically excited and a proportion of the excited molecules move to a triplet state. The lifetime of this state is long lived (~40 μs)[15,16] relative to the time it takes for the two ends of a disordered protein to come into contact. If this contact is made for a long enough time or for a sufficient number of times, quenching of the excited state will occur. If the two ends do not stay in contact long enough, then they will diffuse away without quenching (Figure 3.1).

Figure 3.1. Principle of operation. The tryptophan (red molecule) is excited, and quenching of the triplet state occurs upon contact with a cystine (yellow molecule) after chain reconfiguration.

This can be described empirically as a two state process where the two ends diffuse together at a rate k_{D+}, and then either of two things will occur: the triplet state is quenched by the cystine at a rate q, or the two ends diffuse away without quenching at a rate k_{D-}. The technique measures the observed quenching rate k_{obs}, which is equal to the rate that contact is formed times the probability that quenching occurs.

$$k_{obs} = k_{D+} \frac{q}{k_{D-} + q} \qquad \text{Eq 4}$$

Defining the equilibrium constant for forming the encounter complex as $K_{eq} = k_{D+}/k_{D-}$, the observed rate is rewritten in terms of a diffusion-limited rate k_{D+} and a reaction-limited rate k_R, where $k_R = q*K_{eq}$.

$$\frac{1}{k_{obs}} = \frac{1}{k_R} + \frac{1}{k_{D+}} \qquad \text{Eq 5}$$

The reaction-limited rate corresponds to the case where diffusion is fast enough such that the fraction of encounter complexes is equal to its equilibrium value at all times. When written in this way, the variable that depends on the structure (k_R) is separated from the variable that depends on the dynamics (k_{D+}).

To obtain the reaction limited and diffusion limited rates, we measure k_{obs} as a function of solvent viscosity. In aqueous solution we are close to the reaction limited rate, and at very high viscosities, we are close to the diffusion-limited rate. By plotting the inverse of the observed rate as a function of solvent viscosity, it is possible to obtain the reaction limited and diffusion limited rates (Figure 3.2).

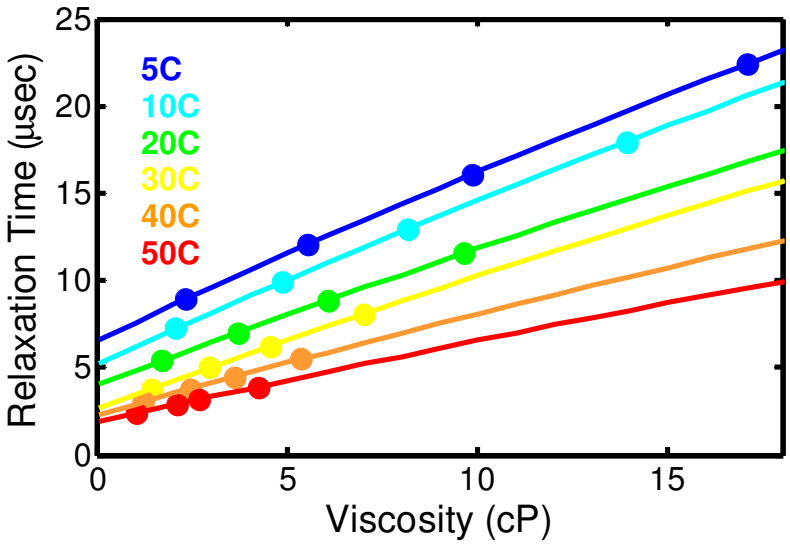

Figure 3.2. Viscosity dependence of the observed quenching rate. The inverse of the observed quenching rate as a function of solvent viscosity for CGRP in 6M GdmCl 50mM NaAc pH 4.9. The intercept at zero viscosity is $1/k_R$, while the slope is $1/\eta k_{D+}$.

3.2.2.3.SPECTROPHOTOMETER AND DATA COLLECTION

To measure the end-to-end contact formation rates of CGRP, a home-built spectrophotometer was constructed in the Laser Spectroscopy and Biophysics Lab (LSBL) of Dr. Sara M. Vaiana in the Department of Physics and Center for Biological Physics at Arizona State University. Planning and construction was done by Alejandro Solis with help from Sebastian Haefner, with further calibration and adjustments done by Stephanie Cope, Danmei Bian and Sara Sizemore, all under the supervision of Dr. Sara M. Vaiana. A general description of the spectrophotometer setup and collection of the experimental data is described below.

Prepared samples of IDPs in solution were irradiated by a 10 Hz, 7ns pulse at 290 nm generated by an Nd:YAG laser (Continuum) which excites the tryptophan in the protein, a proportion of which moves to a triplet state. The quenching of the triplet state of tryptophan by cystine was measured by monitoring the triplet-triplet absorption at 458 nm, with an Argon ion laser (Coherent) at 458 nm continuously irradiating the sample to keep the tryptophan in the triplet state until quenching by cystine could occur. A schematic of the photophysics is shown in Figure 3.3.

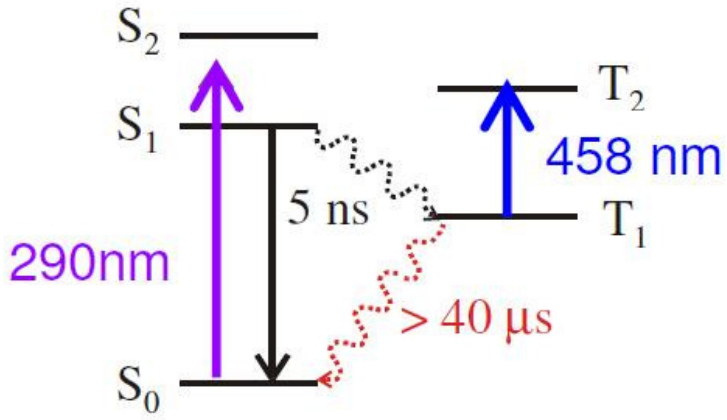

Figure 3.3. Photophysics of the triplet state of tryptophan.

As this is a two state process, the triplet-triplet absorption of the sample at 458 nm, which corresponds to the population of molecules in the triplet state, decays in time exponentially as it is quenched by cystine with a characteristic rate k_{obs}. Fitting this decay with a single exponential function gives the observed rate of quenching. To account for the decay of free radicals in the solution,[10,19] the data were fit to an exponential decay, together with a second offset function which varied linearly with log(t) for times greater

than 4e-5 s and a time-independent offset constant, as shown in Figure 3.4. A single measurement corresponds to the average absorption at 458 nm of 256 events, with five measurements performed at each temperature and then averaged.

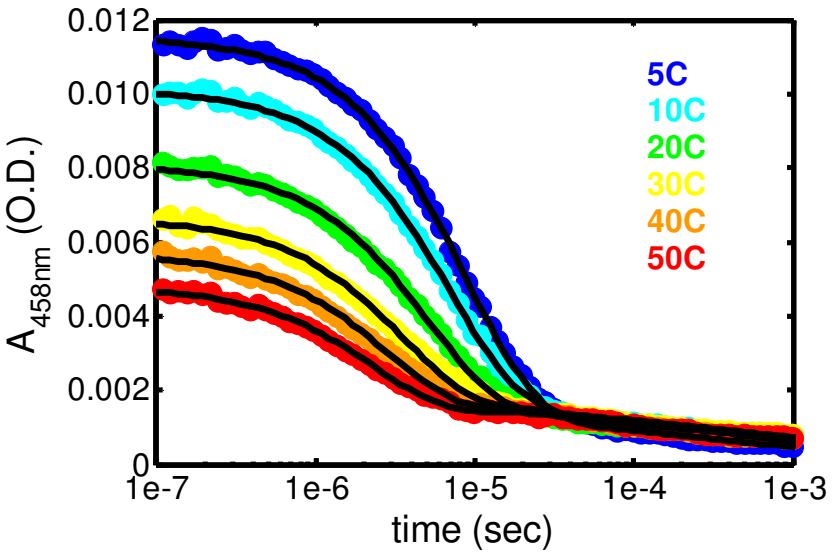

Figure 3.4. Decay of the triplet-triplet absorption at 458 nm. The temperature dependence of the triplet-triplet absorption of CGRP in 6M GdmCl 50mM NaAc pH 4.9 is fit with a single exponential function with a sloped decay at long times. The characteristic decay times from these fits are used to calculate the reaction and diffusion limited rates.

The temperature of the sample was adjusted by a peltier temperature stage so that measurements could be performed as a function of temperature from 5 to 50C. A schematic of the setup is shown in Figure 3.5.

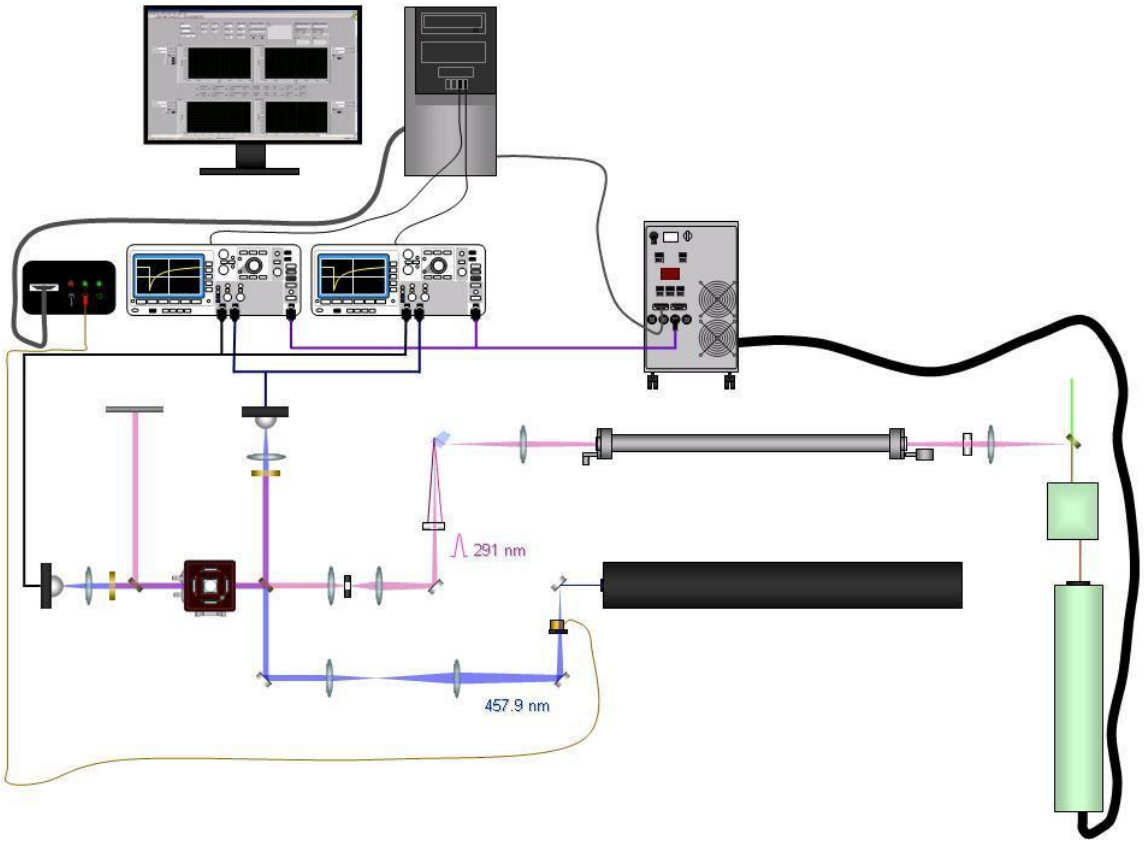

Figure 3.5. Schematic of the home-built laser pump-probe spectrophotometer. The Nd:YAG laser pumps the tryptophan to its triplet state at 290 nm, while the argon laser probes the triplet-triplet absorption at 458 nm.

To extract structural and dynamical information, viscosity and temperature dependent measurements were performed by addition of sucrose at each solvent condition (up to 40% w/v) and performing a temperature scan from 5-50C. The raw data, after correcting for background, was assembled into an array of approximately 120 traces, and singular value decomposition (SVD) was performed, with the 12 largest components used to reconstruct the data. This reduces noise in the signal and decreases uncertainty in the fit, without affecting the experimental fit for the observed rate of quenching. To reduce noise

further after performing SVD, the data sets for each temperature and viscosity condition were averaged. The temperature and viscosity data were then globally fit using the exponential decay described above and assuming that the reaction limited k_R and diffusion limited k_{D+} rates have a temperature and viscosity dependence that can be characterized by

$$k_R = k_R(T) \qquad \text{Eq 6}$$

$$k_{D+} = \eta(T)^{-1} k_{D+}(T) \qquad \text{Eq 7}$$

where $\eta(T)$ is viscosity of the solvent measured at the given temperature. The values of k_{obs} corresponding to the exponential decay of the triplet state are plotted as a function of the solvent viscosity, as in Figure 3.2. The temperature and viscosity dependence of k_{obs} is given in Eq 8 below.

$$\frac{1}{k_{obs}(\eta,T)} = \frac{1}{k_R(T)} + \frac{1}{k_{D+}(\eta,T)} \qquad \text{Eq 8}$$

When analyzed this way, $1/k_R$ is obtained as the intercept at zero viscosity, and $1/\eta k_{D+}$ as the initial slope. These values for k_R and ηk_{D+} for CGRP exhibit Arrhenius-like temperature dependence so for easy visualization, Arrhenius plots of the rates are given throughout this paper.

3.2.2.4. INFORMATION EXTRACTED

Although the quenching of tryptophan was described as a two state model above, the actual quenching rate q(r) has a distance dependence. SSS theory models this process in which the rate of end-to-end contact formation can be described as 1-D diffusion along the end-to-end distance coordinate.[20,21] In this way, the observed rate of quenching k_{obs} from Eq 5 can be described in terms of k_R and k_{D+} below:

$$k_R(T) = \int_{a_0}^{l_c} P(r,T)q(r,T)dr \qquad \text{Eq 9}$$

$$k_{D+}(T) = \left(\int_{a_0}^{l_c} \left(D(T) \cdot P(r,T)\right)^{-1} \left[\int_{x}^{l_c} \delta q(x,T)P(x,T)dx \right]^2 dr \right)^{-1} \qquad \text{Eq 10}$$

In this way, measurements of the reaction and diffusion limited rates allow us to extract information on the structure through the equilibrium end-to-end distance distribution P(r) and information on the dynamics through the intra-chain diffusion coefficient D. Both k_R and k_{D+} have an explicit dependence on temperature,[18,22] and with the quenching rate *q* having a complicated dependence on temperature, this work does not attempt to explain how CGRP's structure and dynamics depend on temperature. The temperature dependence of k_{obs} was measured in order to do global fits of the experimental data, and in this work, k_{obs}, k_R, and ηk_{D+} will be plotted on Arrhenius plots to guide the eye only,

and we will not attempt to give interpretations of the enthalpy, ΔH, and instead will only discuss shifts in the rates that occur at all temperatures.

Despite the fact that IDPs are unfolded with little regular structure, their end to end distances can vary significantly from one IDP to another, and can experience significant compaction or expansion under different solvent conditions. In order to quantify these changes in structure, we can use basic polymer models to calculate how the end to end distances change. For the analysis in this work, we use the ideal chain or Gaussian model, in which the monomer is divided into segments of equal lengths, or effective segment lengths, *b*. In this model, each segment is uncorrelated and freely rotating, effectively approximating a 3-D random walk, with the average end-to-end distance $\sqrt{\langle r^2 \rangle}$ taking the form

$$\sqrt{\langle r^2 \rangle} = N^{1/2} b \qquad \text{Eq 11}$$

where N is the number of segments, or amino acids, making up the polymer. Although a Gaussian model is idealized, other groups have found that a Gaussian P(r) is sufficient to describe changes in $\sqrt{\langle r^2 \rangle}$ when performing end-to-end contact formation measurements,[23,24] so for the purposes of this work, all end-to-end distances are calculated assuming a Gaussian P(r).

Tryptophan triplet quenching when used in conjunction with SSS theory and polymer models, is a powerful way to characterize the structure and dynamics of disordered

proteins in solution. Through the deployment of the techniques described in this chapter, this work seeks to characterize the structure and internal dynamics of CGRP to help understand how the monomer state of CGRP interacts with itself and its receptor.

REFERENCES

[1]Marsh, J. A., & Forman-Kay, J. D. (2010). Sequence determinants of compaction in intrinsically disordered proteins. *Biophysical journal*, *98*(10), 2383-2390.

[2]Romero, P., Obradovic, Z., Li, X., Garner, E. C., Brown, C. J., & Dunker, A. K. (2001). Sequence complexity of disordered protein. *Proteins: Structure, Function, and Bioinformatics*, *42*(1), 38-48.

[3]Rogers, J. M., Steward, A., & Clarke, J. (2013). Folding and binding of an intrinsically disordered protein: fast, but not 'diffusion-limited'. *Journal of the American Chemical Society*, *135*(4), 1415-1422.

[4]Manning, M. C. (1989). Conformation of the alpha form of human calcitonin gene-related peptide (CGRP) in aqueous solution as determined by circular dichroism spectroscopy. *Biochemical and biophysical research communications*, *160*(1), 388-392.

[5]Hubbard, J. A., Martin, S. R., Chaplin, L. C., Bose, C., Kelly, S. M., & Price, N. C. (1991). Solution structures of calcitonin-gene-related-peptide analogues of calcitonin-gene-related peptide and amylin. *Biochem. J*, *275*, 785-788.

[6]Mimeault, M., St-Pierre, S., & Fournier, A. (1993). Conformational characterization by circular dichroism spectroscopy of various fragments and analogs of calcitonin gene−related peptide. *European Journal of Biochemistry*, *213*(3), 927-934.

[7]Breeze, A. L., Harvey, T. S., Bazzo, R., & Campbell, I. D. (1991). Solution structure of human calcitonin gene-related peptide by proton NMR and distance geometry with restrained molecular dynamics. *Biochemistry*, *30*(2), 575-582.

[8]Boulanger, Y., Khiat, A., Chen, Y., Senecal, L., Tu, Y., St-Pierre, S., & Fournier, A. (1994). Structure of human calcitonin gene-related peptide (hCGRP) and of its antagonist hCGRP 8-37 as determined by NMR and molecular modeling. *Peptide research*, *8*(4), 206-213.

[9]O'Connell, J. P., Kelly, S. M., Raleigh, D. P., Hubbard, J. A., Price, N. C., Dobson, C. M., & Smith, B. J. (1993). On the role of the C-terminus of alpha-calcitonin-gene-related peptide (alpha CGRP). The structure of des-phenylalaninamide37-alpha CGRP and its interaction with the CGRP receptor. *Biochem. J*, *291*, 205-210.

[10]Vaiana, S. M., Best, R. B., Yau, W. M., Eaton, W. A., & Hofrichter, J. (2009). Evidence for a partially structured state of the amylin monomer. *Biophysical journal*, *97*(11), 2948-2957.

[11]Miller, C., Zerze, G.H., & Mittal, J. (2014). Molecular simulations indicate marked differences in the structure of amylin mutants, correlated with known aggregation propensity. *The Journal of Physical Chemistry B. 117*(50), 16066-16075.

[12]Cho, J.H., Sato, S., & Raleigh, D.P. (2004). Thermodynamics and kinetics of non-native interactions in protein folding: a single point mutation significantly stabilizes the N-terminal domain of L9 by modulating non-native interactions in the denatured state. *Journal of molecular biology, 338*(4), 827-837.

[13]Clore, G. M., & Iwahara, J. (2009). Theory, practice, and applications of paramagnetic relaxation enhancement for the characterization of transient low-population states of biological macromolecules and their complexes. *Chemical reviews*, *109*(9), 4108-4139.

[14]Cope, S.M. (2013). *Interactions driving the collapse of islet amyloid polypeptide: implications for amyloid aggregation* (Doctoral Dissertation).

[15]Gonnelli, M., & Strambini, G. B. (1995). Phosphorescence lifetime of tryptophan in proteins. *Biochemistry*, *34*(42), 13847-13857.

[16]Strambini, G. B., Kerwin, B. A., Mason, B. D., & Gonnelli, M. (2004). The Triplet-state Lifetime of Indole Derivatives in Aqueous Solution. *Photochemistry and photobiology*, *80*(3), 462-470.

[17]Lapidus, L. J., Eaton, W. A., & Hofrichter, J. (2000). Measuring the rate of intramolecular contact formation in polypeptides. *Proceedings of the National Academy of Sciences*, *97*(13), 7220-7225.

[18]Lapidus, L. J., Steinbach, P. J., Eaton, W. A., Szabo, A., & Hofrichter, J. (2002). Effects of chain stiffness on the dynamics of loop formation in polypeptides. Appendix: Testing a 1-dimensional diffusion model for peptide dynamics. *The Journal of Physical Chemistry B*, *106*(44), 11628-11640.

[19]Gonnelli, M., & Strambini, G. B. (2005). Intramolecular Quenching of Tryptophan Phosphorescence in Short Peptides and Proteins¶. *Photochemistry and photobiology*, *81*(3), 614-622.

[20]Szabo, A., Schulten, K., & Schulten, Z. (1980). First passage time approach to diffusion controlled reactions. *The Journal of Chemical Physics*, *72*(8), 4350-4357.

[21]Schulten, K., Schulten, Z., & Szabo, A. (1981). Dynamics of reactions involving diffusive barrier crossing. *The Journal of Chemical Physics*, *74*(8), 4426-4432.

[22]Buscaglia, M., Lapidus, L. J., Eaton, W. A., & Hofrichter, J. (2006). Effects of denaturants on the dynamics of loop formation in polypeptides. *Biophysical journal*, *91*(1), 276-288

[23]Müller-Späth, S., Soranno, A., Hirschfeld, V., Hofmann, H., Rüegger, S., Reymond, L., Nettels, D., & Schuler, B. (2010). Charge interactions can dominate the dimensions of intrinsically disordered proteins. *Proceedings of the National Academy of Sciences*, *107*(33), 14609-14614.

[24]Hofmann, H., Soranno, A., Borgia, A., Gast, K., Nettels, D., & Schuler, B. (2012). Polymer scaling laws of unfolded and intrinsically disordered proteins quantified with single-molecule spectroscopy. *Proceedings of the National Academy of Sciences*, *109*(40), 16155-16160.

CHAPTER 4

CGRP IN AQUEOUS SOLVENT AND DENATURANT

4.1. INTRODUCTION

The aim of this work is to understand the types of intra-chain interactions which modulate the structure and dynamics of CGRP, in order to better understand the types of interactions that might drive receptor binding and activation. It is thought that the high cross receptor cross-reactivity among Ct peptide family members[1-3] are due to their structural similarities. In particular, the focus of this work is the study of the structure and dynamics of CGRP, whose structure, as Chapter Two reveals, is relatively unknown and unexplored. Therefore it is interesting to compare the structure of CGRP with IAPP, a Ct family peptide that has been studied extensively, with which CGRP shares a 47% sequence homology.[4-6] As CGRP is very soluble compared to IAPP[4] and has very similar sequence composition, comparison of the structure and dynamics of the two peptides can allow us to explore differences and similarities in the method of receptor binding and activation.

We first set out to understand what structural and dynamical similarities exist between the Ct family peptides CGRP and IAPP that allow for receptor cross-reactivity. As mentioned in Chapter Two, all Ct family peptides have a characteristic N-terminal disulfide loop, N_loop, which is required for activation of cell response.[6-10] The loop could promote interactions between the peptide chain and the receptor, which is

supported by studies that show that removal of the N_loop or conversion to a linear analog by breaking the disulfide bond abolishes receptor activity.[8-10] Previous experiments and molecular dynamics simulations showed that the N_loop causes both human and rat IAPP variants to prefer a collapsed state in aqueous solvent, with the N_loop forming favorable non-local intra-chain interactions with the rest of the chain.[11] Earlier work in the Vaiana Lab group found that the N_loop readily self-associates, forming favorable inter-chain interactions, suggesting a potential mechanism for receptor binding and aggregation.[12] All of this hints at an important role that the characteristic N_loop found in Ct family peptides likely plays in their structure and function, and might be a potential mechanism for pathological aggregation.

Circular dichroism measurements done on both CGRP and IAPP show that CGRP and IAPP have very different secondary structure content in aqueous solvent, with CGRP having more alpha helix than IAPP, which appears to preferentially adopt a random coil structure.[13] In addition, CD and NMR measurements show that when the loop found in CGRP and IAPP is truncated, both peptides lose their alpha helical propensity.[13-15] This suggests that CGRP, despite having a similar sequence to IAPP, might have more helix promoting residues, and that the N_loop in the Ct family peptides help stabilize the transient secondary structure.

In this chapter, tryptophan triplet quenching measurements on CGRP in both buffer and denaturant as well as circular dichroism measurements were performed to explore both the effect of the solution environment on the secondary and tertiary structure of CGRP

and to compare it with previous measurements on IAPP in the same solution conditions. TTQ studies on the disulfide loop found in CGRP were also performed to explore how the structure of CGRP depends on the N_loop. In this way, we explore how peptides of the same length in the same solvent, with 47% sequence homology, adopt different structural characteristics.

4.2. EXPERIMENTAL METHODS

MATERIALS

Fmoc(9-fluorenylmethoxycarbonyl)-protected amino acids were purchased from Novabiochem. HOBt (N-hydroxy benzotriazole) and HBTU (O-Benzotriazole-N, N, N', N'-tetramethyl-uronium-hexafluoro-phosphate) were purchased from Genscript. N,N-iisopropylethylamine, or Hünig's base (DIPEA), and N-Methyl-2-pyrrolidone (NMP), used as base in solid phase peptide synthesis, were purchased from Sigma Aldrich. Piperidine (Sigma-Aldrich) was used for deprotection. Rink Amide ChemMatrix® was purchased from Matrix Innovations. Dimethyl formamide, Dichloromethane and Acetonitrile were purchased from Fisher Scientific and were used without further purification.

In addition, >95% purity CGRP wild-type and CGRP D3N mutants, both with the F37W mutation, were purchased from Genscript and purity verified via HPLC on a C18 analytical column. Circular dichroism and TTQ measurements on CGRP F37W purchased from Genscript was identical to measurements on CGRP F37W that was

synthesized and purified as described below, and show no difference in secondary or tertiary structure between the two sources.

PEPTIDE SYNTHESIS AND PURIFICATION

CGRP F37W was synthesized on a 0.1 mmol scale using a CEM Liberty Automated Microwave Peptide Synthesizer and PALChem Matrix resin. After synthesis, the peptide was thoroughly washed 5 times by DMF followed by DCM. After washing, the peptide was stored on the resin at -20°C. For deprotection, the peptide was shaken for one hour in 20% piperdine, 0.1M HOBt in DMF. The cleavage cocktail consisted of 81.5% trifluoroacetic acid + 5% Water +5% Anisole + 5% Thioanisole + 2.5% 1,2-Ethanedithiol + 1% triisopropylsilane at the ratio of 150 µL/ 10 mgs of resin. CGRP F37W was purified using reverse phase high performance liquid chromatography (HPLC) on a Waters 600E system. Crude peptide was purified on a C4 semi-preparative column (Vydac/Grace Deerfield, IL) from 5-50% Acetonitrile with 0.1% (v/v) TFA at a gradient of 1% every three minutes.

DISULFIDE FORMATION AND FURTHER PURIFICATION

1.0 mM of lyopholized peptide was dissolved in 30% DMSO and 3% Acetic Acid. The sample was stirred with a magnetic stir bar at 800 rpm. During this time, the formation of the intra-molecular disulfide bonds was monitored via HPLC on a C18 analytical column. The reaction was deemed complete when the reduced peptide's HPLC peak was no longer apparent: approximately 12 hours. After this time, the sample was frozen and

lyophilized. Oxidized peptide was re-purified on a C18 semi-preparative column to further purify and separate any un-reacted peptide.

Calibrated matrix-assisted laser desorption/ionization - time of flight mass spectrometry (MALDI-TOF) mass spectrometry indicated the presence of a -2 Da species (above the margin of error the instrument), corresponding to the oxidized form of the peptide. To further support these findings, a maleimide sulfhydryl reaction was performed. 1 mg 3-(N-Maleimidopropionyl)-biocytin (Cayman Chemical Company Ann Arbor, MI) was dissolved in 180uL 20mM PBS buffer, pH=7.0 and 20µL acetonitrile. 1mg pure, oxidized CGRP F37W was dissolved in 90µL 20mM PBS buffer, pH=7.0 and 10µL acetonitrile. This solution was combined with the 3-(N-Maleimidopropionyl)-biocytin solution and shaken for four hours. At 1 hour increments, 20 µL aliquot was removed and frozen in dry ice. After four hours, the four aliquots were analyzed via MALDI-TOF.

HPLC peaks were analyzed by a Voyager Systems 4320 (Applied Biosystems) MALDI-TOF. The peak corresponding to a molecular weight of 3828Da (corresponding to the amidated and oxidized form of CGRP F37W) was analyzed further for purity by analytical HPLC, using a reverse phase C18 analytical column 214TP54 (Length 250mm × ID 4.6mm) particle size 5µm using the same gradient conditions with 0.9 mL/min flow rate. A single peak eluting at a gradient corresponding to the hydrophobicity of CGRP was collected, immediately frozen in liquid nitrogen, lyophilized, and kept at -20°C.

END TO END CONTACT FORMATION BY TRYPTOPHAN TRIPLET QUENCHING

The quenching of the triplet state of tryptophan by cystine in 100uM CGRP samples were measured in either 50mM NaAc at pH 3 or 4.9, or 20mM $NaPO_4$ pH 8 buffers (Sigma-Aldrich). The pHs of the buffers were checked by an Accumet BASIC AB15 pH meter (Fisher Sci) and the final solution pH was adjusted using either 1M NaOH or 1M HCl as needed. In order to measure CGRP in denaturant and to do viscosity dependent measurements, guanadinium chloride, or GdmCl (as measured by calculated molar concentration) and/or sucrose (as measured by percent weight by volume) were added to prepared buffer and the pH readjusted as needed. The buffers were kept at 4C and filtered with a 0.02 um Whatman Anotop 10 filter before further sample preparation. Lyophilized peptide was weighed out to yield 100uM in ~3 mL of sample (~0.38 mg/mL) and added directly to freshly filtered buffer. Absorbance was checked in a 1cm quartz cuvette using an extinction coefficient of $\varepsilon = 5774\ m^2/mol$, and the concentration adjusted to 100uM if needed. The CGRP samples were filtered directly into long-neck quartz cuvettes (Starna Cells) with a Whatman Anotop 10 0.2 um filter, and degassed with nitrous oxide for at least two hours to eliminate free oxygen from the sample before measurement.

For TTQ measurements of CGRP in TCEP-HCl (tris(2-carboxyethyl)phosphine hydrochloride), samples of CGRP at pH 4.9 in both buffer and 6M GdmCl were prepared as above. However, before degassing, a two-fold (200μM) excess of TCEP (Pierce) was weighed out and added directly to the CGRP samples and stirred gently.

For TTQ experiments on CGRP C7S and C2S, due to the possibility of oxidization of the cysteines, both the peptide and buffer are deoxygenated before the addition of peptide to buffer, with sample preparation proceeding as usual afterwards.

The triplet-triplet absorption of the sample at 457 nm, which corresponds to the decay of the triplet state of tryptophan as it is quenched by cystine, was measured with New Focus Model 1621 nanosecond photodetectors, and the data recorded by Tektronic DP03032 digital phosphor oscilloscopes. The temperature of the sample was adjusted by a Quantum Northwest TLC50 turret peltier stage so that measurements could be performed as a function of temperature from 5 to 50C.

As CGRP does not have a naturally occurring tryptophan, the phenylalanine at residue 37 was mutated to a tryptophan that will be quenched by the naturally occurring cystine at the N terminus. As both amino acids have aromatic rings, the structure of CGRP is not expected to be significantly perturbed by this mutation. This was checked by comparing the circular dichroism structure of CGRP F37W to already published spectra from literature.[13,16] No change in CGRP's secondary structure was observed due to this mutation. In addition, NMR studies that actually truncated the chain by removing the phenylalanine at residue 37 saw no change in structure, and was still able to bind to the CGRP receptors although biological activity was abolished.[17] Because of this, it is assumed that little to no change in the structure of CGRP occurs due to this mutation.

CIRCULAR DICHROISM SPECTROSCOPY

CD Spectra of the samples were measured in 1mm quartz cuvettes (Starna Cells). Aliquots of solutions prepared for TCQ were diluted with Millipore H_2O, resulting in final peptide concentrations ranging from 10-40 μM. Samples were measured by a Jasco J-710 spectropolarimeter (Jasco Company) with a 1 nm bandwidth. For each sample, eight spectra taken with a 0.2 nm pitch at a 50 nm/min scan speed were averaged. Before data analysis, spectra were buffer subtracted.

4.3 THE CGRP MONOMER SAMPLES STATES WITH SHORT END-TO-END DISTANCES IN SOLUTION

4.3.1. OBSERVED RELAXATION RATE OF CGRP

Using tryptophan triplet quenching, the observed quenching rate k_{obs} of CGRP was measured, which is the rate that cystine quenches the triplet state of tryptophan. This rate k_{obs} is equal to the rate that the two ends of the peptide chain come into contact, k_{D+} times the probability that quenching occurs. As this rate depends on the volume of the chain, k_{obs} can be used as a first approximation of the expansion or compaction of the chain. The observed quenching rates of CGRP in both 50mM NaAc buffer pH 5 and in 6M GdmCl are shown on an Arrhenius plot in Figure 4.1. We see that CGRP has a three fold increase in rates when going from denaturant (6M GdmCl) to buffer, indicating that CGRP samples highly compact states (characterized by short end-to-end distances) in aqueous solvent relative to denaturant.

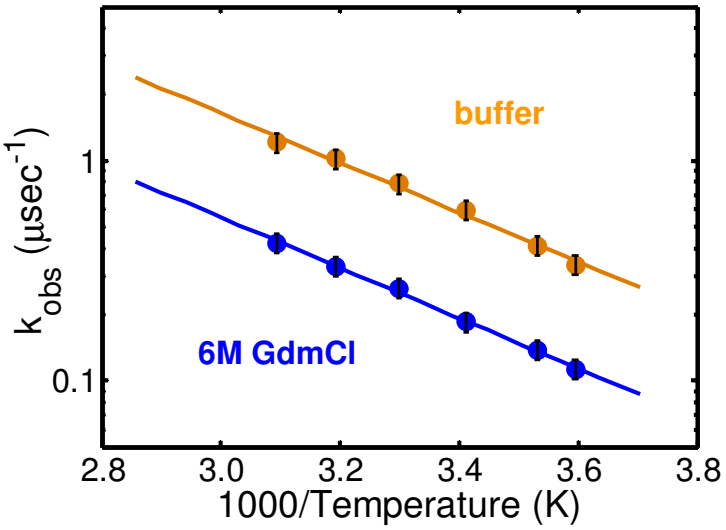

Figure 4.1. Arrhenius plot of the observed quenching rate of CGRP. CGRP was measured in 50mM NaAc pH 4.9 buffer (orange) and denaturant (6M GdmCl- blue).

This collapse means that CGRP has intra-chain interactions that form non-local contacts in aqueous solvent, such as electrostatic interactions and hydrophobic interactions. To further explore CGRP in both buffer and denaturant, viscosity dependent measurements must be performed.

4.3.2. STRUCTURE AND DYNAMICS OF CGRP

To determine whether the increase in k_{obs} in buffer is due to chain collapse rather than faster chain dynamics, k_{obs} was measured as a function of viscosity and k_R and ηk_{D+} were obtained from the intercept and slope, as described in Chapter 3.2.2. Figure 4.2 shows the inverse of the observed quenching rate as a function of solvent viscosity for CGRP in

both buffer and denaturant. The reaction limited rate is extracted from the intercept at zero viscosity, and the diffusion limited rate is the initial slope.

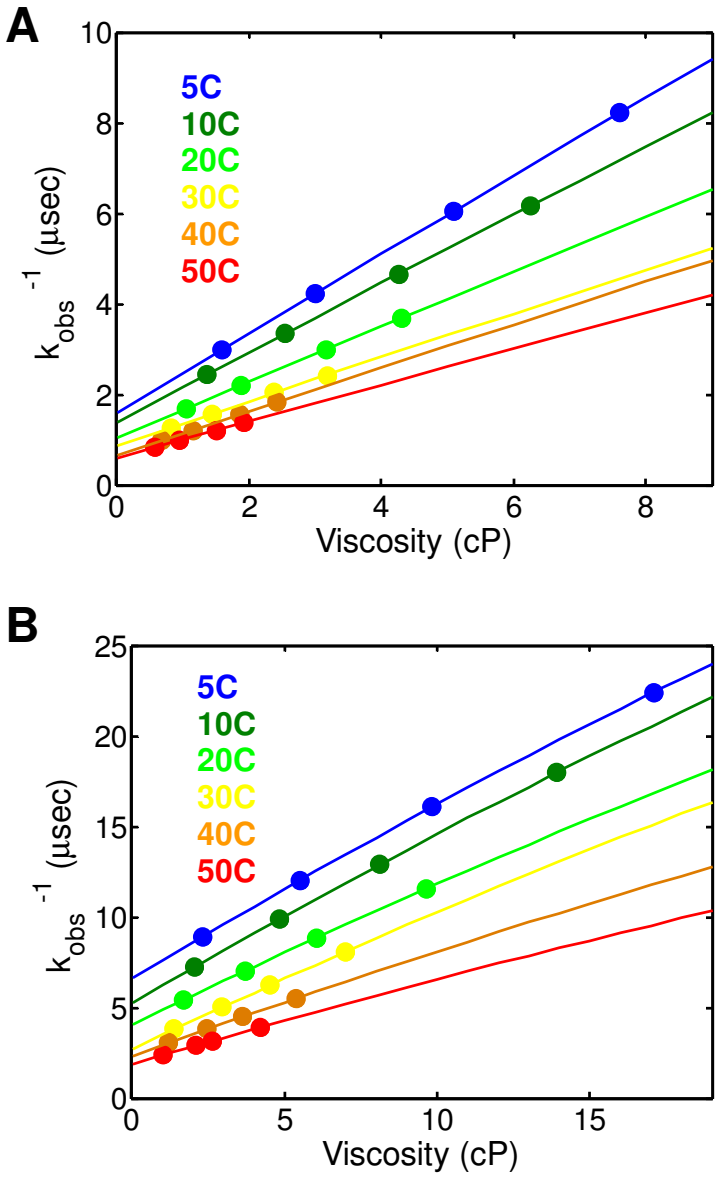

Figure 4.2. Viscosity dependence of the observed quenching rate of CGRP in buffer and denaturant. The figures plot the temperature dependence of the inverse of the observed quenching rate of CGRP as a function of solvent viscosity in buffer (A) and denaturant (B).

Arrhenius plots of both the reaction limited rates and diffusion limited rates of CGRP obtained from analysis of Figure 4.2 above in buffer and denaturant are shown in Figure 4.3A and 4.3B respectively. In this chapter we will only focus on the reaction limited rates while the diffusion limited rates will be discussed in Chapter Six. The plot in Figure 4.3.A shows that the three fold increase in k_{obs} when going from denaturant to buffer are also seen in k_R, confirming the conclusions drawn in the previous section that the increase in rates is due to chain compaction rather than faster chain dynamics. In the next section, these experimental values for k_R will be used to estimate the increase in the end-to-end distance of CGRP in buffer and denaturant (Table 4.2). To further explore and quantify the types of attractive interactions on the structure of CGRP, measurements of CGRP in different pH, salt and denaturant conditions must be performed. In Chapter Five, I will present the results of these measurements.

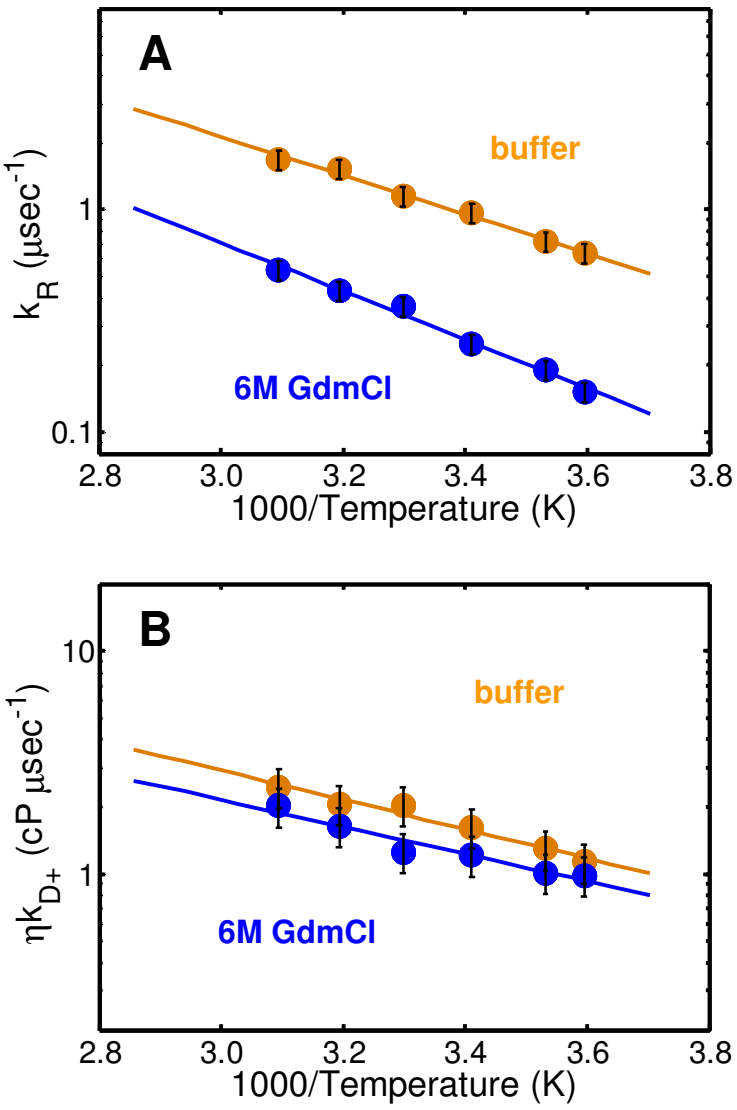

Figure 4.3. Arrhenius plots of the reaction limited (A) and diffusion limited (B) rates of CGRP. CGRP was measured in 50mM NaAc pH 4.9 buffer (orange) and denaturant (6M GdmCl- blue).

4.3.3. COMPARISON OF CGRP WITH IAPP

The reaction limited rate of CGRP in both buffer and denaturant were then compared to analogous experimental data of IAPP from Vaiana et al, 2009, in the same solution conditions.[11] The rates of CGRP compared IAPP at 20C in both buffer and denaturant are presented in Table 4.1. In both buffer and denaturant, CGRP has smaller values of k_R corresponding to a more expanded chain than IAPP.

Peptide	Solvent	k_{obs} (μs^{-1})	k_R (μs^{-1})
CGRP	Buffer	0.57 ± 0.06	0.93 ± 0.09
	6M GdmCl	0.19 ± 0.02	0.25 ± 0.03
hIAPP	Buffer	0.92 ± 0.09	1.3 ± 0.12
	6M GdmCl	0.22 ± 0.02	0.32 ± 0.03

Table 4.1. k_{obs} and k_R for CGRP and IAPP in buffer and denaturant at 20C.

The data are also presented in an Arrhenius plot of the temperature dependence of the reaction limited rates (Figure 4.4). As evident in Figure 4.4 and easily observed in Table 4.1, while CGRP populates compact states in aqueous solvent (a three fold increase in k_R compared to the expected 1.8 fold increase in k_R for an ideal chain),[18] CGRP still has a smaller increase in k_R than observed in IAPP (which has a five fold increase in k_R when going from denaturant to buffer).

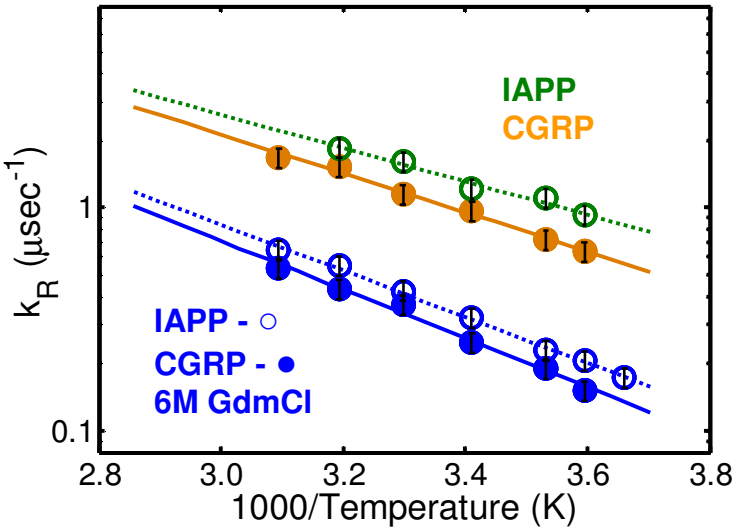

Figure 4.4. Arrhenius plot of the reaction limited rates of CGRP and IAPP. Both peptides are in both 50mM NaAc pH 4.9 buffer or denaturant (6M GdmCl)- CGRP in 6M GdmCl (closed blue circles), IAPP in 6M Gdmcl (open blue circles), and CGRP in buffer (closed orange circles,) and IAPP (open green circles).

Using the measured values of k_R for CGRP (and those previously measured for IAPP) we can estimate the relative end-to-end distances, for example in the simple case of a Gaussian P(r) distribution. In this way we can quantify how much more compact CGRP is in aqueous solvent than in denaturant.

$$P(r) = 4\pi r^2 \left(\frac{1}{\frac{2}{3}\pi \langle R^2 \rangle} \right)^{3/2} \exp\left(-\frac{3r^2}{2\langle R^2 \rangle} \right) \qquad \text{Eq 1}$$

The Gaussian model does not take into account excluded volume interactions, but has been found to be a good first approximation in disordered proteins. Analyzing the reaction limited rates found for CGRP in buffer and denaturant using a Gaussian model give the average end to end distances found in Table 4.2.

Peptide	Solvent	$\sqrt{\langle r^2 \rangle}$ (nm)
CGRP	Buffer	2.39
	6M GdmCl	3.72
IAPP	Buffer	2.14
	6M GdmCl	3.43

Table 4.2 End-to-end distances of CGRP and IAPP in buffer and denaturant

We see that the end-to-end distance of CGRP increases from 2.4 nm to 3.7 nm in buffer and denaturant, respectively. In Figure 4.5, comparison of the equilibrium end-to end-distance calculated using the previously published reaction limited rates for IAPP[11] show that while in denaturant CGRP has a similar $\sqrt{<r^2>}$ to IAPP, CGRP is more expanded than IAPP in buffer (2.4 vs 2.1 nm), supporting the conclusion that in buffer, IAPP has larger attractive intra-chain interactions than CGRP.

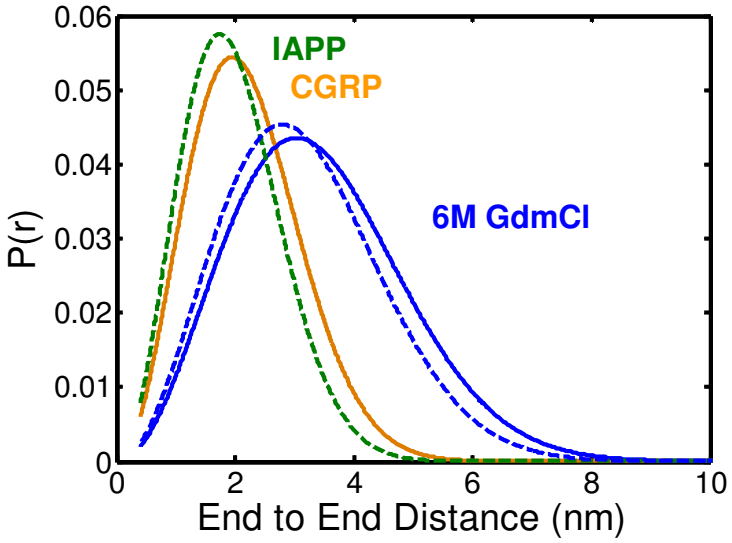

Figure 4.5. The equilibrium end-to-end distance distribution of CGRP (orange- buffer, solid blue line- 6M GdmCl) and IAPP (green dashed line- buffer, blue dashed line- 6M GdmCl) assuming a Gaussian P(r).

To further understand the structural differences between CGRP and IAPP, the CD spectrum of CGRP was measured and compared to that of IAPP. Circular dichroism measurements on both CGRP and rat IAPP (rIAPP) in aqueous solvent (50mM NaAc pH 4.9) show that CGRP adopts more alpha helix than rIAPP which is primarily random coil (Figure 4.6). CD measurements were done on rIAPP because human IAPP aggregates readily, and previous studies have shown little difference in secondary structure between human IAPP (hIAPP) and rIAPP.[19]

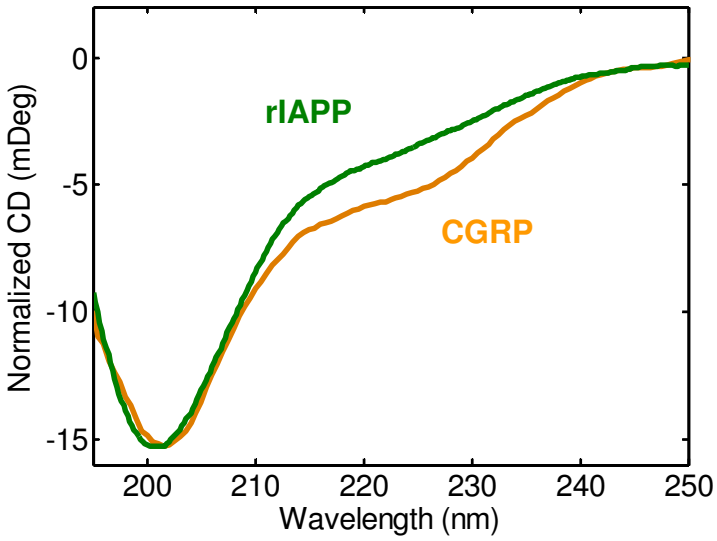

Figure 4.6. CD spectra of comparing CGRP and rIAPP. The CD spectra of CGRP (orange) has a larger shoulder at 220 nm than rIAPP (green).

Figure 4.6 supports previous CD studies that found that CGRP has about 20% alpha helix.[13,16,20] The peptide with greater apparent helical content (CGRP) therefore has a larger end-to-end distance than the peptide with a higher percentage of random coil (IAPP); this might suggest that the greater alpha helical content might lead to a stiffer chain. We note however that Marsh and Forman-Kay showed that the amount of compaction in disordered peptides does not correlate with secondary structure content and is primarily due to electrostatics and hydrophobic effects.[21]

4.4 N_LOOP CONTRIBUTES TO COLLAPSE IN CGRP

To explore why CGRP populates collapsed states in buffer, a closer look at the sequence of CGRP was required. The most significant structural feature of CGRP is the disulfide

bond forming a loop between the cysteine residues at 2 and 7 (N_loop). Vaiana, et al found that by attaching the disulfide loop, residues 1-8 of IAPP, which differs from CGRP's by only three residues (Figure 2.2), to a model peptide with no hydrophobic or charged residues $CC(AGQ)_9W$, the reaction limited rates increased seven fold from denaturant to buffer.[11] A seven fold increase in the reaction limited rate means that there is a large collapse in buffer, which was surprising as the same sequence without the loop only had a roughly 1.8 fold increase in rates when going from denaturant to buffer (as expected from polymer models of peptides of the same length).[18] As this model peptide does not have any obvious hydrophobic or attractive intra-chain interactions, this collapse must be due to interactions between the N_loop and the disordered chain. Since this collapse is present in both the model peptide and in IAPP, which have significantly different sequences, these interactions must be between the side chains and backbone of the N_loop and the backbone atoms of the disordered chain. Molecular dynamics simulations showed that residues 3 and 4 of the N_loop are especially favorable to forming side chain and backbone interactions with the backbone of the rest of the chain, especially with amino acids near the N_loop, with these interactions effectively decreasing the chain length and therefore increasing the rate that the two ends come into contact.[11] Cope, et al found that the N_loop by itself strongly self associates,[12] supporting the argument that the rigid structure of the N_loop in Ct family peptides reduces the entropy cost for the formation of intrachain hydrogen bonds.

To test whether a similar mechanism was at play in CGRP, the quenching rate of linear analogs of CGRP were measured. A twofold excess of TCEP was added to the intact

form of CGRP in both aqueous solvent and denaturant, breaking the disulfide bond by oxidative reduction. In addition, TTQ experiments were performed on two mutants where a serine residue was substituted for each of the cysteine residues, so that the cysteine quencher is in position 2 in one peptide (CGRP C7S), and position 7 in the other (CGRP C2S). In both of these experiments, the observed quenching rate increased only by a factor of two when going from denaturant to aqueous solvent; the results are discussed in more detail below.

In TCEP at 5C, CGRP's observed quenching rate increases two fold when going from denaturant to aqueous solvent, which is smaller than the three fold increase observed for wild type CGRP with the intact N_loop (Table 4.3). We note that TTQ measurements on CGRP reduced by TCEP in buffer and denaturant have significantly larger observed rates than CGRP with the intact N_loop due to the fact that two quenchers are now present (the cysteines at position 2 and 7). This makes quantitative analysis more complicated than in the case of a single quencher.

Peptide	Solvent	k_{obs} (μs^{-1})	$\frac{k_{obs}\text{ (buffer)}}{k_{obs}\text{ (GdmCl)}}$
CGRP	Buffer	0.34 ± 0.03	3.1
	6M GdmCl	0.11 ± 0.01	
CGRP w/ TCEP	Buffer	0.42 ± 0.04	2.1
	6M GdmCl	0.20 ± 0.02	

Table 4.3. Observed quenching rate of CGRP with and without TCEP at 5C. The ratio of k_{obs} in buffer versus denaturant is related to the compaction of CGRP in buffer.

To avoid the complications due to the presence of two quenchers, the cysteine at position 2 or the one at position 7 was replaced with a serine to produce CGRP C2S and CGRP C7S respectively. With this mutation, the linear analog of CGRP now has one quencher provided by a substitution that is not expected to change its conformation. The location of the quencher along the peptide chain is also not expected to significantly alter the quenching efficiency or prohibit comparison of k_{obs} between CGRP variants.[18] For completeness however, experiments were performed with both of these mutations in both denaturant and buffer to compare to CGRP wild type, to eliminate the effects that the type and position of the quencher might have on the observed quenching rates.

Peptide	Solvent	k_{obs} (μs^{-1})	$\frac{k_{obs}\text{ (buffer)}}{k_{obs}\text{ (GdmCl)}}$
CGRP	Buffer	0.59 ± 0.06	3.1
	6M GdmCl	0.19 ± 0.02	
CGRP C7S	Buffer	0.43 ± 0.04	2.1
	6M GdmCl	0.21 ± 0.02	
CGRP C2S	Buffer	0.48 ± 0.05	2.2
	6M GdmCl	0.22 ± 0.02	

Table 4.4 k_{obs} of CGRP wt, C7S, C2S at 20C in buffer and denaturant

Experimental measurements of the observed quenching rates of the linear analogs of CGRP, CGRP C2S and C7S at 20C, in both buffer and denaturant are shown in Table 4.4. The observed quenching rates of C7S and C2S in denaturant are similar to CGRP wild

type, however the linear analogs of CGRP show only a twofold increase in rates when going from denaturant to buffer, compared to the threefold increase in rates found in CGRP wild type.

Our data therefore suggests that a mechanism similar to the one proposed for IAPP might contribute to the collapse of CGRP in buffer. The N_loop has also been shown to stabilize the alpha helical content, with a linear analog, $CGRP_{8-37}$ with vastly decreased secondary structure.[14,15] Both these mechanisms could be important for the binding of CGRP to its receptor, since in addition to increasing binding affinity, the intact N_loop is required in order to activate cell response.[8-10]

We note that the difference in the observed quenching rates for these linear analogs of CGRP are similar to the 1.8-fold increase in rates between denaturant and buffer observed by Buscaglia, et al 2006, for the model peptide $C(AGQ)_9W$, which was shown behave like a worm-like chain good solvent (denaturant) versus bad solvent (water).[18] This is very close to our observed factor of 2.1-2.2 for the linear analogs of CGRP suggesting that in the absence of the N_loop , the peptide behaves similarly to the model peptide $C(AGQ)_9W$ and that the presence of the disulfide bond in N_loop is responsible for most of the increase in rates.

4.5. DISCUSSION

Our findings show that CGRP adopts more compact states in buffer than in denaturant, with k_R increasing threefold in buffer compared to denaturant instead of the expected two fold increase for a polymer of the same length. As k_R depends on the equilibrium end-to-end distance, CGRP is significantly more compact than expected in buffer which is likely due to attractive non-local intra-chain interactions present in CGRP. CGRP also does not become as compact as a similar peptide IAPP, despite sharing 47% sequence homology. CD measurements also show that CGRP has more secondary structure in aqueous solvent than IAPP. It was also shown that the disulfide loop (N_loop: residues 1-8) found at the N-terminus of CGRP accounts for some of this collapse, possibly through the formation of interactions with the rest of the peptide chain, similar to the mechanism seen in IAPP.[11]

The observed differences between the structure of CGRP and IAPP must be due to differences in the sequence. CGRP shares a 47% sequence homology with IAPP, however IAPP aggregates into amyloid fibrils while CGRP is otherwise soluble.[4-6] A glance at the sequence composition of CGRP and IAPP in Figure 4.7 does not reveal significant differences in the average side-chain excluded volume, but CGRP does have a higher average side-chain hydrophobicity despite being more expanded than IAPP. However, CGRP does have a higher net charge with charges distributed relatively equally along the chain compared to IAPP, which has a smaller net charge with charges clustered around the N-terminal region (as evidenced in the Uversky plot in Figure 2.4).

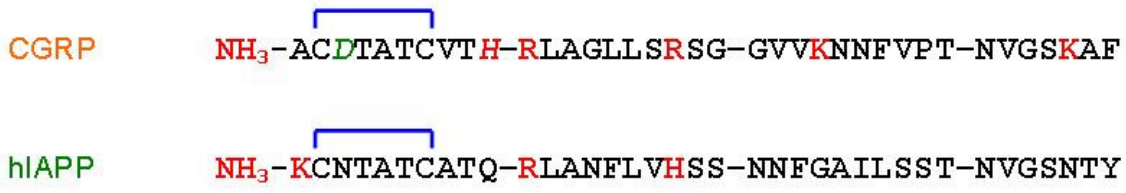

Figure 4.7. Sequence and charge composition of Ct family peptides. The positively charged amino acids at pH 4.9 are indicated with red letters, while the negatively charged amino acids are indicated with green letters. Both CGRP and IAPP have a disulfide bond between residues 2 and 7, and both have an amidated C-terminus.

Therefore it is possible that electrostatic interactions, rather than hydrophobic interactions, could account for the observed differences between CGRP and IAPP. The effect of electrostatic interactions on the structure and dynamics of CGRP as well as a closer comparison between CGRP and IAPP's structure and dynamics will be explored in Chapters Five and Six, respectively.

REFERENCES

[1]Van Rossum, D., Hanisch, U. K., & Quirion, R. (1997). Neuroanatomical localization, pharmacological characterization and functions of CGRP, related peptides and their receptors. *Neuroscience & Biobehavioral Reviews*, *21*(5), 649-678.

[2]Moore, E. L., & Salvatore, C. A. (2012). Targeting a family B GPCR/RAMP receptor complex: CGRP receptor antagonists and migraine. *British journal of pharmacology*, *166*(1), 66-78.

[3]Galeazza, M. T., O'Brien, T. D., Johnson, K. H., & Seybold, V. S. (1991). Islet amyloid polypeptide (IAPP) competes for two binding sites of CGRP. *Peptides*, *12*(3), 585-591.

[4]Westermark, P., Wernstedt, C., Wilander, E., & Sletten, K. (1986). A novel peptide in the calcitonin gene related peptide family as an amyloid fibril protein in the endocrine pancreas. *Biochemical and biophysical research communications*, *140*(3), 827-831.

[5]Cooper, G. J., Willis, A. C., Clark, A., Turner, R. C., Sim, R. B., & Reid, K. B. (1987). Purification and characterization of a peptide from amyloid-rich pancreases of type 2 diabetic patients. *Proceedings of the National Academy of Sciences*, *84*(23), 8628-8632.

[6]Wimalawansa, S. J. (1997). Amylin, calcitonin gene-related peptide, calcitonin, and adrenomedullin: a peptide superfamily. *Critical Reviews™ in Neurobiology*, *11*(2-3).

[7]Brain, S. D., & Grant, A. D. (2004). Vascular actions of calcitonin gene-related peptide and adrenomedullin. *Physiological Reviews*, *84*(3), 903-934.

[8]Dennis, T., Fournier, A., St Pierre, S., & Quirion, R. (1989). Structure-activity profile of calcitonin gene-related peptide in peripheral and brain tissues. Evidence for receptor multiplicity. *Journal of Pharmacology and Experimental Therapeutics*, *251*(2), 718-725.

[9]Tippins, J. R., Di Marzo, V., Panico, M., Morris, H. R., & MacIntyre, I. (1986). Investigation of the structure/activity relationship of human calcitonin gene-related peptide (CGRP). *Biochemical and biophysical research communications*, *134*(3), 1306-1311.

[10]Saha, S., Waugh, D. J. J., Zhao, P., Abel, P. W., & Smith, D. D. (1998). Role of conformational constraints of position 7 of the disulphide bridge of h-α-CGRP derivatives in their agonist versus antagonist properties. *The journal of peptide research*, *52*(2), 112-120.

[11]Vaiana, S. M., Best, R. B., Yau, W. M., Eaton, W. A., & Hofrichter, J. (2009). Evidence for a partially structured state of the amylin monomer. *Biophysical journal*, *97*(11), 2948-2957.

[12]Cope, S. M., Shinde, S., Best, R. B., Ghirlanda, G., & Vaiana, S. M. (2013). Cyclic N-Terminal Loop of Amylin Forms Non Amyloid Fibers. *Biophysical journal*, *105*(7), 1661-1669.

[13]Hubbard, J. A., Martin, S. R., Chaplin, L. C., Bose, C., Kelly, S. M., & Price, N. C. (1991). Solution structures of calcitonin-gene-related-peptide analogues of calcitonin-gene-related peptide and amylin. *Biochem. J*, *275*, 785-788.

[14]Mimeault, M., St-Pierre, S., & Fournier, A. (1993). Conformational characterization by circular dichroism spectroscopy of various fragments and analogs of calcitonin gene−related peptide. *European Journal of Biochemistry*, *213*(3), 927-934.

[15]Boulanger, Y., Khiat, A., Chen, Y., Senecal, L., Tu, Y., St-Pierre, S., & Fournier, A. (1994). Structure of human calcitonin gene-related peptide (hCGRP) and of its antagonist hCGRP 8-37 as determined by NMR and molecular modeling. *Peptide research*, *8*(4), 206-213.

[16]Manning, M. C. (1989). Conformation of the alpha form of human calcitonin gene-related peptide (CGRP) in aqueous solution as determined by circular dichroism spectroscopy. *Biochemical and biophysical research communications*, *160*(1), 388-392.

[17]O'Connell, J. P., Kelly, S. M., Raleigh, D. P., Hubbard, J. A., Price, N. C., Dobson, C. M., & Smith, B. J. (1993). On the role of the C-terminus of alpha-calcitonin-gene-related peptide (alpha CGRP). The structure of des-phenylalaninamide37-alpha CGRP and its interaction with the CGRP receptor. *Biochem. J*, *291*, 205-210.

[18]Buscaglia, M., Lapidus, L. J., Eaton, W. A., & Hofrichter, J. (2006). Effects of denaturants on the dynamics of loop formation in polypeptides. *Biophysical journal*, *91*(1), 276-288.

[19]Andrews, M. N., & Winter, R. (2011). Comparing the structural properties of human and rat islet amyloid polypeptide by MD computer simulations. *Biophysical chemistry*, *156*(1), 43-50.

[20]Breeze, A. L., Harvey, T. S., Bazzo, R., & Campbell, I. D. (1991). Solution structure of human calcitonin gene-related peptide by proton NMR and distance geometry with restrained molecular dynamics. *Biochemistry*, *30*(2), 575-582.

[21]Marsh, J. A., & Forman-Kay, J. D. (2010). Sequence determinants of compaction in intrinsically disordered proteins. *Biophysical journal*, *98*(10), 2383-2390.

CHAPTER 5

EFFECTS OF CHARGE INTERACTIONS, SALT SCREENING, AND DENATURANT EXPANSION ON THE STRUCTURE OF CGRP

5.1. INTRODUCTION

The results in the previous chapter showed that CGRP adopts compact states in aqueous solvent compared to denaturant, with the disulfide loop at the N-terminus of CGRP potentially causing some of this collapse through the formation of attractive intra-chain interactions, as previously seen in IAPP.[1] In this chapter, we study the effects of electrostatic interactions, salt screening, and denaturant expansion on the structure of CGRP and rationalize them in terms of sequence specific effects and potential mechanisms for biological activation.

Due to the fact that electrostatic interactions are the strongest kinds of interactions that occur at long distances, electrostatic interactions have long been known to greatly affect protein structure in folded proteins as well as the binding of proteins to their receptors.[2-4] It is also well known that electrostatic interactions influence aggregation rates;[5,6] for example, a study found that the lag time of IAPP (or the time it takes for fibrilization to occur) decreased when IAPP is in strongly ionic solutions.[7] In addition, recent studies have shown that electrostatic interactions also appear to affect the structure of disordered proteins, despite the fact that they are not folded. Marsh and Forman-Kay's 2010 review of IDPs pointed out that electrostatics appears to be a primary determinant of chain

expansion of disordered proteins.[8] Other studies of IDPs show that both the secondary and tertiary structure content are highly sensitive to addition of counterions in solution.[3,7] This interplay between the protein and an ionic solvent has already been seen in the diffusive binding of two folded proteins, with the binding rate of the two proteins strongly correlating with the Debye length of the solution.[2] While the mechanism for how electrostatic interactions affect the aggregation propensity of IAPP is unknown, it is likely that charge screening allows other attractive intra-chain interactions that promote oliogmerization and fibrilization of IAPP.

Other studies on disordered and unfolded proteins showed that some proteins have a complicated interplay with the solvent, which is largely dependent on their net charge. In the case of the N-terminal domain of HIV-1 integrase, which folds only upon binding of Zn^{2+} ions but is otherwise disordered and human prothymosin α (ProTα), a highly charged IDP, GdmCl was shown to exhibit both a charge screening and denaturant expansion effect on disordered proteins, while non-ionic denaturants, such as Urea, show only denaturant expansion.[9,10] These proteins were found to compact due to charge screening at low GdmCl concentrations, with denaturant expansion effect taking over at higher concentrations. It was found that these proteins can be modeled as polyampholytes, where the proportion of charged residues as well as the net charge on the chain are important, with more collapsed structures in proteins with an even mix of positive and negative charges along the sequence.[11,12] However, other studies have pointed out the importance of charge patterning in polymer models, rather than just net charge.[12,13]

Whether simple polymer models are sufficient to describe the behavior of IDPs is still under debate and is something that needs to be quantitatively modeled for IDPs.

This chapter sets out to understand why CGRP, despite having a high sequence homology with IAPP with similar net charge and hydrophobicity, is less compact than IAPP in aqueous solvent. To do this, the effect of electrostatic and solvent interactions in CGRP is explored through specific site directed mutations and by changing the solution environment of CGRP through changing the solvent pH and the addition of counter-ions and denaturant. These studies are important because as I will more fully discuss at the end of this chapter, the release of CGRP is known to be triggered by tissue acidosis and the presence of excess ions in the extracellular region of cells. Possible changes in the structure or the dynamics of the unbound CGRP monomer due to variations in pH or salt concentration can affect the affinity and rate of binding of CGRP to its receptor, which is relevant to its biological function. As the results of this chapter show, CGRP is highly sensitive to the solution environment and that electrostatic interactions modulate the dimensions of CGRP.

5.2. EXPERIMENTAL METHODS

The experimental methods were previously described in Chapter Four, but with the following modifications:

MATERIALS

Peptide with >95% purity (CGRP wild-type and CGRP D3N mutants, both with the F37W mutation) were purchased from Genscript or synthesized as described previously. All peptide used in these experiments were stored in the lyophilized state at -20C before use.

TRYPTOPHAN TRIPLET QUENCHING MEASUREMENTS

Samples were prepared for TTQ and data were analyzed as described previously. For pH 3 and pH 4.9 experiments, 50mM sodium acetate buffer was used, and pH 7 and 8 experiments were in 20mM sodium phosphate buffer. To explore the solvent effects on CGRP through the addition of solutes, sucrose (as measured by percent weight by volume), potassium chloride (KCl), GdmCl and Urea (as measured by calculated molar concentration) were added to the buffer and the final solution pH was adjusted using either 1M NaOH or 1M HCl as needed.

CIRCULAR DICHROISM MEASUREMENTS

To measure the CD spectra of CGRP, samples were prepared and measured as before, with a few differences in the sample preparation when titrating the solvent. For CD measurements that titrate the solvent, two stock samples of ~30 uM peptide were prepared as for TTQ measurements, but at both the high and low solvent concentrations for use as stock solutions. The stock solutions were combined at the proper ratio to get 200uL of sample at each solvent concentration desired, in order to fully titrate the CD spectra of the peptide with respect to the solvent.

5.3. COMPACTION OF CGRP DEPENDS ON NET CHARGE

5.3.1. CGRP EXPANDS AS NET CHARGE INCREASES

To explore the effect of electrostatic interactions on the structure of CGRP, the net charge on CGRP was changed by adjusting the solvent pH. A look at Figure 2.2 shows that CGRP has two charged residues that can easily be titrated: the aspartic acid at C3 and the histidine at C11. By measuring the quenching rate of CGRP at pH 3, pH 4.9 and pH 8, we effectively change the net charge on CGRP from +6 to +4 and in this way explore the effect of electrostatic interactions on the structure of CGRP.

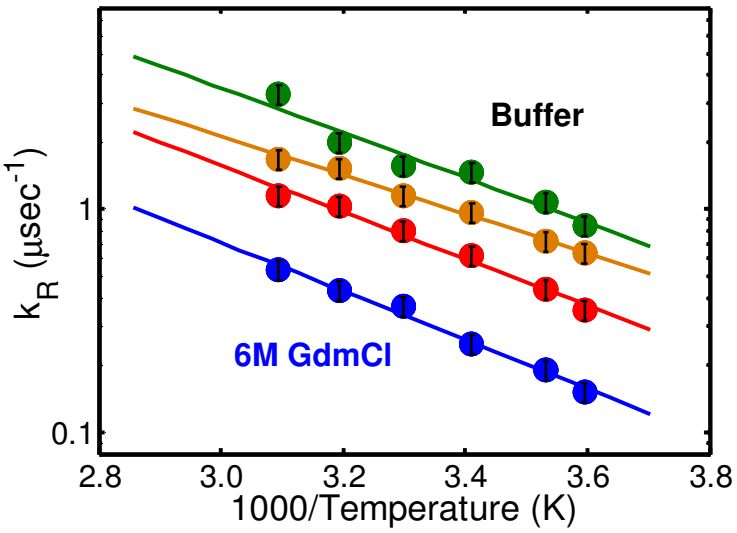

Figure 5.1. The pH dependence of the reaction limited rates of CGRP at pH 8 (green), pH 4.9 (orange), pH 3 (red) and 6M GdmCl (blue).

Arrhenius plots of CGRP at +4 (pH 3), +5 (pH 4.9) and +6 (pH 8) net charge are presented in Figure 5.1. Here k_R decreases when the net charge increases, with CGRP at a net charge of +4 populating states with shorter end-to-end distances than with a net charge of +6. Table 5.1 shows the pH dependence on the end-to-end distance of CGRP at 20C assuming a Gaussian chain, where the end to end distance increases from a compact 2.10 nm to 2.80 nm in buffer due to changes in the net charge of CGRP. Interestingly, even at a +6 net charge, CGRP is still more compact than in GdmCl where it has an end-to-end distance of 2.80 nm versus 3.72 nm in 6M GdmCl, suggesting even with repulsive electrostatic interactions, there are still other attractive interactions present in CGRP in buffer.

Solvent	$\sqrt{\langle r^2 \rangle}$ (nm)
pH 3	2.80
pH 4.9	2.39
pH 8	2.10
6M GdmCl	3.72

Table 5.1. pH dependence of end-to-end distances for CGRP at 20C.

Briefly, a few controls were done to verify that the change in k_R observed when changing the solvent pH is due to a change in P(r), and that this change is due to the change in overall net charge. Since k_R also depends on the quenching rate q(r), the bimolecular

quenching rates were measured in each solvent condition. These results are not shown in this work, but it was found that the solvent pH has very little effect on the quenching rate q(r) and do not follow the trend seen in CGRP. In addition, control experiments of CGRP with a D3N mutation (chosen because the asparagine at C3 is present in both IAPP and βCGRP)[14] were performed to check that the change in k_R is due to a change in overall net charge and not due to other possible direct pH effects (Figure 5.2). As these figures show, the values for k_R are indistinguishable for CGRP wild-type and CGRP D3N when they have the same net charge.

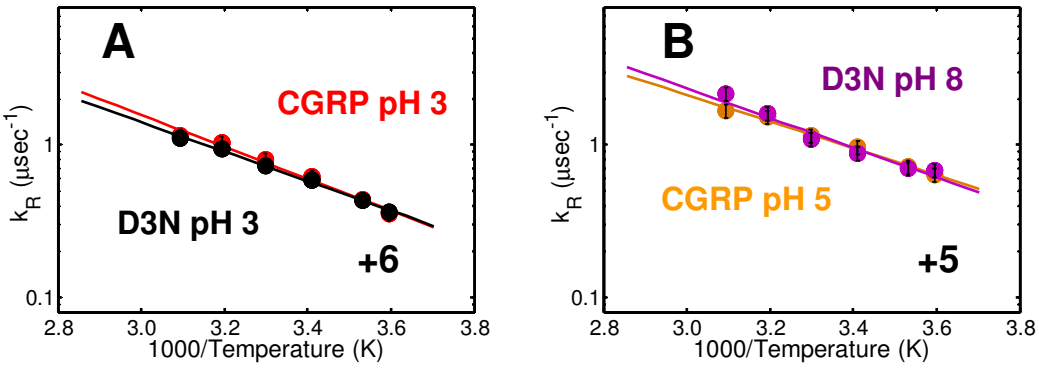

Figure 5.2. Reaction limited rates of CGRP and CGRP D3N with same net charge. In (A), CGRP pH 3 (red) has the same net charge (+6) and reaction limited rate of CGRP D3N at pH 3 (black), similarly in (B), CGRP pH 5 (orange) has the same net charge (+5) and reaction limited rate as CGRP D3N pH 8 (maroon).

Estimates of the end-to-end distance of CGRP, from the measured values of k_R and assuming a simple Gaussian P(r), are shown in Figure 5.3 as a function of pH. As shown in the figure, the end-to-end distance increases from 2.10 nm to 2.80 nm when the net charge increases from roughly +4 to +6.

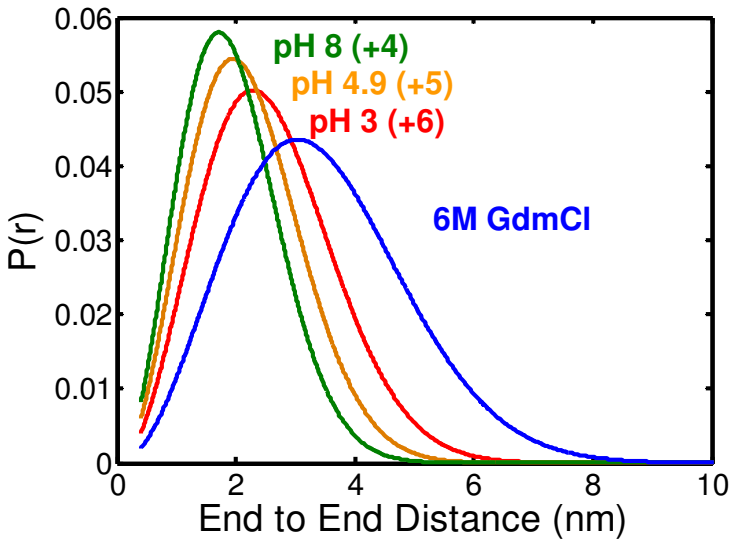

Figure 5.3. pH dependence of the equilibrium end-to-end distance distribution of CGRP at pH 8 (green), pH 4.9 (orange), pH 3 (red) and 6M GdmCl (blue).

To determine whether these short end-to-end distances at low net charge are due to changes in the local secondary structure of CGRP or due to changes that affect the long range, non-local interactions present in CGRP, CD measurements were done for CGRP wild-type at pH 7 (+4 net charge) and compared to those at pH 3 (+6 net charge). For practical reasons, the D3N mutant was used for the latter although comparison with wild-type showed no change (not shown).

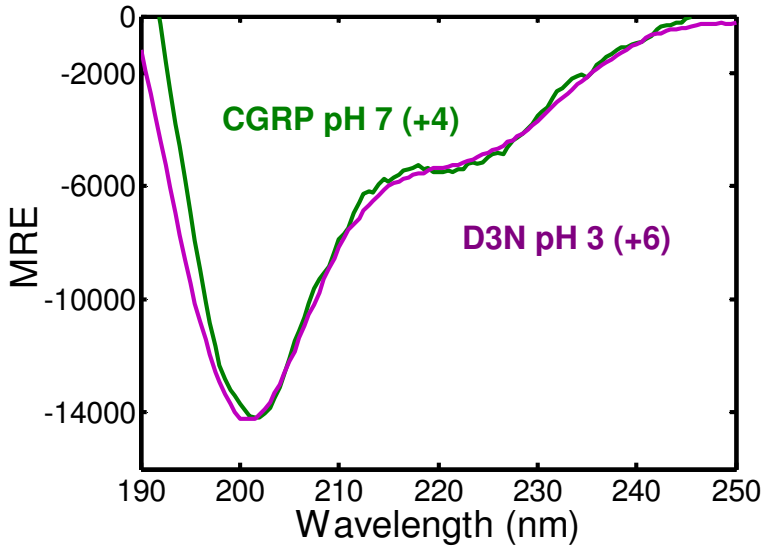

Figure 5.4. CD spectra of the pH dependence of CGRP. The CD spectra of CGRP pH 7 (green) overlaps with CGRP D3N pH 3 (maroon), despite having different end-to-end distances.

Figure 5.4 shows that the secondary structure of CGRP does not change when the net charge changes. This is consistent with previous CD measurements which found that CGRP exhibits no pH dependence in the far UV, which reports on secondary structure, but observed a small change in the near UV, which was attributed to increased solvent exposure of the cystine as the histidine was titrated.[15] This agrees with our experimental evidence that CGRP populates larger end-to-end distances as the net charge increases, and that this expansion is due to non-local contact formation rather than to changes in secondary structure.

5.3.2. COMPACTION DUE TO CHARGE SCREENING SCALES WITH DEBYE LENGTH

In order to quantify the effect of electrostatic interactions on the end-to-end distance of CGRP and check whether the results in the previous section are due to changes in the net charge or specific electrostatic interactions with the histidine and aspartic acid, salt was added to the buffer to uniformly screen all six charges on the amino acid side chains. For these measurements, TTQ experiments were done in increasing salt (KCl) concentrations on the CGRP peptide with the highest net charge: CGRP D3N in pH 3 buffer (+6 net charge). The amount of salt screening can be related to the Debye length κ^{-1}, which depends on the ionic strength of the solution *I*, as shown in Eq 1 below.

$$\kappa^{-1} = \sqrt{\frac{\varepsilon_r \varepsilon_0 k_B T}{2 N_A e^2 I}} \qquad \text{Eq 1}$$

As salt is added and the ionic strength of the solution increases, the Debye length becomes shorter meaning that charges are more effectively screened. By measuring CGRP by TTQ as a function salt concentration we monitor how salt screening changes the observed rate of quenching.

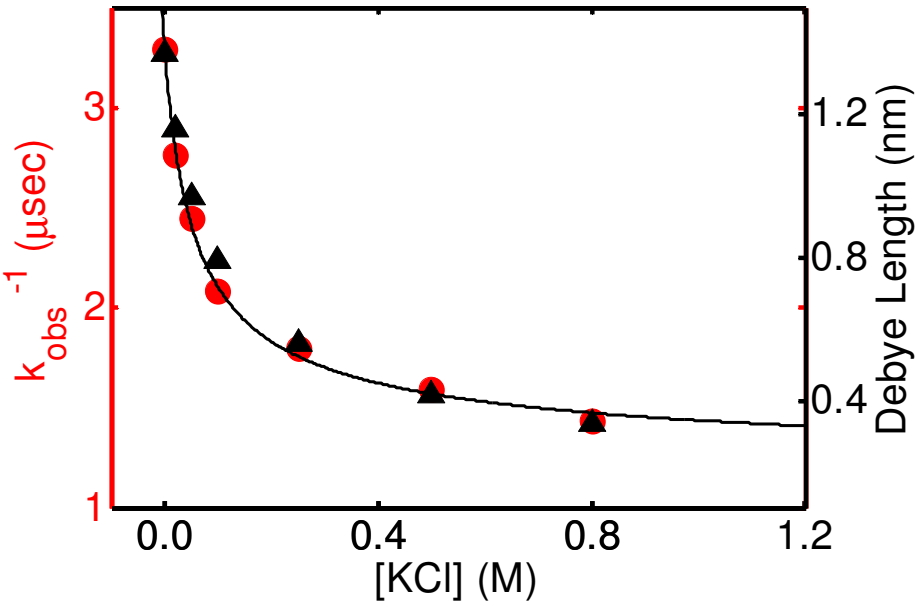

Figure 5.5. Plot of the inverse of the observed rate of CGRP D3N at pH 3 (red circles) as a function of KCl concentration, overlaid upon a plot of the Debye length of the solvent (black trianges) as a function of KCl concentration.

Our results showed that as the concentration of KCl increases, k_{obs} becomes larger indicating as the charges on the chain are screened CGRP becomes more compact. In fact, a plot of $1/k_{obs}$ as a function of KCl concentration overlaid on a plot of the Debye length of the solvent as a function of KCl concentration shows a clear correlation between the two variables (Figure 5.5).

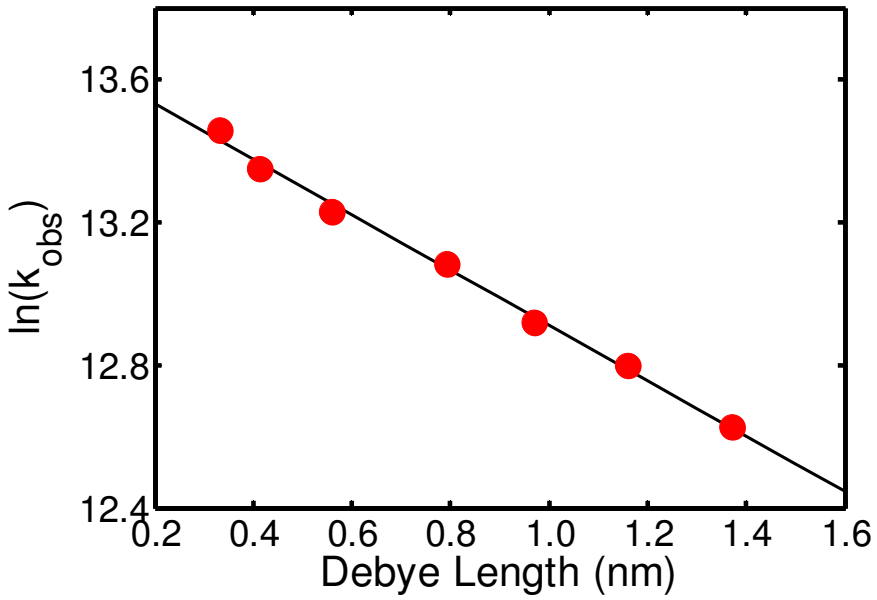

Figure 5.6. Plot of the log of the observed quenching rate of CGRP D3N (red circles) as a function of the Debye length of the solvent. The data was fit to a linear fit line (black line), from which the electrostatic contribution to the free energy difference between the open and closed states of CGRP was calculated.

Interestingly, further analysis showed that the log of k_{obs} of CGRP is linearly proportional to the Debye length of the solvent, as in Figure 5.6. As the observed quenching rate k_{obs} is proportional to the equilibrium rate K_{eq} between the open and closed states of CGRP, the electrostatic contribution to the free energy cost of forming a contact ΔG_{OC}^* in CGRP is related to k_{obs} via Eq 2 below.

$$k_{obs} \propto K_{eq} = e^{-\Delta G_{OC}^* / RT} \qquad \text{Eq 2.}$$

More specifically, ΔG_{OC}^* is the free energy difference between the two sub-ensembles of the equilibrium ensemble where the two sub-ensembles are defined as the following: the

closed ensemble, where all configurations of the equilibrium ensemble where $\sqrt{<r^2>}$ is less than 0.4 nm, and the open ensemble, where all configurations of the equilibrium ensemble where $\sqrt{<r^2>}$ is greater than 0.4 nm. Since the log of k_{obs} depends linearly on κ^{-1}, we now have an expression relating ΔG_{OC}* to the Debye length:

$$\Delta G_{OC}^{*} / RT = A + B \cdot \kappa^{-1} \qquad \text{Eq 3}$$

where B = 13.68 is the slope and A = -0.773 nm^{-1} is the intercept in Figure 5.6 above.

5.3.3. SCREENING OF ELECTROSTATIC INTERACTIONS CAUSE COMPACTION IN CGRP

In the previous section, a change in k_{obs} when adding salt was attributed to compaction of CGRP. However to determine whether the increase in the observed quenching rate with the addition of salt to the buffer is due to chain compaction or faster intra-chain diffusion, viscosity dependent measurements were done in 500mM KCl.

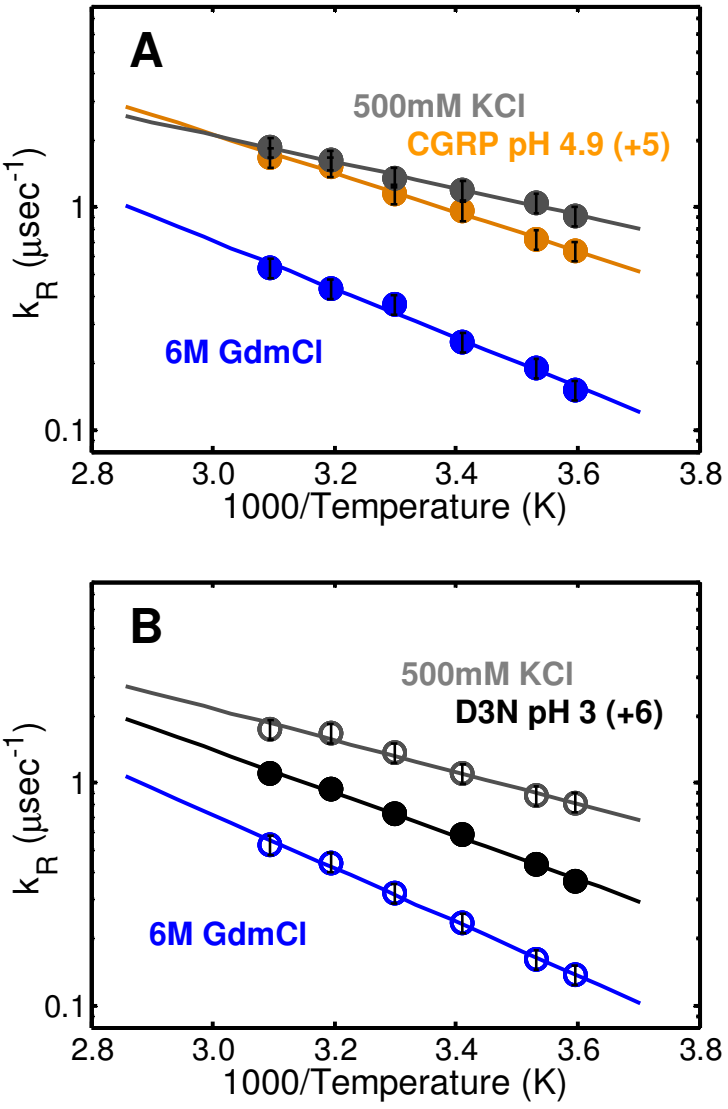

Figure 5.7. Reaction limited rates of (A) CGRP pH 4.9 in 6M GdmCl (closed blue circles), buffer (orange circles) and 500mM KCl (closed grey circles), and (B) CGRP D3N pH 3 in 6M GdmCl (open blue circles), buffer (black circles) and 500mM KCl (open grey circles).

Figure 5.7 shows k_R of CGRP wt and CGRP D3N in both buffer and 500mM KCl, which increase in 500mM KCl relative to buffer for both variants, with shorter end-to-end distances in salt consistent with screening of electrostatic interactions. A Gaussian P(r)

was used to model these changes in k_R and a significant decrease in the end-to-end distances from 2.39 nm to 2.19 nm for CGRP wt and 2.83 nm to 2.25 nm for CGRP D3N were seen when salt was added (Table 5.2)

Peptide	Solvent	$\sqrt{\langle r^2 \rangle}$ (nm)
CGRP	pH 4.9	2.39
	500mM KCl	2.19
CGRP D3N	pH 3	2.83
	500mM KCl	2.25

Table 5.2 End-to-end distances of CGRP and CGRP D3N in buffer and 500mM KCl

As a visualization of how much these end-to-end distances change in 500mM KCl relative to buffer, a plot of the Gaussian P(r) for CGRP D3N with and without 500mM KCl shows significant compaction of CGRP D3N in salt (Figure 5.8). From these viscosity dependent measurements, we know that the changes in the observed quenching rates measured in Figures 5.5 & 5.6 above are reflected by changes in the end-to-end distance of CGRP and are due to screening of electrostatic interactions in CGRP.

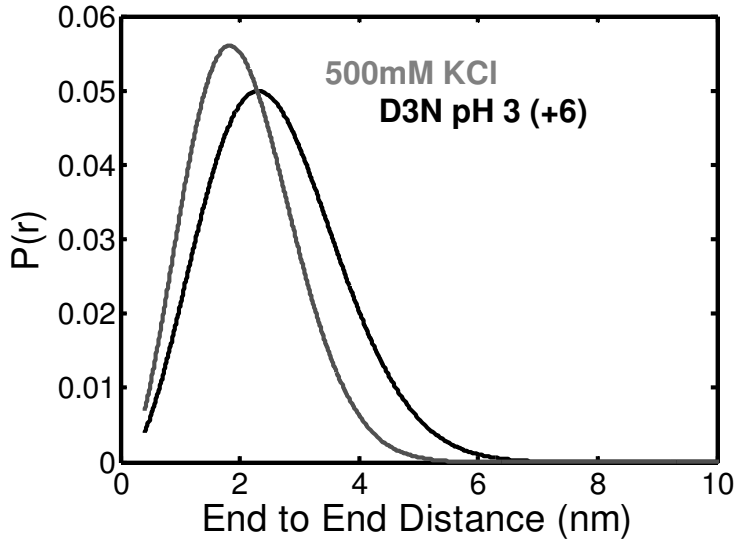

Figure 5.8. Equilibrium end-to-end distance distribution of CGRP D3N pH 3 in buffer (black) and 500mM KCl (grey) for a Gaussian chain.

5.3.4. A CLOSER COMPARISON BETWEEN CGRP AND IAPP, CONSIDERING THE EFFECT OF CHARGES

So far, this chapter has explored the effect of electrostatic interactions on the structure of CGRP with increasing net charge causing expansion of CGRP, while the previous chapter briefly discussed the differences in structure between CGRP and IAPP, where CGRP was more expanded than IAPP in the same solution conditions. Here, we compare CGRP and IAPP with the same net charge to see if electrostatic interactions account for the observed differences in end-to-end distance in Ct family peptides.

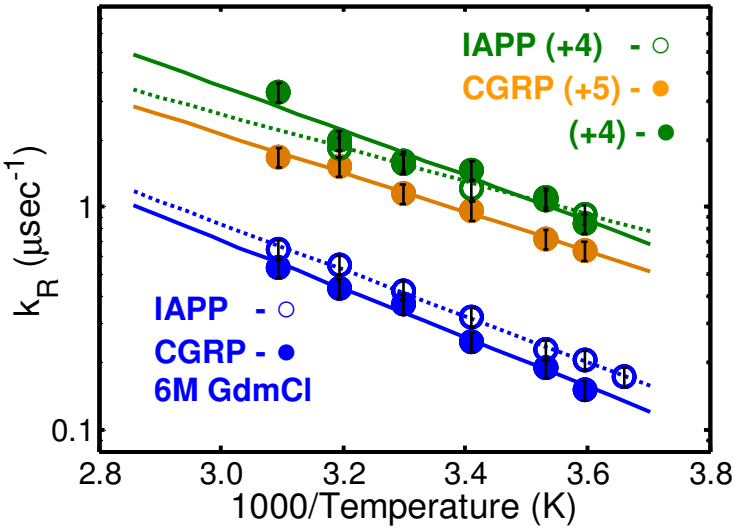

Figure 5.9. Reaction limited rates for CGRP in 6M GdmCl (closed blue circles), pH 4.9 buffer (orange circles) and pH 8 buffer (closed green circles), and IAPP in 6M GdmCl (open blue circles) and pH 4.9 buffer (open green circles).

As Figure 5.9 shows, when CGRP and IAPP have the same net charge of +4, their reaction limited rates become very similar with both populating very compact states. The Gaussian end-to-end distance distributions (Figure 5.10) show that CGRP and IAPP with the same net charge have virtually the same end-to-end distance of about 2.1 nm. This suggests that for these peptides, electrostatic interactions are the main contribution to the observed differences in end-to-end distance.

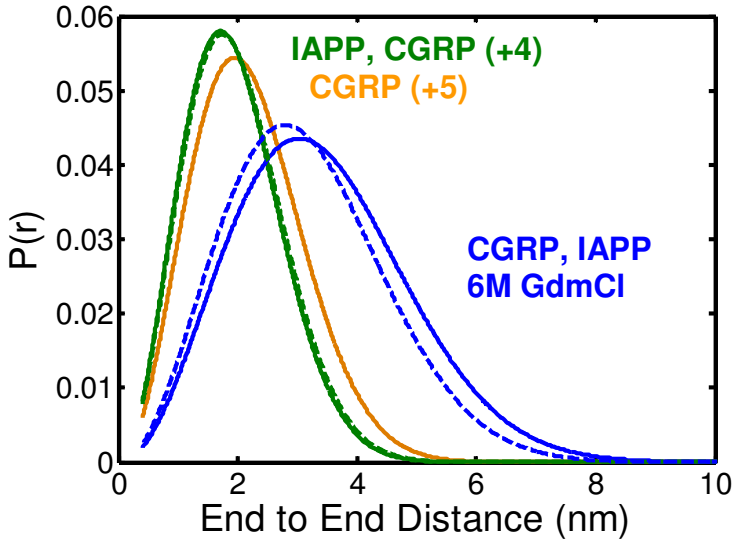

Figure 5.10. Equilibrium end-to-end distance distribution for CGRP in 6M GdmCl (solid blue line), pH 4.9 buffer (orange line) and pH 8 buffer (solid green line), and IAPP in 6M GdmCl (dashed blue line) and pH 4.9 buffer (dashed green line) for a Gaussian chain.

5.4. DENATURANT EXPANSION VERSUS CHARGE SCREENING IN CGRP

5.4.1. COLLAPSE DUE TO CHARGE SCREENING SEEN IN GDMCL BUT NOT UREA

So far we have seen that electrostatic interactions modulate the structure of CGRP, however as Figure 5.1 shows, CGRP with a high + 6 net charge still has a shorter end-to-end distance than in 6M GdmCl. The denaturant binding of GdmCl to CGRP must be stronger than other attractive intra-chain interactions present in CGRP with a +6 net charge. GdmCl and Urea were titrated to see how denaturant binding affects the end-to-end contact formation rates of CGRP.

First, we looked at CGRP and CGRP D3N in 6M GdmCl and 8M Urea to explore how the end-to-end distance changes when the peptide is fully denatured. As Figure 5.11 shows, 6M GdmCl and 8M Urea "fully" denatures CGRP, with very similar, but smaller k_R values in all experimental conditions. This makes sense, as in 6M GdmCl and 8M Urea the denaturant will have broken all attractive intra-chain interactions through preferential binding of the denaturant with the peptide.

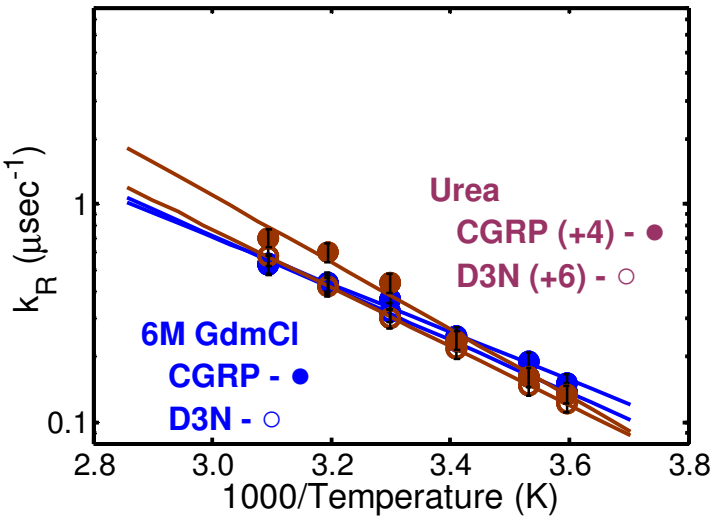

Figure 5.11. Reaction limited rates of CGRP variants in denaturant: CGRP wt in 6M GdmCl pH 4.9 (closed blue circles), CGRP wt in 8M Urea pH 8 (closed maroon circles), CGRP D3N in 6M GdmCl pH 3 (open blue circles), CGRP D3N in 8M Urea pH 3 (open maroon circles).

Next, the concentrations of GdmCl and Urea in the solution were titrated to explore the effect of increasing denaturant binding on the end-to-end distances of CGRP. In order to quantify the effect that changing the GdmCl and Urea concentrations have on the structure of CGRP, the radius of gyration was calculated from k_{obs} of quenching as described in Appendix III. The experimental results in Figure 5.12 below show how the radius of gyration of CGRP at 10C changes as a function of denaturant concentration.

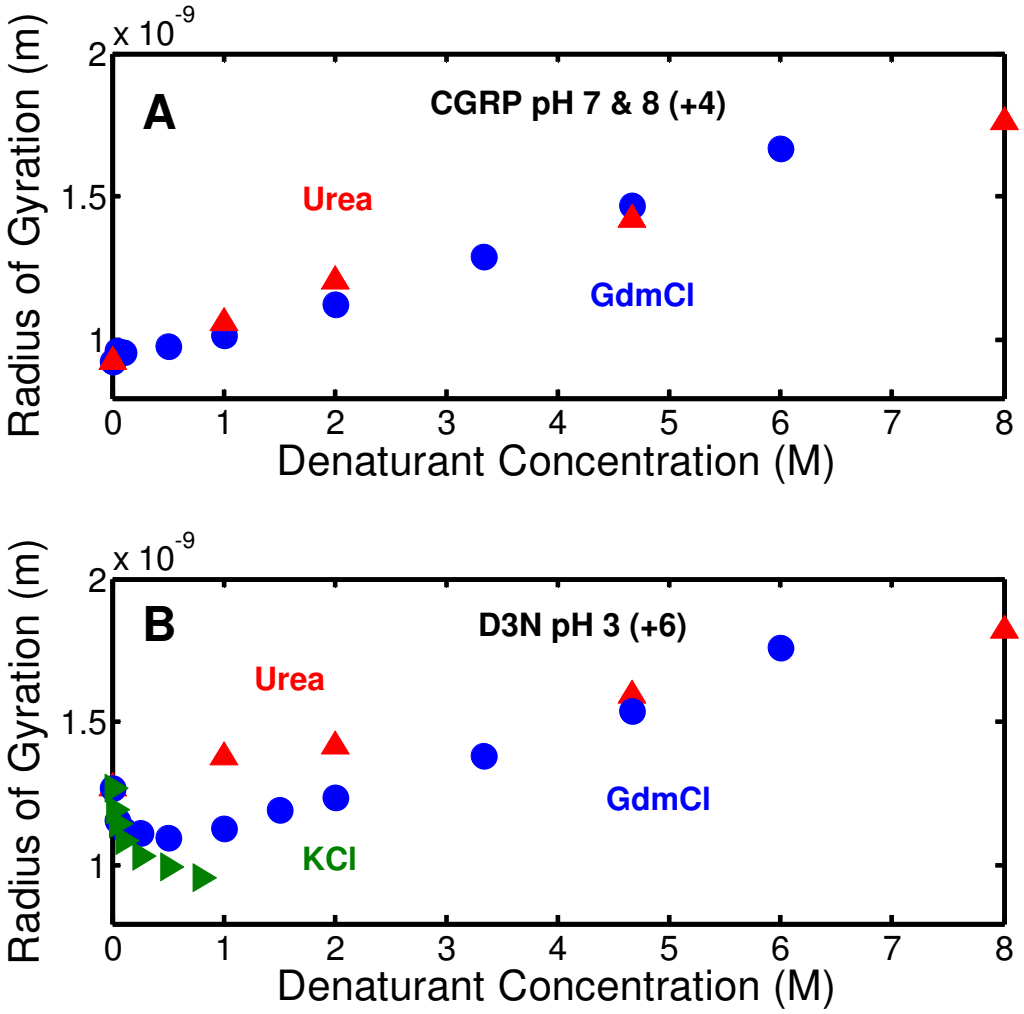

Figure 5.12. The radius of gyration of CGRP variants as a function of denaturant concentration. A. CGRP wild-type in GdmCl pH 7 (blue circles) and Urea pH 8 (red triangles), B. CGRP D3N pH 3 in GdmCl (blue circles), Urea (red triangles), and KCl (green arrows).

In all cases, the radius of gyration increases as the concentration of denaturant increases. However, while the radius of gyration of CGRP with a +4 net charge increases monotonically in GdmCl and Urea, the radius of gyration of CGRP D3N with a +6 net charge decreases at low GdmCl concentrations (but increases monotonically in Urea).

According to Figure 5.12, the turnover point at which the concentration of GdmCl where the denaturant binding effect starts to take over charge screening occurs at around 500mM GdmCl at 10C. It is surprising that such a relatively small change in net charge has a dramatic effect on the charge screening effect in GdmCl. To further explore this, we used polymer models to fit the data.

5.4.2. CHARGE POSITION NEEDS TO BE TAKEN INTO ACCOUNT

The discovery that a +2 difference in net charge is sufficient to change the behavior of CGRP in GdmCl was surprising as compared to other IDPs, CGRP has a low net charge per residue (Figure 2.4) and a +2 difference in net charge is relatively small. Previous studies noted that this compaction at low GdmCl concentrations only occurred in IDPs that were charge balanced[9] and a similar study on a unfolded protein where the net charge went from -4 to +10 by changing the solvent pH always collapsed at low GdmCl concentrations.[10] To understand why a +2 net charge difference in CGRP can change the way it behaves in denaturant, a collaboration was established with Andrea Soranno from the University of Zurich. A. Soranno first fit the experimental data on CGRP from Figure 5.12 to a polyampholyte model which has successfully been used to model the dimensions of the disordered proteins, prothymosin α and the N-terminal domain of HIV-1 integrase,[9,10,16] with CGRP having $N = 37$ monomers of length $b = 0.36$ nm. This model is based on the original model by Higgs and Joanny[16] with the electrostatic contribution to the radius of gyration is modeled using Eq 4.

$$R_g = \alpha \frac{N^{0.5} b}{6^{0.5}} \qquad \text{Eq 4}$$

$$\alpha^5 - \alpha^3 = \frac{4}{3}\left(\frac{3}{2\pi}\right)^{1.5} N^{0.5} \nu^* \qquad \text{Eq 5}$$

where the effective excluded volume $\nu^* b^3$ in Eq 5 has an electrostatic contribution $\nu_{el} b^3$ such that

$$\nu^* b^3 = \nu_0 b^3 + \nu_{el} b^3 \qquad \text{Eq 6}$$

The polyampholyte model is given by:

$$\nu_{el}^{PA} = \frac{4\pi l_b (f-g)^2}{\kappa(I)^2 b^3} - \frac{\pi l_b^2 (f+g)^2}{\kappa(I) b^3} \qquad \text{Eq 7}$$

where l_b is the Bjerrum length, I is the ionic strength of the solvent, and f and g are the positive and negative fractions of the chain, respectively.[16] In polyampholyte theory, the first term in Eq 7 is the contribution of electrostatic repulsion to the excluded volume, while the second term is the electrostatic attraction contribution to the excluded volume of the polymer chain. As CGRP is a relatively short protein and is a weak polyampholyte (and in the case of CGRP D3N, a polyelectrolyte only), this model overestimated the contribution of electrostatic interactions to the compaction of CGRP so, the data were

then fit with a polyelectrolyte model,[17] which eliminates the contribution of electrostatic attraction of oppositely charged amino acids.

$$v_{el}^{PE} = \frac{4\pi l_b (f-g)^2}{\kappa(I)^2 b^3} \qquad \text{Eq 8}$$

The polyelectrolyte contribution Eq 8 to the excluded volume estimation of CGRP also overestimates the compaction at low GdmCl concentrations.

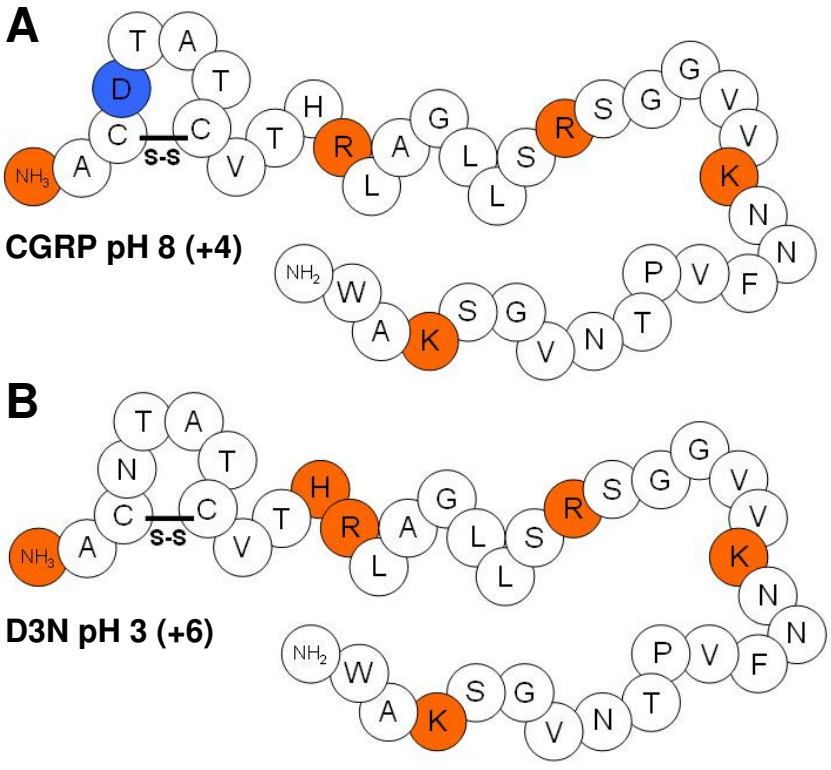

Figure 5.13. Sequence of CGRP variants with positive (red) and negative (blue) charges highlighted. (A) CGRP wild-type at pH 8, (B) CGRP D3N at pH 3.

A close look at the position of the charges in the sequences of CGRP and CGRP D3N reveal some subtle differences (Figure 5.13). Besides a difference in the overall net charge, the differences (including a plus/minus charge attraction) between the two variants are limited to the N-terminal region, suggesting that CGRP might be sensitive to the type and position of the charges in the sequence. To model the position of the charges, A. Soranno used a simple Gaussian model that explicitly calculates the electrostatic contribution to the excluded volume by taking into account the relative distance between charges along the chain,[13] seen in Eq 9 below.

$$\nu_{el} = \frac{l_b}{Nb^3} \sum_{i,j} \frac{c_i c_j}{|i-j|^{0.5} \alpha b} e^{-\kappa(I)|i-j|^{0.5} \alpha b} \qquad \text{Eq 9}$$

In Eq 9, i and j are the position of the charged residues, with c_i and c_j being the charge on those residues based on the pKa of the amino acids and the solvent conditions. To take into account the expansion of CGRP due to denaturant binding, the charge screening is modeled in conjunction with a Schellman denaturant binding model[9,18] given in Eq 10 below:

$$R_G = N^{0.5} \alpha b \left(1 + \rho \frac{Ka}{1+Ka} \right) \qquad \text{Eq 10}$$

where ρ is the denaturant expansion coefficient, K is the denaturant binding constant, and a is the activity of the denaturant. This combined model takes into account charge screening at low GdmCl concentrations and denaturant binding and expansion at higher denaturant concentrations. For CGRP, the radius of gyration is rescaled to:

$$R_g(I,\rho,K,a) = \alpha(I,\nu)\frac{n^{0.5}b}{6^{0.5}}\left(1+\rho\frac{Ka}{1+Ka}\right) \qquad \text{Eq 11}$$

Experimental data for CGRP at +4 and CGRP D3N at +6 were successfully fit to Eq 9 and 11 above. The fits for CGRP and CGRP D3N are shown in Figure 5.14.

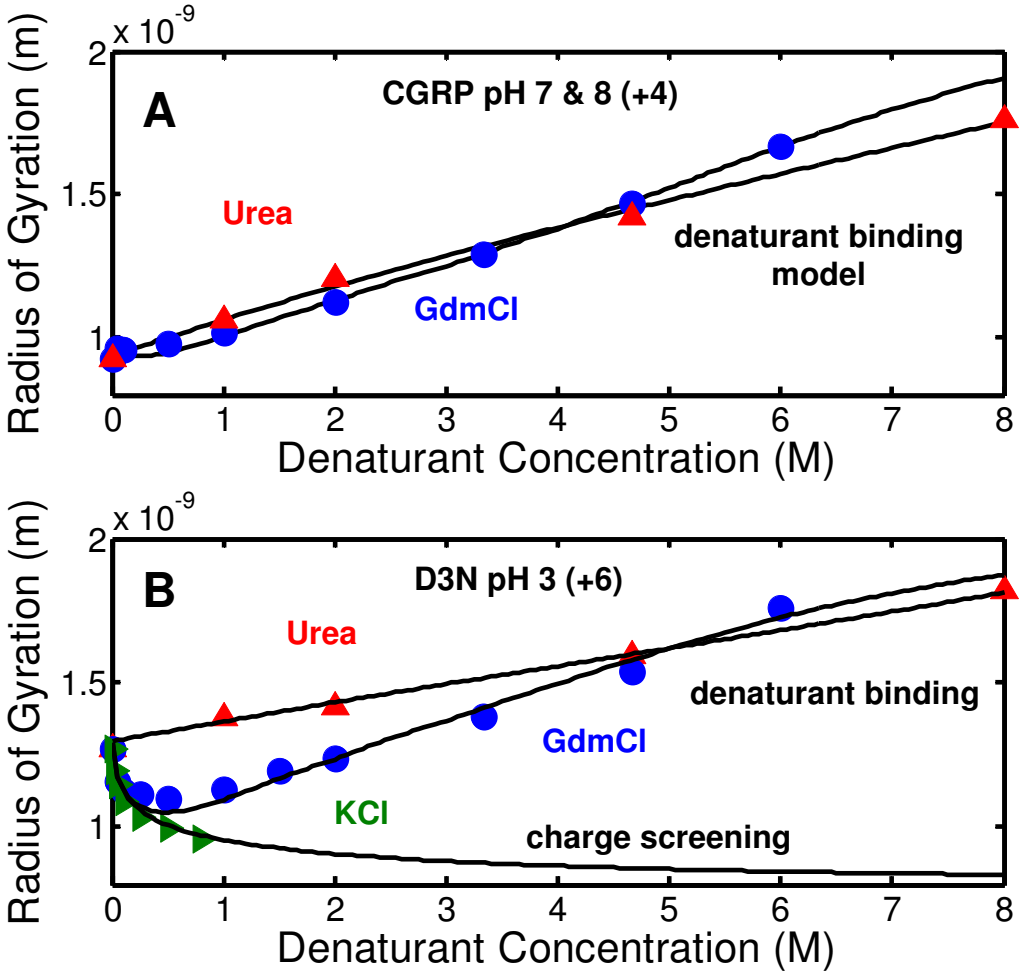

Figure 5.14. The radius of gyration of CGRP variants as a function of denaturant concentration. A. CGRP wild-type in GdmCl pH 7 (blue circles) and Urea pH 8 (red triangles), B. CGRP D3N in GdmCl pH 3 (blue circles), Urea pH 3 (red triangles), and KCl pH 3 (green arrows). The black lines are the fit from the charge patterning model described in Eq 11.

From these fits, we now have values for the excluded volume term with the electrostatic contribution and the denaturant binding term, given in Table 5.3 below.

Net Charge	Solvent	N	K	ρ
+6 (pH 3)	GdmCl	0.00 ± 0.06	0.04 ± 0.03	1.6 ± 0.1
	Urea		0.01 ± 0.02	6 ± 10
+4 (pH 7 & 8)	GdmCl	0.20 ± 0.04	0.16 ± 0.07	1.6 ± 0.4
	Urea	0.09 ± 0.06	0.04 ± 0.03	4 ± 2

Table 5.3 Fitting parameters for fits for CGRP titration. For CGRP with a +6 or +4 net charge in GdmCl and Urea, the parameters ar: ν - excluded volume of CGRP, ρ - denaturant expansion coefficient, K - denaturant binding constant.

As expected, GdmCl binds more efficiently than Urea and the electrostatic contribution to the excluded volume is small for these peptides compared to other disordered proteins. This suggests that CGRP cannot be characterized as a "simple" polyampholyte or polyelectrolyte, but instead the position of the charges and the types of charge interactions must be taken into account. However, through the modification of a polyampholyte polymer model to take into account the position of the charges, we can quantitatively account for the data, extracting effective denaturant binding constants and effective excluded volumes for CGRP. Specifically in the case of CGRP, the single N3 charge has a dramatic effect on the structure of CGRP, due to its specific location along the sequence, which suggests a possible functional role for this charge.

5.4.3. SECONDARY STRUCTURE IS NOT AFFECTED BY ELECTROSTATICS

To determine whether the decrease in the radius of gyration at low GdmCl concentrations is due to changes in non-local interactions or secondary structure at low GdmCl concentrations, CD measurements titrating GdmCl were performed on CGRP wild type at pH 7 and CGRP D3N at pH 3. The CD minima at 222 nm was measured and plotted as a function of GdmCl concentration with the minima at 222 nm corresponds to the amount of secondary structure in CGRP.

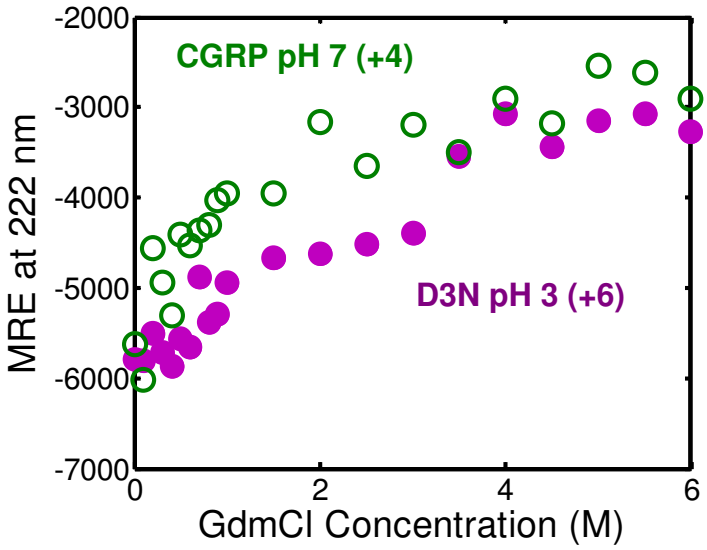

Figure 5.15. GdmCl titration of the CD signal at 222 nm of CGRP variants. The CD of CGRP wild-type in pH 7 buffer (open green circles) and CGRP D3N in pH 3 buffer (closed maroon circles) were measured as a function of GdmCl concentration, and the signal at 222nm, which reports on the secondary structure, decreases monotonically.

As Figure 5.15 shows, the CD signal at 222 nm for both peptides decrease in a monotonic way, consistent with the loss of secondary structure in disordered proteins. Therefore, the compaction in CGRP D3N at low GdmCl concentrations are due to non-local interactions that directly affect the end-to-end distances of CGRP and its variants.

5.5. DISCUSSION

In this chapter, we explored the effect of electrostatic interactions on CGRP. Unlike previous reports on secondary structure of CGRP[15] we found that the end-to-end distance (a non-local property) is highly sensitive to electrostatic interactions between charged residues in the sequence. This emphasized the importance of measuring non-local (tertiary) structural properties of IDPs in addition to local (secondary) structural properties. Screening the charges with salt caused CGRP to populate compact states, with this compaction depending linearly on the Debye length of the solution. When exploring this charge screening effect by measurements of the end-to-end contact formation rates of CGRP in an ionic denaturant (GdmCl), it was found that with a +6 net charge, CGRP will compact at low ionic concentrations before the denaturant effect takes over. As discussed in Chapter One these findings are relevant to current studies on the effect of electrostatic interactions on the structure of IDPs. As described in that chapter, the structure of the disordered unbound state of IDPs is expected to affect the both the affinity and the kinetics of binding to receptors, and therefore their biological function.

Moreover, these findings are directly relevant to current models on the mechanism by which CGRP is responsible for the transmission of pain signals and triggering migraines. As discussed in Chapter Two, CGRP is known for its vasodilatory effects and role in the transmission of pain in the body. The release of CGRP in sensory neurons triggers a vasodilatory response which provides a cardiac protective effect and reduces ischemia and other inflammation[19,20] and there is a significant body of evidence that the release of CGRP is triggered by a drop in the extracellular pH, either through the release of protons via anaerobic respiration or the release of lactic acid during cell damage.[20] Multiple experiments have found an increase in CGRP levels or an increase in CGRP immunoreactivity when lowering the pH of the medium or with the addition of calcium or proton ions.[21-24] This suggests that the mechanism that triggers the release of CGRP, thereby providing a cardioprotective vasodilatory response, is the lowered pH of the extracellular medium due to cell damage.

Low extracellular pH is even suspected to play a role in the transmission of pain in the body via the release of CGRP. Cancer cells actually cause significant sprouting of CGRP-producing sensory nerve fibers nearby[25,26] while other studies have found that cancer cells have a reverse pH gradient, with lower extracellular pH.[26] As mentioned in Chapter Two, CGRP plays an important role in back pain, and there is a new theory that the genesis of back pain is due to the low pH in the intervertebral disks due to high levels of lactate in the disks from inflammation.[27] As the release of CGRP and activation of the CGRP receptor is sensitive to acidic conditions in the body, the experimental evidence presented

in this work showing CGRP's structural sensitivity to solution pH suggests that the binding of CGRP to its receptor is sensitive to variations in the structure of CGRP. In short, there is a significant body of evidence that lowering the pH of the extracellular medium triggers the release of CGRP, thereby transmitting pain or prompting a vasodilatory response.

REFERENCES

[1]Vaiana, S. M., Best, R. B., Yau, W. M., Eaton, W. A., & Hofrichter, J. (2009). Evidence for a partially structured state of the amylin monomer. *Biophysical journal*, *97*(11), 2948-2957.

[2]Schreiber, G., & Fersht, A. R. (1996). Rapid, electrostatically assisted association of proteins. *Nature Structural & Molecular Biology*, *3*(5), 427-431.

[3]Uversky, V. N. (2009). Intrinsically disordered proteins and their environment: effects of strong denaturants, temperature, pH, counter ions, membranes, binding partners, osmolytes, and macromolecular crowding. *The protein journal*, *28*(7-8), 305-325.

[4]Johansson, J., Gudmundsson, G. H., Rottenberg, M. E., Berndt, K. D., & Agerberth, B. (1998). Conformation-dependent antibacterial activity of the naturally occurring human peptide LL-37. *Journal of Biological Chemistry*, *273*(6), 3718-3724.

[5]Su, Y., & Chang, P. T. (2001). Acidic pH promotes the formation of toxic fibrils from β-amyloid peptide. *Brain research*, *893*(1), 287-291.

[6]Kamihira, M., Oshiro, Y., Tuzi, S., Nosaka, A. Y., Saitô, H., & Naito, A. (2003). Effect of electrostatic interaction on fibril formation of human calcitonin as studied by high resolution solid state ^{13}C NMR. *Journal of Biological Chemistry*, *278*(5), 2859-2865.

[7]Marek, P. J., Patsalo, V., Green, D. F., & Raleigh, D. P. (2012). Ionic strength effects on amyloid formation by amylin are a complicated interplay among Debye screening, ion selectivity, and Hofmeister effects. *Biochemistry*, *51*(43), 8478-8490.

[8]Marsh, J. A., & Forman-Kay, J. D. (2010). Sequence determinants of compaction in intrinsically disordered proteins. *Biophysical journal*, *98*(10), 2383-2390.

[9]Müller-Späth, S., Soranno, A., Hirschfeld, V., Hofmann, H., Rüegger, S., Reymond, L., Nettels, D., & Schuler, B. (2010). Charge interactions can dominate the dimensions of intrinsically disordered proteins. *Proceedings of the National Academy of Sciences*, *107*(33), 14609-14614.

[10]Hofmann, H., Nettels, D., & Schuler, B. (2013). Single-molecule spectroscopy of the unexpected collapse of an unfolded protein at low pH. *The Journal of chemical physics*, *139*(12), 121930.

[11]Mao, A. H., Crick, S. L., Vitalis, A., Chicoine, C. L., & Pappu, R. V. (2010). Net charge per residue modulates conformational ensembles of intrinsically disordered proteins. *Proceedings of the National Academy of Sciences*, *107*(18), 8183-8188.

[12]Das, R. K., & Pappu, R. V. (2013). Conformations of intrinsically disordered proteins are influenced by linear sequence distributions of oppositely charged residues. *Proceedings of the National Academy of Sciences*, *110*(33), 13392-13397.

[13]Zhou, H. X. (2002). A Gaussian-chain model for treating residual charge-charge interactions in the unfolded state of proteins. *Proceedings of the National Academy of Sciences*, *99*(6), 3569-3574.

[14]Wimalawansa, S. J. (1997). Amylin, calcitonin gene-related peptide, calcitonin, and adrenomedullin: a peptide superfamily. *Critical Reviews™ in Neurobiology*, *11*(2-3).

[15]Hubbard, J. A., Martin, S. R., Chaplin, L. C., Bose, C., Kelly, S. M., & Price, N. C. (1991). Solution structures of calcitonin-gene-related-peptide analogues of calcitonin-gene-related peptide and amylin. *Biochem. J*, *275*, 785-788.

[16]Higgs, P. G., & Joanny, J. F. (1991). Theory of polyampholyte solutions. *The Journal of chemical physics*, *94*(2), 1543-1554.

[17]Ha, B. Y., & Thirumalai, D. (1992). Conformations of a polyelectrolyte chain. *Physical Review A*, *46*(6), R3012.

[18]Schellman, J. A. (1987). Selective binding and solvent denaturation. *Biopolymers*, *26*(4), 549-559.

[19]Lechleitner, P., Genser, N., Mair, J., Dienstl, A., Haring, C., Wiedermann, C. J., Puschendorf, B., Saria, A., & Dienstl, F. (1992). Calcitonin gene-related peptide in patients with and without early reperfusion after acute myocardial infarction. *American heart journal*, *124*(6), 1433-1439.

[20]Bevan, S., & Geppetti, P. (1994). Protons: small stimulants of capsaicin-sensitive sensory nerves. *Trends in neurosciences*, *17*(12), 509-512.

[21]Geppetti, P., Del Bianco, E., Patacchini, R., Santicioli, P., Maggi, C. A., & Tramontana, M. (1991). Low pH-induced release of calcitonin gene-related peptide from capsaicin-sensitive sensory nerves: mechanism of action and biological response. *Neuroscience*, *41*(1), 295-301.

[22]Franco-Cereceda, A., & Lundberg, J. M. (1992). Capsazepine inhibits low pH-and lactic acid-evoked release of calcitonin gene-related peptide from sensory nerves in guinea-pig heart. *European journal of pharmacology*, *221*(1), 183-184.

[23]Cheng, L., de la Monte, S., Ma, J., Hong, J., Tong, M., Cao, W., Behar, J.,Biancani, P., & Harnett, K. M. (2009). HCl-activated neural and epithelial vanilloid receptors (TRPV1)

in cat esophageal mucosa. *American Journal of Physiology-Gastrointestinal and Liver Physiology*, *297*(1), G135-G143.

[24]Fanciullacci, M., Tramontana, M., Del Bianco, E., Alessandri, M., & Geppetti, P. (1991). Low pH medium induces calcium dependent release of CGRP from sensory nerves of guinea-pig dural venous sinuses. *Life sciences*, *49*(8), PL27-PL30.

[25]Bloom, A. P., Jimenez-Andrade, J. M., Taylor, R. N., Castañeda-Corral, G., Kaczmarska, M. J., Freeman, K. T., Coughlin, K.A., Ghilardi, J.R., Kuskowski, M.A., & Mantyh, P. W. (2011). Breast cancer-induced bone remodeling, skeletal pain, and sprouting of sensory nerve fibers. *The Journal of Pain*, *12*(6), 698-711.

[26]Lozano-Ondoua, A. N., Symons-Liguori, A. M., & Vanderah, T. W. (2013). Cancer-induced bone pain: Mechanisms and models. *Neuroscience letters*, *557*, 52-59.

[27]Liang, C., Li, H., Tao, Y., Shen, C., Li, F., Shi, Z., Han, B., & Chen, Q. (2013). New hypothesis of chronic back pain: low pH promotes nerve ingrowth into damaged intervertebral disks. *Acta Anaesthesiologica Scandinavica*, *57*(3), 271-277.

CHAPTER 6

EVIDENCE FOR INTERNAL FRICTION IN CGRP

6.1. INTRODUCTION TO INTERNAL FRICTION

Experimental measurements of the internal dynamics of disordered proteins are of interest in the IDP field as there is a significant body of evidence that the dynamics of the monomer state is important for biological function. As discussed in Chapter One, it is thought that the dynamics of disordered proteins can affect the binding rates and the function of these proteins.[1-4] Recently, research has started to focus on "internal friction" or the roughness of the diffusional energy landscape.[5-7] The reconfiguration time of unfolded or disordered proteins have been found to depend on two effects: "wet" or solvent mediated friction (in which the friction is proportional to the viscosity of the solution), and "dry" or solvent viscosity independent friction (in which the dynamics are mediated by interactions within the protein itself).[8-9] Internal friction, or "dry" solvent independent friction, has been found to have an additive effect on the chain reconfiguration time.[8]

As the internal friction of disordered proteins can have a significant effect on the dynamics of the proteins, recent studies have focused identifying sources of internal friction. Previous FRET measurements on disordered proteins found that in low denaturant concentrations, solvent-independent (or "dry") internal friction is greater when the protein populates shorter end-to-end distances, which was attributed to a greater

number of steric clashes slowing down the reconfiguration time of compact proteins.[8] As the solvent concentration increases, the internal friction contribution to the reconfiguration time decreases such that when the protein is fully denatured, only "wet" friction contributes to the reconfiguration time.[8] This is consistent with previous studies that showed a correlation between the dimensions of unfolded proteins and changes to their chain dynamics.[10-11] Simulations on internal friction in unfolded proteins have also shown that despite the presence of non-local interactions which can form "kinetic traps," instead it is concerted dihedral rotations in collapsed states of IDPs that a play a significant role in internal friction, slowing down the dynamics of IDPs.[9] Aside from these studies, there is currently little experimental evidence for internal friction in disordered proteins.

To measure the internal dynamics of CGRP, we look at the diffusion limited rates corrected for solvent viscosity (ηk_{D+}) measured by TTQ, which report on the time it takes to form a contact between the tryptophan and the cystine. Because the diffusion limited rate depends on both the intra-chain diffusion coefficient, D and the end-to-end distance distribution P(r), for a simple analysis of the dynamics of two proteins, they must have the same end-to-end distance so that any differences in the diffusion limited rate is due to intra-chain dynamics rather than a change in the structure of CGRP. Because of this, we must compare both k_R, which depends only on P(r) and ηk_{D+} in order to elucidate the dynamics of CGRP in solution. In this chapter, we will focus on the internal dynamics of CGRP and identifying possible sources for internal friction that might affect the reconfiguration time of CGRP in solution.

6.2. EXPERIMENTAL METHODS

The experimental methods were described previously in Chapters Four and Five.

6.3 INTERNAL FRICTION IN CGRP

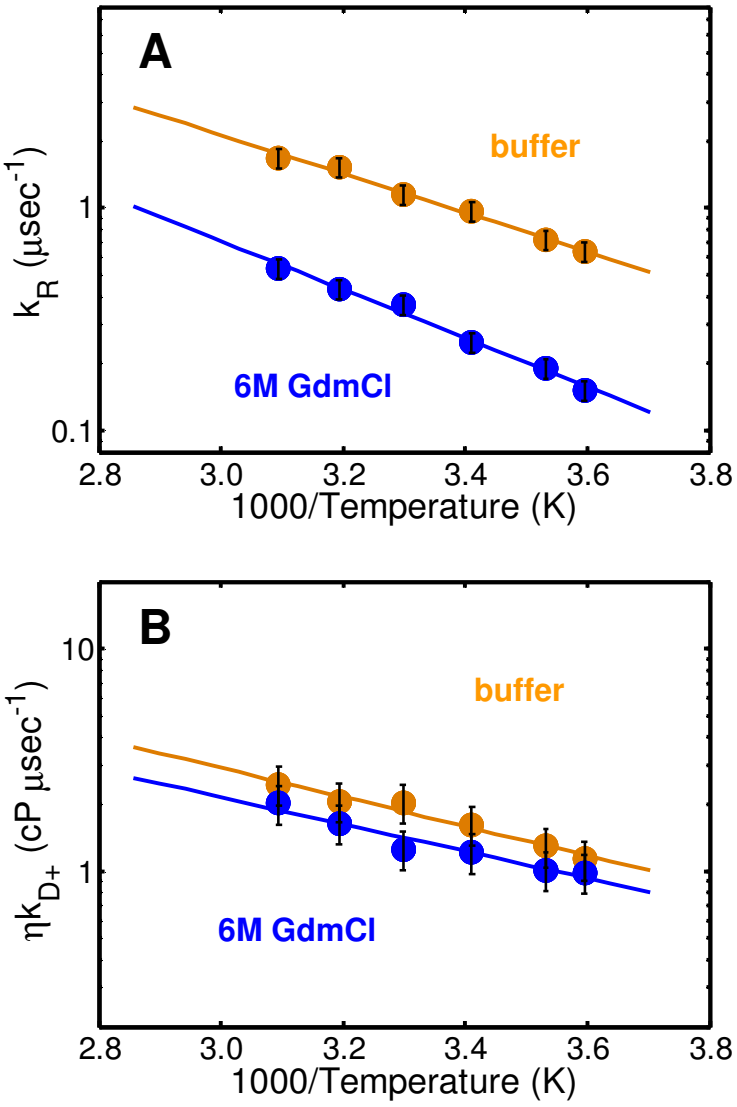

Figure 6.1. Reaction limited (A) and diffusion limited (B) rates of CGRP pH 4.9 in 6M GdmCl (blue) and buffer (orange).

The two graphs in Figure 6.1 above are the reaction and diffusion limited rates of CGRP in both buffer at pH 4.9 and 6M GdmCl. As discussed in Chapter 4, CGRP has shorter end-to-end distances in buffer, with k_R increasing three-fold in buffer compared to denaturant. However, when looking at ηk_{D+}, CGRP now has very similar rates in both buffer and denaturant. As CGRP is significantly more compact in buffer than in GdmCl, the similar ηk_{D+} must be accounted for by CGRP having slower dynamics in buffer compared to denaturant. Intuitively this makes sense because in buffer CGRP will have attractive non-local intra-chain interactions that are "sticky," slowing down the reconfiguration time compared to CGRP in denaturant, in which CGRP will have only excluded volume interactions.

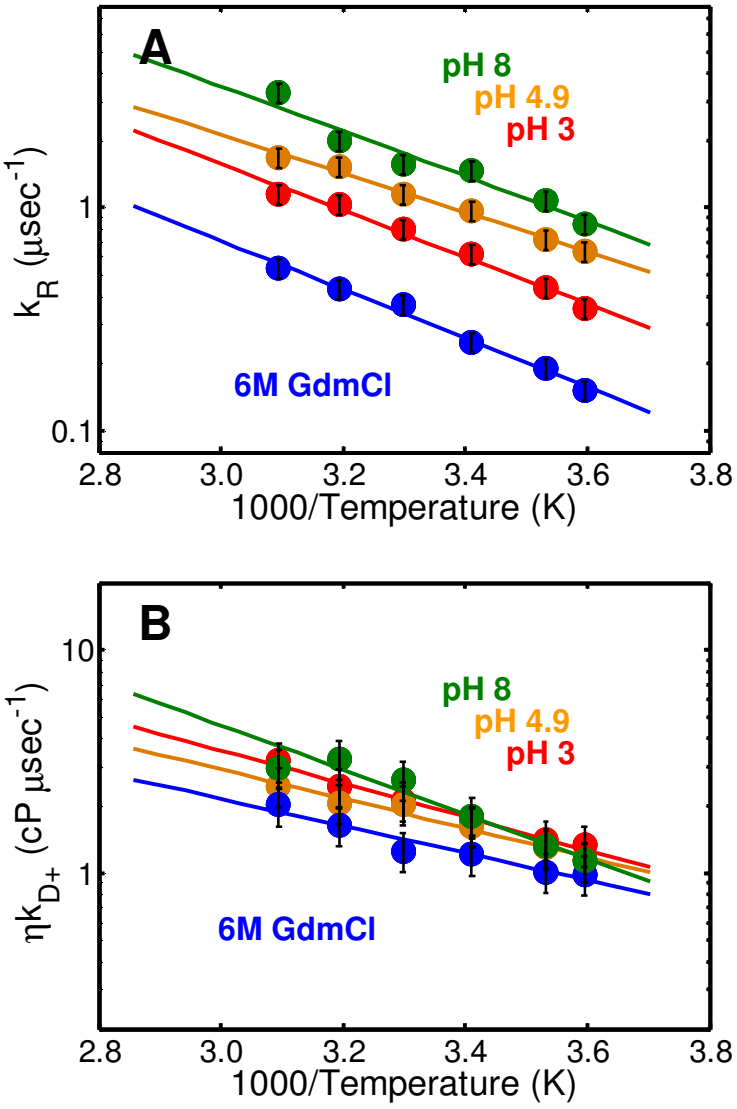

Figure 6.2. Reaction limited (A) and diffusion limited (B) rates of CGRP in 6M GdmCl (blue), pH 3 (red), pH 4.9 (orange) and pH 8 (green).

As reported in Chapter Five, electrostatic interactions strongly modulate the structure of CGRP, with k_R increasing as the net charge on CGRP decreases. However, the pH dependence of the diffusion limited rates stays relatively constant as the net charge on CGRP changes (Figure 6.2), suggesting that as the net charge on CGRP decreases, the

internal dynamics slow down: CGRP with a "high" net charge of +6 has slightly faster dynamics than CGRP with a "low" net charge of +4. Thus the pH dependence of CGRP's dynamics follows the same trend observed in buffer versus denaturant, where the reconfiguration time depends on the net charge of the chain due to "sticky" electrostatic interactions that slow down the internal dynamics of CGRP.

As Figures 6.1 and 6.2 just showed, attractive intra-chain interactions, including electrostatic interactions, slow down the intra-chain dynamics of CGRP. To further explore the role of electrostatic interactions on the internal dynamics of CGRP, electrostatic interactions were screened by the addition of 500mM KCl. Figure 6.3 below shows both kR and ηk_{D+} of CGRP (pH 5, with a net charge of +5) in buffer and salt, and Figure 6.4 shows CGRP D3N (pH 3, with a net charge of +6) in the same conditions. As discussed in Chapter Five, k_R of both CGRP variants in 500mM KCl are faster than in buffer, with the screening of charges causing compaction in CGRP. On the other hand, as Figures 6.3 and 6.4 show, ηk_{D+} are now significantly faster at 500mM KCl than at 0M KCl. This means that despite CGRP populating collapsed states in high salt compared to at 0M KCl, the intra-chain dynamics speed up. This is surprising because previously published experimental and theoretical evidence has shown that compact states increase internal friction and slow down dynamics, rather than speed them up.[8,9] This suggests that at least for CGRP, electrostatic interactions are a primary contributor to internal friction, and elimination of these interactions speed up the internal dynamics.

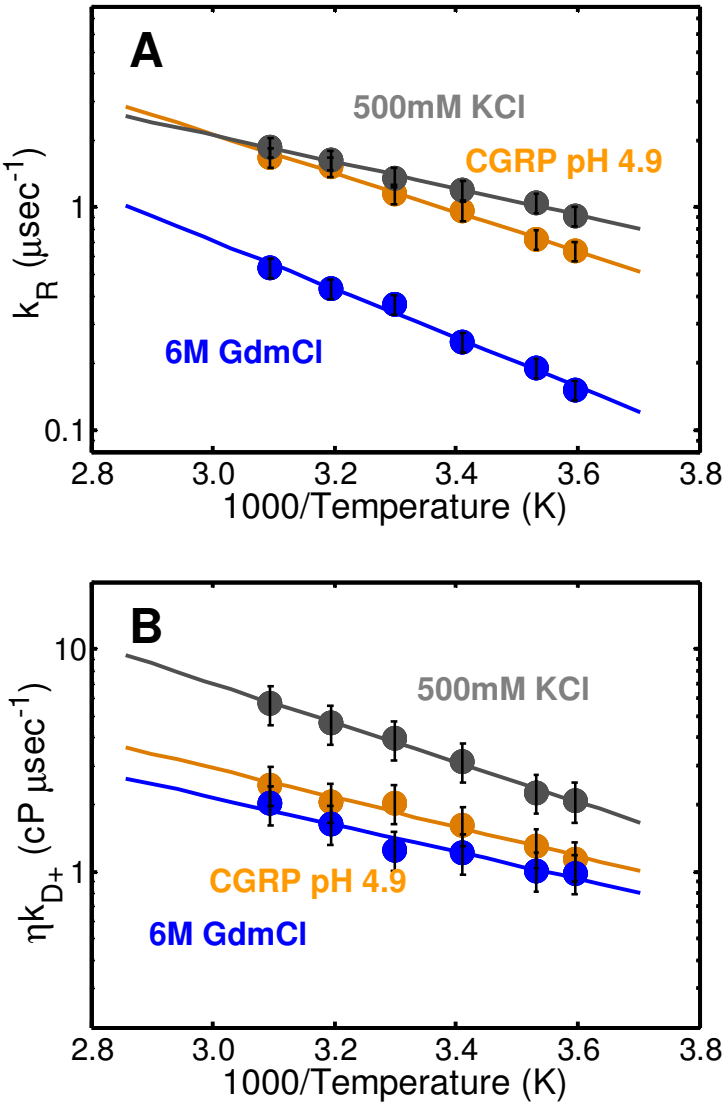

Figure 6.3. Reaction limited (A) and diffusion limited (B) rates of CGRP wild type in 6M GdmCl (closed blue circles), pH 4.9 (orange), and 500mM KCl (closed grey circles).

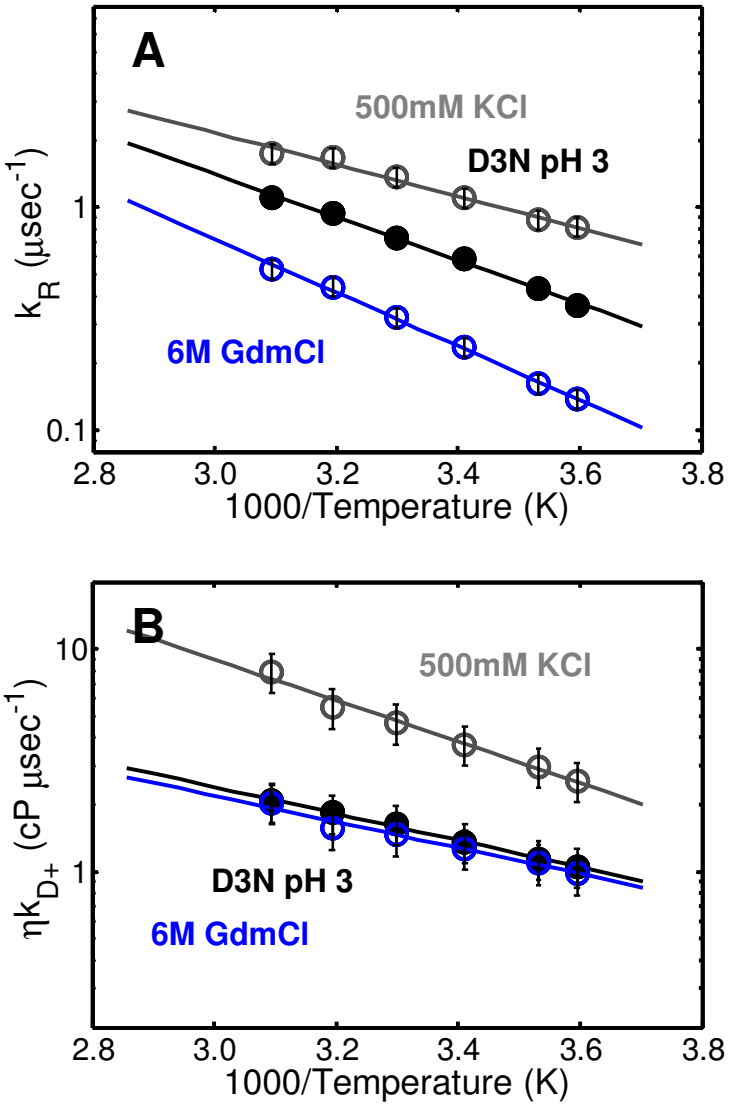

Figure 6.4. Reaction limited (A) and diffusion limited (B) rates of CGRP D3N in 6M GdmCl (open blue circles), pH 3 (black), and 500mM KCl (open grey circles).

6.4. INTERNAL FRICTION IN CT FAMILY PEPTIDES

This chapter has explored how the internal dynamics of CGRP are modulated by electrostatic interactions, with non-local interactions slowing down the dynamics of CGRP relative to GdmCl. Now we can compare the diffusion limited rates for CGRP and IAPP and see how the internal dynamics differ among Ct family peptides. In Figure 6.5, kR and ηk_{D+} for CGRP at pH 8 and IAPP at pH 4.9 in buffer and denaturant are shown. As discussed in Chapter Five, when CGRP and IAPP have the same net charge as they do here, they have similar k_R and very similar end-to-end distances. However, a look at ηk_{D+} shows that IAPP has significantly faster dynamics than CGRP, despite being equally compact as CGRP. This suggests that unlike CGRP, IAPP has few "sticky" intra-chain interactions which would slow down its dynamics in buffer and that even when populating very compact states, IAPP has relatively little internal friction.

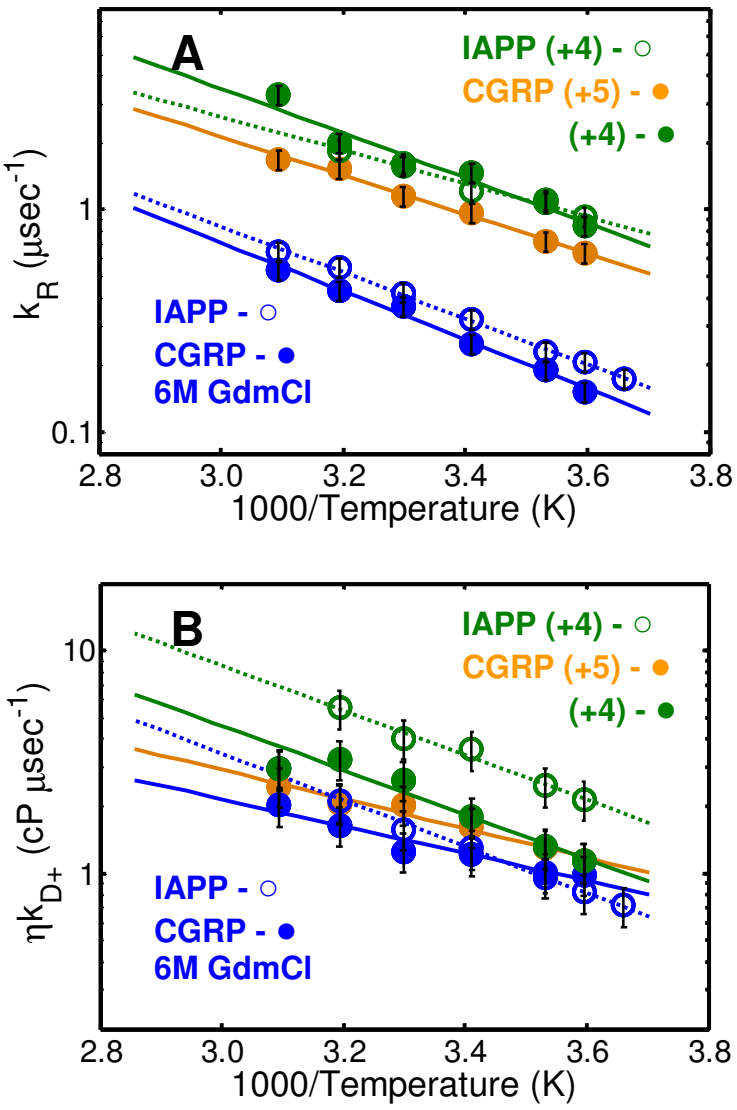

Figure 6.5. Reaction limited (A) and diffusion limited (B) rates of CGRP in 6M GdmCl (closed blue circles), pH 4.9 (orange), and pH 8 (closed green circles) and IAPP in 6M GdmCl (open blue circles) and pH 4.9 buffer (open green circles).

6.5. DISCUSSION

By measuring the diffusion limited rate of CGRP using tryptophan triplet quenching, we were able to determine how the presence of non-local interactions such as electrostatics affect the reconfiguration time. This chapter showed that CGRP has greater internal friction in buffer compared to denaturant due to the presence of attractive interactions present in buffer, while decreasing the net charge of CGRP in buffer appears to slow down CGRP's internal dynamics, suggesting that electrostatic interactions contribute to internal friction and slow down the intra-chain diffusion. Surprisingly however, even when CGRP and IAPP have the same net charge and they both populate compact states with the same end-to-end distance, internal friction is greater in CGRP than IAPP.

The results on CGRP discussed in this chapter are some of the first results showing experimental evidence that electrostatic interactions contribute to internal friction in IDPs. Here we show that non-local electrostatic interactions such as Coulomb interactions contribute to viscosity-independent internal friction in CGRP. Similarly IAPP has faster dynamics than CGRP despite having the same net charge and same end-to-end distance. As IAPP aggregates into amyloid fibrils while CGRP does not, this might contribute to IAPP's aggregation propensity, with the faster dynamics seen in IAPP allowing it to sample transient states quickly compared to CGRP which has "trapped" states slowing down its dynamics. Conversely, as electrostatic interactions slow down the dynamics of CGRP significantly, this suggests that attractive electrostatic interactions between CGRP and its receptor might help CGRP increase its binding rate through attractive inter-

molecule interactions. In agreement with previous literature, at low pH, CGRP is also more expanded with correspondingly faster dynamics, meaning that CGRP quickly goes through its ensemble of conformations which can significantly affect the binding kinetics between CGRP and its receptor. The experimental results presented in this chapter suggest that electrostatic interactions play a significant role in not only the structure of the monomeric state of CGRP, but also its internal dynamics.

REFERENCES

[1]Rogers, J. M., Steward, A., & Clarke, J. (2013). Folding and binding of an intrinsically disordered protein: fast, but not 'diffusion-limited'. Journal of the American Chemical Society, 135(4), 1415-1422.

[2]Borg, M., Mittag, T., Pawson, T., Tyers, M., Forman-Kay, J. D., & Chan, H. S. (2007). Polyelectrostatic interactions of disordered ligands suggest a physical basis for ultrasensitivity. Proceedings of the National Academy of Sciences, 104(23), 9650-9655.

[3]Dunker, A. K., Silman, I., Uversky, V. N., & Sussman, J. L. (2008). Function and structure of inherently disordered proteins. Current opinion in structural biology, 18(6), 756-764.

[4]Wright, P. E., & Dyson, H. J. (2009). Linking folding and binding. Current opinion in structural biology, 19(1), 31-38.

[5]Best, R. B., & Hummer, G. (2010). Coordinate-dependent diffusion in protein folding. *Proceedings of the National Academy of Sciences*, *107*(3), 1088-1093.

[6]Best, R. B., & Hummer, G. (2011). Diffusion models of protein folding. *Physical Chemistry Chemical Physics*, *13*(38), 16902-16911.

[7]J Hagen, S. (2010). Solvent viscosity and friction in protein folding dynamics. *Current Protein and Peptide Science*, *11*(5), 385-395.

[8]Soranno, A., Buchli, B., Nettels, D., Cheng, R. R., Müller-Späth, S., Pfeil, S. H., Hoffmann, A., Lipman, E.A., Makarov, D.E., & Schuler, B. (2012). Quantifying internal friction in unfolded and intrinsically disordered proteins with single-molecule spectroscopy. *Proceedings of the National Academy of Sciences*, *109*(44), 17800-17806.

[9]Echeverria, I., Makarov, D. E., & Papoian, G. A. (2014). Concerted dihedral rotations give rise to internal friction in unfolded proteins. *Journal of the American Chemical Society*, *136*(24), 8708-8713.

[10]Waldauer, S. A., Bakajin, O., & Lapidus, L. J. (2010). Extremely slow intramolecular diffusion in unfolded protein L. *Proceedings of the National Academy of Sciences*, *107*(31), 13713-13717.

[11]Möglich, A., Joder, K., & Kiefhaber, T. (2006). End-to-end distance distributions and intrachain diffusion constants in unfolded polypeptide chains indicate intramolecular hydrogen bond formation. *Proceedings of the National Academy of Sciences*, *103*(33), 12394-12399.

CHAPTER 7

CONCLUSIONS

The characterization of the non-local structural and dynamical properties of the CGRP monomer in solution was the focus of this work. The unbound, free state of CGRP was measured using a nanosecond laser-pump spectrophotometer, by which the end-to-end distance (a structural property) and the rate of end-to-end contact formation (intra-chain diffusional dynamics) was measured. Using this technique, it was revealed that CGRP adopts very compact states in buffer relative to denaturant, populating states with very short end-to-end distances. Our findings also show that the disulfide loop (N_loop) found at the N-terminus of CGRP is partly responsible for some of this collapse, similar to the mechanism seen in IAPP.[1] However, CGRP does not become as compact as a similar peptide IAPP, despite sharing 47% sequence homology,[2,3] therefore the observed differences between the structure (or degree of compaction) of CGRP and IAPP are modulated by differences in the sequence.

While previous reports on the secondary structure of CGRP found little pH dependence[4] we found that electrostatic interactions between charged residues in the sequence appear to modulate compaction in CGRP. When titrating charged residues by changing the solvent pH, we found that the end-to-end distance of CGRP is sensitive to the net charge on the chain and the observed differences in the structure of CGRP and IAPP can be accounted for by differences in net charge. In addition, uniformly screening the charges by the addition of salt allow CGRP to populate compact states, with this compaction

depending linearly on the Debye length of the solution. We also found that in ionic denaturant, there is an interplay between charge screening and denaturant expansion, with charge patterning determining how the radius of gyration of CGRP changes with denaturant concentration.

Finally, through measurements of the rate of end-to-end contact formation in CGRP, this work presents the first experimental evidence of internal friction in Ct family peptides. We show that CGRP has greater internal friction in buffer compared to denaturant, with attractive intra-chain interactions present in buffer slowing down the diffusional dynamics of CGRP. It was also found that decreasing the net charge of CGRP in buffer appears to slow down CGRP's internal dynamics, suggesting that electrostatic interactions contribute to internal friction. Surprisingly however, CGRP was found to have slower intra-chain diffusion than IAPP in buffer, but not in denaturant, even when they both populate compact states with the same end-to-end distance, suggesting that internal friction is greater in CGRP than IAPP.

The results of this work show that for CGRP, electrostatic interactions play an important role in both the structure and dynamics of CGRP. As discussed in Chapter One, the structure and dynamics of disordered proteins is thought to play an important role in the thermodynamics and kinetics of receptor binding and activation. Therefore, the results of this work suggest that electrostatic interactions might help CGRP modulate its binding rate to the CGRP receptor through attractive inter-molecule interactions between CGRP and its receptor. Electrostatic interactions also affect the speed which CGRP goes through

the ensemble of conformations, which can significantly affect the binding kinetics between CGRP and its receptor. As the release of CGRP and activation of the CGRP receptor is sensitive to acidic conditions in the body,[5-8] the experimental evidence presented in this work showing CGRP's sensitivity to electrostatic interactions suggests a potential mechanism for the modulation of the binding of CGRP to its receptor.

In addition, this work compares CGRP with IAPP, a Ct family member with high sequence homology, expanding upon previous work done by Vaiana group members.[1] This work explored sequence specific effects that affect the structure and dynamics of CGRP and IAPP, including electrostatic interactions and intra-chain interactions modulated by the N_loop. In the last few years migraine research has shifted focus to disrupting the CGRP-receptor pathway through the design of pharmacological drugs that bind to either CGRP or its receptor, inhibiting receptor activation and therefore preventing or reducing the frequency of migraine attacks.[9] Therefore, it is important to design therapeutics that are able to selectively target CGRP and its receptor only, and not other, similar Ct family members. By comparing CGRP and IAPP, the results of this work help understand what types of non-local interactions affect the binding affinities of Ct family peptides and will allow better and more precise drug engineering.

REFERENCES

[1]Vaiana, S. M., Best, R. B., Yau, W. M., Eaton, W. A., & Hofrichter, J. (2009). Evidence for a partially structured state of the amylin monomer. Biophysical journal, 97(11), 2948-2957.

[2]Wimalawansa, S. J. (1997). Amylin, calcitonin gene-related peptide, calcitonin, and adrenomedullin: a peptide superfamily. *Critical Reviews™ in Neurobiology*, *11*(2-3).

[3]Tippins, J. R., Di Marzo, V., Panico, M., Morris, H. R., & MacIntyre, I. (1986). Investigation of the structure/activity relationship of human calcitonin gene-related peptide (CGRP). *Biochemical and biophysical research communications*, *134*(3), 1306-1311.

[4]Hubbard, J. A., Martin, S. R., Chaplin, L. C., Bose, C., Kelly, S. M., & Price, N. C. (1991). Solution structures of calcitonin-gene-related-peptide analogues of calcitonin-gene-related peptide and amylin. *Biochem. J*, *275*, 785-788.

[5]Geppetti, P., Del Bianco, E., Patacchini, R., Santicioli, P., Maggi, C. A., & Tramontana, M. (1991). Low pH-induced release of calcitonin gene-related peptide from capsaicin-sensitive sensory nerves: mechanism of action and biological response. *Neuroscience*, *41*(1), 295-301.

[6]Franco-Cereceda, A., & Lundberg, J. M. (1992). Capsazepine inhibits low pH-and lactic acid-evoked release of calcitonin gene-related peptide from sensory nerves in guinea-pig heart. *European journal of pharmacology*, *221*(1), 183-184.

[7]Cheng, L., de la Monte, S., Ma, J., Hong, J., Tong, M., Cao, W., Behar, J.,Biancani, P., & Harnett, K. M. (2009). HCl-activated neural and epithelial vanilloid receptors (TRPV1) in cat esophageal mucosa. *American Journal of Physiology-Gastrointestinal and Liver Physiology*, *297*(1), G135-G143.

[8]Fanciullacci, M., Tramontana, M., Del Bianco, E., Alessandri, M., & Geppetti, P. (1991). Low pH medium induces calcium dependent release of CGRP from sensory nerves of guinea-pig dural venous sinuses. *Life sciences*, *49*(8), PL27-PL30.

[9]Moore, E. L., & Salvatore, C. A. (2012). Targeting a family B GPCR/RAMP receptor complex: CGRP receptor antagonists and migraine. *British journal of pharmacology*, *166*(1), 66-78.

REFERENCES

Amara, S. G., Jonas, V., Rosenfeld, M. G., Ong, E. S., & Evans, R. M. (1982). Alternative RNA processing in calcitonin gene expression generates mRNAs encoding different polypeptide products. *Nature,* 298 (240-244).

Andrews, M. N., & Winter, R. (2011). Comparing the structural properties of human and rat islet amyloid polypeptide by MD computer simulations. *Biophysical chemistry*, *156*(1), 43-50.

Ansari, A., Jones, C. M., Henry, E. R., Hofrichter, J., & Eaton, W. A. (1992). The role of solvent viscosity in the dynamics of protein conformational changes. *Science*, *256*(5065), 1796-1798.

Arvinte, T., Cudd, A., & Drake, A. F. (1993). The structure and mechanism of formation of human calcitonin fibrils. *Journal of Biological Chemistry*, *268*(9), 6415-6422.

Ashton, I. K., Roberts, S., Jaffray, D. C., Polak, J. M., & Eisenstein, S. M. (1994). Neuropeptides in the human intervertebral disc. *Journal of orthopaedic research*, *12*(2), 186-192.

Best, R. B., & Hummer, G. (2010). Coordinate-dependent diffusion in protein folding. *Proceedings of the National Academy of Sciences*, *107*(3), 1088-1093.

Best, R. B., & Hummer, G. (2011). Diffusion models of protein folding. *Physical Chemistry Chemical Physics*, *13*(38), 16902-16911.

Bevan, S., & Geppetti, P. (1994). Protons: small stimulants of capsaicin-sensitive sensory nerves. *Trends in neurosciences*, *17*(12), 509-512.

Bloom, A. P., Jimenez-Andrade, J. M., Taylor, R. N., Castañeda-Corral, G., Kaczmarska, M. J., Freeman, K. T., Coughlin, K.A., Ghilardi, J.R., Kuskowski, M.A., & Mantyh, P. W. (2011). Breast cancer-induced bone remodeling, skeletal pain, and sprouting of sensory nerve fibers. *The Journal of Pain*, *12*(6), 698-711.

Borg, M., Mittag, T., Pawson, T., Tyers, M., Forman-Kay, J. D., & Chan, H. S. (2007). Polyelectrostatic interactions of disordered ligands suggest a physical basis for ultrasensitivity. *Proceedings of the National Academy of Sciences*, *104*(23), 9650-9655.

Boulanger, Y., Khiat, A., Chen, Y., Senecal, L., Tu, Y., St-Pierre, S., & Fournier, A. (1994). Structure of human calcitonin gene-related peptide (hCGRP) and of its antagonist hCGRP 8-37 as determined by NMR and molecular modeling. *Peptide research*, *8*(4), 206-213.

Brain, S. D., & Grant, A. D. (2004). Vascular actions of calcitonin gene-related peptide and adrenomedullin. *Physiological Reviews*, *84*(3), 903-934.

Brain, S. D., Williams, T. J., Tippins, J. R., Morris, H. R., & MacIntyre, I. (1985). Calcitonin gene-related peptide is a potent vasodilator. *Nature,* 308 (653-655).

Breeze, A. L., Harvey, T. S., Bazzo, R., & Campbell, I. D. (1991). Solution structure of human calcitonin gene-related peptide by proton NMR and distance geometry with restrained molecular dynamics. *Biochemistry*, *30*(2), 575-582.

Bunker, C. B., Dowd, P. M., Terenghi, G., Springall, D. R., & Polak, J. M. (1990). Deficiency of calcitonin gene-related peptide in Raynaud's phenomenon. *The Lancet*, *336*(8730), 1530-1533.

Bunker, C. B., Reavley, C., Dowd, P. M., & O'Shaughnessy, D. J. (1993). Calcitonin gene-related peptide in treatment of severe peripheral vascular insufficiency in Raynaud's phenomenon. *The Lancet*, *342*(8863), 80-83.

Buscaglia, M., Lapidus, L. J., Eaton, W. A., & Hofrichter, J. (2006). Effects of denaturants on the dynamics of loop formation in polypeptides. *Biophysical journal*, *91*(1), 276-288.

Chantry, A., Leighton, B., & Day, A. J. (1991). Cross-reactivity of amylin with calcitonin-gene-related peptide binding sites in rat liver and skeletal muscle membranes. *Biochem. J*, *277*, 139-143.

Cheng, L., de la Monte, S., Ma, J., Hong, J., Tong, M., Cao, W., Behar, J.,Biancani, P., & Harnett, K. M. (2009). HCl-activated neural and epithelial vanilloid receptors (TRPV1) in cat esophageal mucosa. *American Journal of Physiology-Gastrointestinal and Liver Physiology*, *297*(1), G135-G143.

Cho, J.H., Sato, S., & Raleigh, D.P. (2004). Thermodynamics and kinetics of non-native interactions in protein folding: a single point mutation significantly stabilizes the N-terminal domain of L9 by modulating non-native interactions in the denatured state. *Journal of molecular biology, 338*(4), 827-837.

Clore, G. M., & Iwahara, J. (2009). Theory, practice, and applications of paramagnetic relaxation enhancement for the characterization of transient low-population states of biological macromolecules and their complexes. *Chemical reviews*, *109*(9), 4108-4139.

Cooper, G. J., Willis, A. C., Clark, A., Turner, R. C., Sim, R. B., & Reid, K. B. (1987). Purification and characterization of a peptide from amyloid-rich pancreases of type 2 diabetic patients. *Proceedings of the National Academy of Sciences*, *84*(23), 8628-8632.

Cope, S.M. (2013). *Interactions driving the collapse of islet amyloid polypeptide: implications for amyloid aggregation* (Doctoral Dissertation).

Cope, S. M., Shinde, S., Best, R. B., Ghirlanda, G., & Vaiana, S. M. (2013). Cyclic N-Terminal Loop of Amylin Forms Non Amyloid Fibers. *Biophysical journal*, *105*(7), 1661-1669.

Crick, S. L., Jayaraman, M., Frieden, C., Wetzel, R., & Pappu, R. V. (2006). Fluorescence correlation spectroscopy shows that monomeric polyglutamine molecules form collapsed structures in aqueous solutions. *Proceedings of the National Academy of Sciences*, *103*(45), 16764-16769.

Cruwys, S. C., Kidd, B. L., Mapp, P. I., Walsh, D. A., & Blake, D. R. (1992). The effects of calcitonin gene-related peptide on formation of intra-articular oedema by inflammatory mediators. *British journal of pharmacology*, *107*(1), 116-119.

Das, R. K., & Pappu, R. V. (2013). Conformations of intrinsically disordered proteins are influenced by linear sequence distributions of oppositely charged residues. *Proceedings of the National Academy of Sciences*, *110*(33), 13392-13397.

De Gennes, P. G. (1979). *Scaling concepts in polymer physics*. Cornell university press.
Dennis, T., Fournier, A., St Pierre, S., & Quirion, R. (1989). Structure-activity profile of calcitonin gene-related peptide in peripheral and brain tissues. Evidence for receptor multiplicity. *Journal of Pharmacology and Experimental Therapeutics*, *251*(2), 718-725.

Doods, H., Arndt, K., Rudolf, K., & Just, S. (2007). CGRP antagonists: unravelling the role of CGRP in migraine. *Trends in pharmacological sciences*, *28*(11), 580-587.

Dunker, A. K., Brown, C. J., Lawson, J. D., Iakoucheva, L. M., & Obradovic, Z. (2002). Intrinsic disorder and protein function. *Biochemistry*, *41*(21), 6573-6582.

Dunker, A. K., Romero, P., Obradovic, Z., Garner, E. C., & Brown, C. J. (2000). Intrinsic protein disorder in complete genomes. *Genome Informatics*, *11*, 161-171.

Dunker, A. K., Silman, I., Uversky, V. N., & Sussman, J. L. (2008). Function and structure of inherently disordered proteins. *Current opinion in structural biology*, *18*(6), 756-764.

Echeverria, I., Makarov, D. E., & Papoian, G. A. (2014). Concerted dihedral rotations give rise to internal friction in unfolded proteins. *Journal of the American Chemical Society*, *136*(24), 8708-8713.

Fanciullacci, M., Tramontana, M., Del Bianco, E., Alessandri, M., & Geppetti, P. (1991). Low pH medium induces calcium dependent release of CGRP from sensory nerves of guinea-pig dural venous sinuses. *Life sciences*, *49*(8), PL27-PL30.

Franco-Cereceda, A., & Lundberg, J. M. (1992). Capsazepine inhibits low pH-and lactic acid-evoked release of calcitonin gene-related peptide from sensory nerves in guinea-pig heart. *European journal of pharmacology*, *221*(1), 183-184.

Galeazza, M. T., O'Brien, T. D., Johnson, K. H., & Seybold, V. S. (1991). Islet amyloid polypeptide (IAPP) competes for two binding sites of CGRP. *Peptides*, *12*(3), 585-591.

Gennari, C., Nami, R., Agnusdei, D., & Fischer, J. A. (1990). Improved cardiac performance with human calcitonin gene related peptide in patients with congestive heart failure. *Cardiovascular research*, *24*(3), 239-241.

Geppetti, P., Del Bianco, E., Patacchini, R., Santicioli, P., Maggi, C. A., & Tramontana, M. (1991). Low pH-induced release of calcitonin gene-related peptide from capsaicin-sensitive sensory nerves: mechanism of action and biological response. *Neuroscience*, *41*(1), 295-301.

Gonnelli, M., & Strambini, G. B. (1995). Phosphorescence lifetime of tryptophan in proteins. *Biochemistry*, *34*(42), 13847-13857.

Gonnelli, M., & Strambini, G. B. (2005). Intramolecular Quenching of Tryptophan Phosphorescence in Short Peptides and Proteins¶. *Photochemistry and photobiology*, *81*(3), 614-622.

Ha, B. Y., & Thirumalai, D. (1992). Conformations of a polyelectrolyte chain. *Physical Review A*, *46*(6), R3012.

Higgs, P. G., & Joanny, J. F. (1991). Theory of polyampholyte solutions. *The Journal of chemical physics*, *94*(2), 1543-1554.

Ho, T. W., Edvinsson, L., & Goadsby, P. J. (2010). CGRP and its receptors provide new insights into migraine pathophysiology. *Nature Reviews Neurology*, *6*(10), 573-582.

Hoffmann, J., & Goadsby, P. J. (2014). Emerging targets in migraine. *CNS drugs*, *28*(1), 11-17.

Hofmann, H., Nettels, D., & Schuler, B. (2013). Single-molecule spectroscopy of the unexpected collapse of an unfolded protein at low pH. *The Journal of chemical physics*, *139*(12), 121930.

Hofmann, H., Soranno, A., Borgia, A., Gast, K., Nettels, D., & Schuler, B. (2012). Polymer scaling laws of unfolded and intrinsically disordered proteins quantified with single-molecule spectroscopy. *Proceedings of the National Academy of Sciences*, *109*(40), 16155-16160.

Hubbard, J. A., Martin, S. R., Chaplin, L. C., Bose, C., Kelly, S. M., & Price, N. C. (1991). Solution structures of calcitonin-gene-related-peptide analogues of calcitonin-gene-related peptide and amylin. *Biochem. J*, *275*, 785-788.

J Hagen, S. (2010). Solvent viscosity and friction in protein folding dynamics. *Current Protein and Peptide Science*, *11*(5), 385-395.

Johansson, J., Gudmundsson, G. H., Rottenberg, M. E., Berndt, K. D., & Agerberth, B. (1998). Conformation-dependent antibacterial activity of the naturally occurring human peptide LL-37. *Journal of Biological Chemistry*, *273*(6), 3718-3724.

Kamihira, M., Oshiro, Y., Tuzi, S., Nosaka, A. Y., Saitô, H., & Naito, A. (2003). Effect of electrostatic interaction on fibril formation of human calcitonin as studied by high resolution solid state ^{13}C NMR. *Journal of Biological Chemistry*, *278*(5), 2859-2865.

Krieger, F., Möglich, A., & Kiefhaber, T. (2005). Effect of proline and glycine residues on dynamics and barriers of loop formation in polypeptide chains. *Journal of the American Chemical Society*, *127*(10), 3346-3352.

Lapidus, L. J., Eaton, W. A., & Hofrichter, J. (2000). Measuring the rate of intramolecular contact formation in polypeptides. *Proceedings of the National Academy of Sciences*, *97*(13), 7220-7225.

Lapidus, L. J., Eaton, W. A., & Hofrichter, J. (2001). Dynamics of intramolecular contact formation in polypeptides: distance dependence of quenching rates in a room-temperature glass. *Physical review letters*, *87*(25), 258101.

Lapidus, L. J., Steinbach, P. J., Eaton, W. A., Szabo, A., & Hofrichter, J. (2002). Effects of chain stiffness on the dynamics of loop formation in polypeptides. Appendix: Testing a 1-dimensional diffusion model for peptide dynamics. *The Journal of Physical Chemistry B*, *106*(44), 11628-11640.

Lechleitner, P., Genser, N., Mair, J., Dienstl, A., Haring, C., Wiedermann, C. J., Puschendorf, B., Saria, A., & Dienstl, F. (1992). Calcitonin gene-related peptide in patients with and without early reperfusion after acute myocardial infarction. *American heart journal*, *124*(6), 1433-1439.

Liang, C., Li, H., Tao, Y., Shen, C., Li, F., Shi, Z., Han, B., & Chen, Q. (2013). New hypothesis of chronic back pain: low pH promotes nerve ingrowth into damaged intervertebral disks. *Acta Anaesthesiologica Scandinavica*, *57*(3), 271-277.

Lozano-Ondoua, A. N., Symons-Liguori, A. M., & Vanderah, T. W. (2013). Cancer-induced bone pain: Mechanisms and models. *Neuroscience letters*, *557*, 52-59.

Lynch, B., & Kaiser, E. T. (1988). Biological properties of two models of calcitonin gene related peptide with idealized amphiphilic alpha-helices of different lengths. *Biochemistry*, *27*(20), 7600-7607.

Mair, J., Lechleitner, P., Längle, T., Wiedermann, C., Dienstl, F., & Saria, A. (1990). Plasma CGRP in acute myocardial infarction. *The Lancet*, *335*(8682), 168.

Manning, M. C. (1989). Conformation of the alpha form of human calcitonin gene-related peptide (CGRP) in aqueous solution as determined by circular dichroism spectroscopy. *Biochemical and biophysical research communications*, *160*(1), 388-392.

Mao, A. H., Crick, S. L., Vitalis, A., Chicoine, C. L., & Pappu, R. V. (2010). Net charge per residue modulates conformational ensembles of intrinsically disordered proteins. *Proceedings of the National Academy of Sciences*, *107*(18), 8183-8188.

Marek, P. J., Patsalo, V., Green, D. F., & Raleigh, D. P. (2012). Ionic strength effects on amyloid formation by amylin are a complicated interplay among Debye screening, ion selectivity, and Hofmeister effects. *Biochemistry*, *51*(43), 8478-8490.

Marsh, J. A., & Forman-Kay, J. D. (2010). Sequence determinants of compaction in intrinsically disordered proteins. *Biophysical journal*, *98*(10), 2383-2390.

McLatchie, L. M., Fraser, N. J., Main, M. J., Wise, A., Brown, J., Thompson, N., Solari, R., Lee, M.G., & Foord, S. M. (1998). RAMPs regulate the transport and ligand specificity of the calcitonin-receptor-like receptor. *Nature*, *393*(6683), 333-339.

Miller, C., Zerze, G.H., & Mittal, J. (2014). Molecular simulations indicate marked differences in the structure of amylin mutants, correlated with known aggregation propensity. *The Journal of Physical Chemistry B. 117*(50), 16066-16075.

Mimeault, M., St-Pierre, S., & Fournier, A. (1993). Conformational characterization by circular dichroism spectroscopy of various fragments and analogs of calcitonin gene-related peptide. *European Journal of Biochemistry*, *213*(3), 927-934.

Möglich, A., Joder, K., & Kiefhaber, T. (2006). End-to-end distance distributions and intrachain diffusion constants in unfolded polypeptide chains indicate intramolecular hydrogen bond formation. *Proceedings of the National Academy of Sciences*, *103*(33), 12394-12399.

Moore, E. L., & Salvatore, C. A. (2012). Targeting a family B GPCR/RAMP receptor complex: CGRP receptor antagonists and migraine. *British journal of pharmacology*, *166*(1), 66-78.

Müller-Späth, S., Soranno, A., Hirschfeld, V., Hofmann, H., Rüegger, S., Reymond, L., Nettels, D., & Schuler, B. (2010). Charge interactions can dominate the dimensions of

intrinsically disordered proteins. *Proceedings of the National Academy of Sciences*, *107*(33), 14609-14614.

Narayanan, R., Ganesh, O. K., Edison, A. S., & Hagen, S. J. (2008). Kinetics of folding and binding of an intrinsically disordered protein: the inhibitor of yeast aspartic proteinase YPrA. *Journal of the American Chemical Society*, *130*(34), 11477-11485.

O'Connell, J. P., Kelly, S. M., Raleigh, D. P., Hubbard, J. A., Price, N. C., Dobson, C. M., & Smith, B. J. (1993). On the role of the C-terminus of alpha-calcitonin-gene-related peptide (alpha CGRP). The structure of des-phenylalaninamide37-alpha CGRP and its interaction with the CGRP receptor. *Biochem. J*, *291*, 205-210.

Olesen, J., Diener, H. C., Husstedt, I. W., Goadsby, P. J., Hall, D., Meier, U., Pollentier, S., & Lesko, L. M. (2004). Calcitonin gene–related peptide receptor antagonist BIBN 4096 BS for the acute treatment of migraine. *New England Journal of Medicine*, *350*(11), 1104-1110.

Pappu, R. V., Srinivasan, R., & Rose, G. D. (2000). The Flory isolated-pair hypothesis is not valid for polypeptide chains: implications for protein folding. *Proceedings of the National Academy of Sciences*, *97*(23), 12565-12570.

Raddant, A. C., & Russo, A. F. (2011). Calcitonin gene-related peptide in migraine: intersection of peripheral inflammation and central modulation. *Expert reviews in molecular medicine*, *13*, e36.

Reuter, U. (2014). Anti-CGRP antibodies: a new approach to migraine prevention. *The Lancet Neurology*, *13*(9), 857-859.

Rogers, J. M., Steward, A., & Clarke, J. (2013). Folding and binding of an intrinsically disordered protein: fast, but not 'diffusion-limited'. *Journal of the American Chemical Society*, *135*(4), 1415-1422.

Romero, P., Obradovic, Z., Li, X., Garner, E. C., Brown, C. J., & Dunker, A. K. (2001). Sequence complexity of disordered protein. *Proteins: Structure, Function, and Bioinformatics*, *42*(1), 38-48.

Rosenfeld, M. G., Mermod, J. J., Amara, S. G., Swanson, L. W., Sawchenko, P. E., Rivier, J., Vale, W.W., & Evans, R. M. (1983). Production of a novel neuropeptide encoded by the calcitonin gene via tissue-specific RNA processing. *Nature,* 304 (129-135).

Russo, A. F., & Dickerson, I. M. (2006). CGRP: A multifunctional neuropeptide. In *Handbook of neurochemistry and molecular neurobiology* (pp. 391-426). Springer US.

Saha, S., Waugh, D. J. J., Zhao, P., Abel, P. W., & Smith, D. D. (1998). Role of conformational constraints of position 7 of the disulphide bridge of h-α-CGRP derivatives in their agonist versus antagonist properties. *The journal of peptide research*, *52*(2), 112-120.

Salmon, A. M., Damaj, I., Sekine, S., Picciotto, M. R., Marubio, L., & Changeux, J. P. (1999). Modulation of morphine analgesia in αCGRP mutant mice. *Neuroreport*, *10*(4), 849-854.

Salmon, A. M., Damaj, M. I., Marubio, L. M., Epping-Jordan, M. P., Merlo-Pich, E., & Changeux, J. P. (2001). Altered neuroadaptation in opiate dependence and neurogenic inflammatory nociception in αCGRP-deficient mice. *Nature neuroscience*, *4*(4), 357-358.

Schellman, J. A. (1987). Selective binding and solvent denaturation. *Biopolymers*, *26*(4), 549-559.

Schreiber, G., & Fersht, A. R. (1996). Rapid, electrostatically assisted association of proteins. *Nature Structural & Molecular Biology*, *3*(5), 427-431.

Schulten, K., Schulten, Z., & Szabo, A. (1981). Dynamics of reactions involving diffusive barrier crossing. *The Journal of Chemical Physics*, *74*(8), 4426-4432.

Shoemaker, B. A., Portman, J. J., & Wolynes, P. G. (2000). Speeding molecular recognition by using the folding funnel: the fly-casting mechanism. *Proceedings of the National Academy of Sciences*, *97*(16), 8868-8873.

Soranno, A., Buchli, B., Nettels, D., Cheng, R. R., Müller-Späth, S., Pfeil, S. H., Hoffmann, A., Lipman, E.A., Makarov, D.E., & Schuler, B. (2012). Quantifying internal friction in unfolded and intrinsically disordered proteins with single-molecule spectroscopy. *Proceedings of the National Academy of Sciences*, *109*(44), 17800-17806.

Strambini, G. B., Kerwin, B. A., Mason, B. D., & Gonnelli, M. (2004). The Triplet-state Lifetime of Indole Derivatives in Aqueous Solution. *Photochemistry and photobiology*, *80*(3), 462-470.

Su, Y., & Chang, P. T. (2001). Acidic pH promotes the formation of toxic fibrils from β-amyloid peptide. *Brain research*, *893*(1), 287-291.

Szabo, A., Schulten, K., & Schulten, Z. (1980). First passage time approach to diffusion controlled reactions. *The Journal of Chemical Physics*, *72*(8), 4350-4357.

Teufel, D. P., Johnson, C. M., Lum, J. K., & Neuweiler, H. (2011). Backbone-driven collapse in unfolded protein chains. *Journal of molecular biology*, *409*(2), 250-262.

Tippins, J. R., Di Marzo, V., Panico, M., Morris, H. R., & MacIntyre, I. (1986). Investigation of the structure/activity relationship of human calcitonin gene-related peptide (CGRP). *Biochemical and biophysical research communications*, *134*(3), 1306-1311.

Tjen-A-Looi, S., Ekman, R., Lippton, H., Cary, J., & Keith, I. (1992). CGRP and somatostatin modulate chronic hypoxic pulmonary hypertension. *American Journal of Physiology-Heart and Circulatory Physiology*, *263*(3), H681-H690.

Tompa, P. (2005). The interplay between structure and function in intrinsically unstructured proteins. *FEBS letters*, *579*(15), 3346-3354.

Tso, A. R., & Goadsby, P. J. (2014). New targets for migraine therapy. *Current treatment options in neurology*, *16*(11), 1-11.

Uversky, V. N. (2002). Natively unfolded proteins: a point where biology waits for physics. *Protein science*, *11*(4), 739-756.

Uversky, V. N. (2009). Intrinsically disordered proteins and their environment: effects of strong denaturants, temperature, pH, counter ions, membranes, binding partners, osmolytes, and macromolecular crowding. *The protein journal*, *28*(7-8), 305-325.

Uversky, V. N., Gillespie, J. R., & Fink, A. L. (2000). Why are "natively unfolded" proteins unstructured under physiologic conditions?. *Proteins: Structure, Function, and Bioinformatics*, *41*(3), 415-427.

Uversky, V. N., Li, J., & Fink, A. L. (2001). Metal-triggered Structural Transformations, Aggregation, and Fibrillation of Human α-Synuclein A possible molecular link between Parkinson's disease and heavy metal exposure. Journal of Biological Chemistry, 276(47), 44284-44296.

Uversky, V. N., Oldfield, C. J., & Dunker, A. K. (2005). Showing your ID: intrinsic disorder as an ID for recognition, regulation and cell signaling. *Journal of Molecular Recognition*, *18*(5), 343-384.

Vaiana, S. M., Best, R. B., Yau, W. M., Eaton, W. A., & Hofrichter, J. (2009). Evidence for a partially structured state of the amylin monomer. *Biophysical journal*, *97*(11), 2948-2957.

Van Rossum, D., Hanisch, U. K., & Quirion, R. (1997). Neuroanatomical localization, pharmacological characterization and functions of CGRP, related peptides and their receptors. *Neuroscience & Biobehavioral Reviews*, *21*(5), 649-678.

Waldauer, S. A., Bakajin, O., & Lapidus, L. J. (2010). Extremely slow intramolecular diffusion in unfolded protein L. *Proceedings of the National Academy of Sciences*, *107*(31), 13713-13717.

Watkins, H. A., Rathbone, D. L., Barwell, J., Hay, D. L., & Poyner, D. R. (2013). Structure-activity relationships for α-calcitonin gene-related peptide. *British journal of pharmacology*, *170*(7), 1308-1322.

Westermark, P., Engström, U., Johnson, K. H., Westermark, G. T., & Betsholtz, C. (1990). Islet amyloid polypeptide: pinpointing amino acid residues linked to amyloid fibril formation. *Proceedings of the National Academy of Sciences*, *87*(13), 5036-5040.

Westermark, P., Wernstedt, C., Wilander, E., & Sletten, K. (1986). A novel peptide in the calcitonin gene related peptide family as an amyloid fibril protein in the endocrine pancreas. *Biochemical and biophysical research communications*, *140*(3), 827-831.

Wimalawansa, S. J. (1997). Amylin, calcitonin gene-related peptide, calcitonin, and adrenomedullin: a peptide superfamily. *Critical Reviews™ in Neurobiology*, *11*(2-3).

Wright, P. E., & Dyson, H. J. (2009). Linking folding and binding. *Current opinion in structural biology*, *19*(1), 31-38.

Zhou, H. X. (2002). A Gaussian-chain model for treating residual charge-charge interactions in the unfolded state of proteins. *Proceedings of the National Academy of Sciences*, *99*(6), 3569-3574.

APPENDIX I

VISCOSITY DEPENDENCE OF k_{obs} OF CGRP

The observed quenching rate was measured as a function of temperature and solution viscosity to extract the reaction and diffusion limited rates for analysis of the structure and dynamics of CGRP. The figures below are the plots of the viscosity dependence of CGRP in the solution conditions discussed in this work.

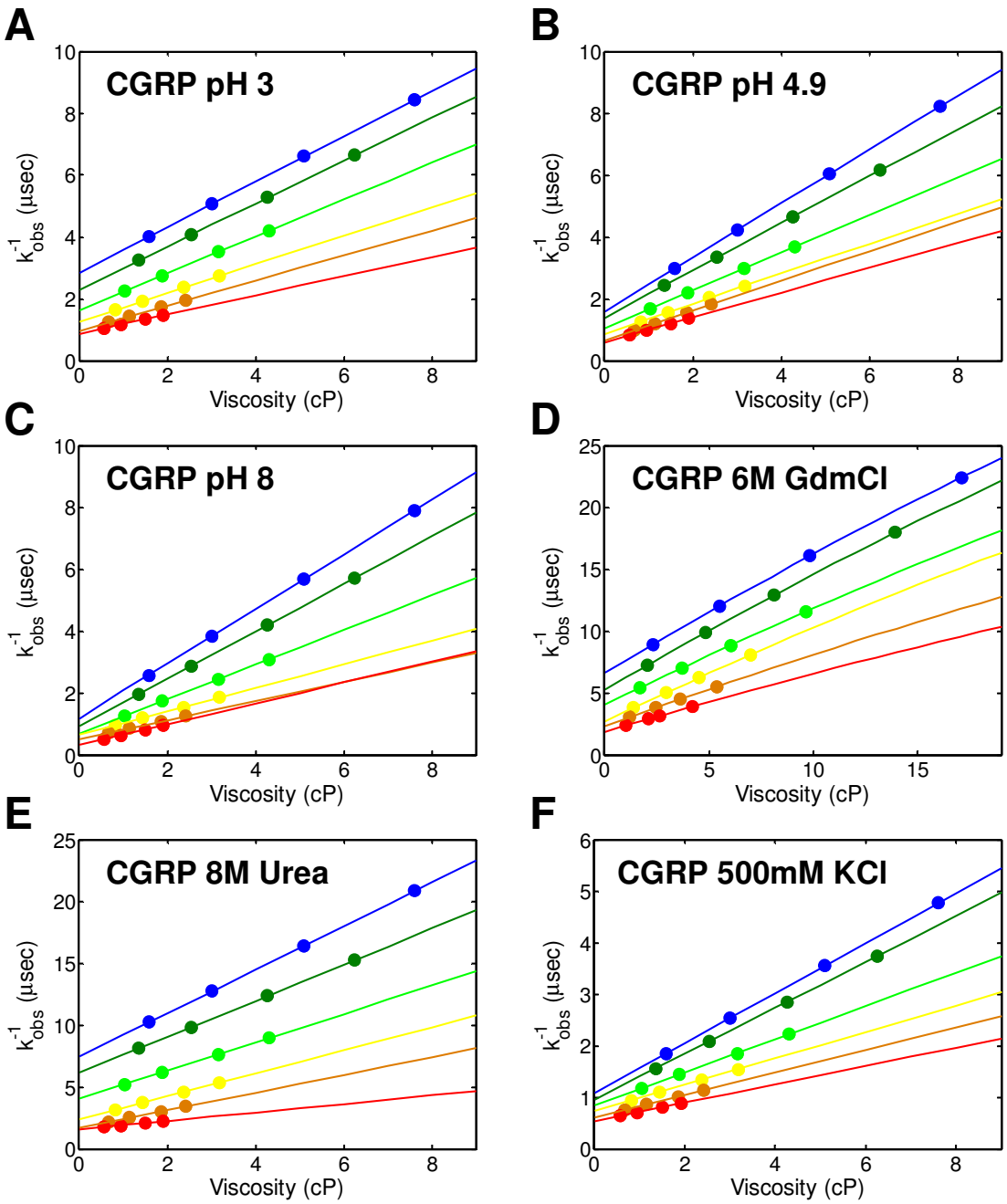

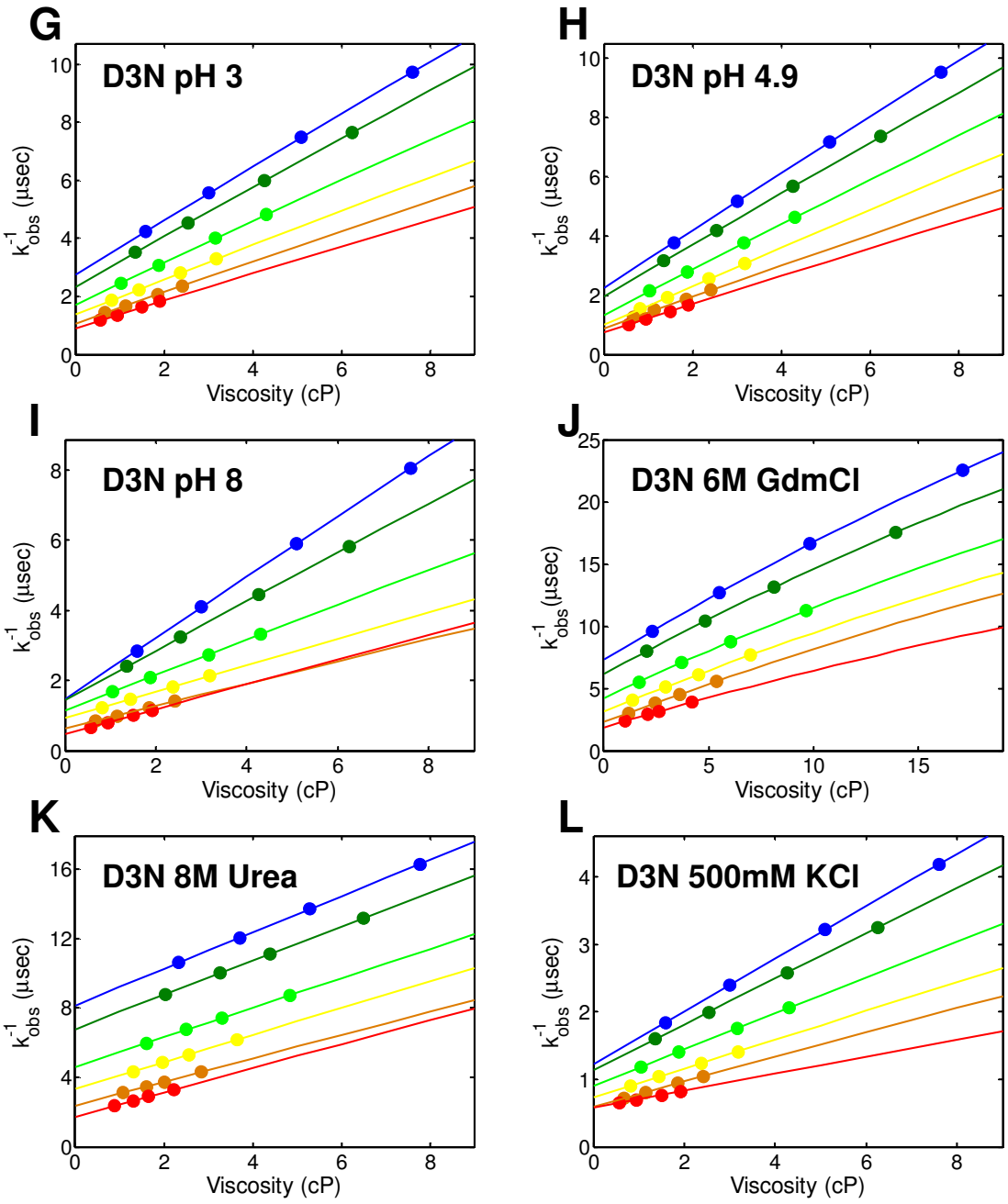

Figure A.1. Viscosity dependence of k_{obs} for CGRP and D3N. The inverse of k_{obs} is plotted as a function of solution viscosity for: CGRP in (A) pH 3, (B) pH 4.9, and (C) pH 8 buffers and (D) 6M GdmCl, (E) 8M Urea and (F) 500mM KCl and D3N in (G) pH 3, (H) pH 4.9, and (I) pH 8 buffers and (J), 6M GdmCl, (K) 8M Urea and (L) 500mM KCl.

APPENDIX II

DETERMINING THE VISCOSITY OF SOLUTIONS

In order to separate the reaction limited and diffusion limited rates, accurate values for the viscosity of the sucrose solutions were needed. Dynamic light scattering (DLS) experiments were performed to verify the viscosity of the sucrose solutions in both aqueous solution and 8M Urea. DLS measures the intensity fluctuations of scattered light over time, with bigger particles diffusing through the solution slower and therefore having slower intensity fluctuations (and vice versa). These intensity fluctuations are time correlated, and in monodisperse samples the second order autocorrelation function corresponds to a single exponential decay, Γ which is given by the expression

$$g^{(2)}(q,\tau) = B + A\exp(-2\Gamma\tau) \qquad \text{Eq 1}$$

where q is the wave vector, and τ is the delay time. The wave vector q is expressed by

$$q = \frac{4\pi n_0}{\lambda}\sin(\theta/2) \qquad \text{Eq 2}$$

where n_0 is the index of refraction, λ is the wavelength of the laser beam (λ = 622 nm) and θ is the scattering angle (90^o). The decay of the autocorrelation function, Γ is related to the diffusion of the particles in solution via the diffusion coefficient, D.

$$\Gamma = q^2 D \qquad \text{Eq 3}$$

The diffusion of particles in solution is characterized by the Stokes-Einstein relation, which relates the diffusion coefficient to the hydrodynamic radius r_h of the particles.

$$D = \frac{k_B T}{6\pi\eta r_h} \qquad \text{Eq 4}$$

As apparent in Eq 4, the diffusion of the particles in solution also depends on the solvent viscosity η and temperature T. As the only variable that will change with each solution besides η is the index of refraction n_0, this was empirically measured to correct for the change in the index of refraction as sucrose is added.

Polystyrene spheres with a radius of 73.5 +/- 1 nm in a 1% suspension from Duke Scientific were used as the control in these experiments. The spheres were carefully sonicated to ensure monodispersity. The sucrose buffer were filtered with a Whatman 0.02 um filter and polystyrene spheres were added to create a 0.01% solution of spheres in buffer. DLS temperature scans were performed on these solutions by taking 200 correlation functions at each temperature used in TTQ experiments, after waiting 40-60 minutes for thermal equilibration at each temperature. DLS measurements of the diffusion coefficient of polystyrene spheres in sucrose solutions were measured using a Wyatt DynaPro NanoStar. The diffusion coefficient D was calculated from the data by Dynamics software v 7.2 (Wyatt). D was substituted into the Stokes-Einstein equation above, using the radius of the spheres as the r_H of particles in solution, thereby giving accurate values of the viscosity of the solutions used for TTQ experiments.

APPENDIX III

CALCULATION OF k_R AND r_G FROM k_{obs}

TTQ experiments involving the titration of GdmCl, Urea, and KCl were performed to explore the effect of the addition of denaturant on the structure of CGRP. Thherefore it is important to determine how the radius of gyration, which is a structural property, depends on the observed quenching rate. It is not feasible to do viscosity dependent measurements at each solvent concentration, due to the large amounts of sample and time involved. Therefore, only extreme solvent concentrations (0M and 6M GdmCl, 0M and 8M Urea, and 0M and 0.5 M KCl) have experimentally determined values for k_R from which the radius of gyration, assuming a Gaussian chain, is calculated. The radius of gyration of CGRP at these intermediate solvent concentrations were calculated as described below.

Using k_R from the viscosity dependent analysis and the observed quenching rate k_{obs} from the independent fit of CGRP at extreme solvent concentrations, a proportionality constant A, was calculated that gives an empirical relationship between the two rates (Eq 1).

$$A = \frac{k_{obs}}{k_R} \qquad \text{Eq 1}$$

There is very little variation in A for all solvent concentrations, so it is assumed that any changes in structure, or k_R, due to changing solvent are reflected by changes in k_{obs}. A linear interpolation of A versus solvent concentration was calculated such that each experimental solvent concentration has a characteristic A that reflects an increase in A with increasing solvent concentration. Using these characteristic values for A, values for k_R can now be calculated from each experimental k_{obs} for each solvent concentration.

A Matlab program was written to calculate the radius of gyration from a set of experimental k_{obs} values by finding an average end-to-end distance for a given k_R. The code takes the experimental values for k_{obs} at 10C, and multiples this by the value for A calculated for that solvent concentration to get a calculated value for k_R. To find the end-to-end distance that gives this value for k_R assuming a Gaussian chain, a matrix of end-to-end distance values from a_0 to ½ the contour length is generated, and a second matrix of k_R values were calculated using these generated values for the end-to-end distance. The computer then uses a minimization search to find the theoretical k_R closest to the experimental value for k_R. The end-to-end distance which gave the calculated value for k_R that most closely matched was then used to find the radius of gyration (Eq 2).

$$r_G = \frac{\sqrt{\langle r^2 \rangle}}{\sqrt{6}} \qquad \text{Eq 2}$$

Using these values of the radius of gyration we can now evaluate how changing solution conditions affect the structure of CGRP.

APPENDIX IV

CALCULATION OF QUENCHING OF TRYPTOPHAN BY N_LOOP

While previous work has found that free cystines have a similar quenching rate as free cysteines,[1] the effect the specific geometry of the N_loop on the quenching rate q(r) must be accounted for as the geometry of the N_loop might decrease the actual accessible area of the cystine. The distance dependence of the quenching rate of tryptophan by cysteine is known to be exponential from measurements done in trehalose glass by Lapidus, et al 2001,[2] and takes the form

$$q(r) = q_0 \exp\left(b(r - a_0)\right) \qquad \text{Eq 1}$$

a_0 is the van der Waals contact (4 Å), while both q_0 (4.2 ns^{-1}) and b (4.0 $Å^{-1}$) were determined experimentally.[2] As the quenching rate of the tryptophan in CGRP is still assumed to have an exponential distance dependence, a rescaling factor that takes into account the geometry of the N_loop was calculated by finding a characteristic q_0* which is proportional to q_0, the quenching coefficient found previously.[2]

Since CGRP and IAPP have a rigid N_loop between residues 2 & 7, we assume the effective polymer length of these peptides is 31 amino acids. We know from previous work that a 31mer has an effective end-to-end distance of 3.45 nm in 6MGdmCl, and R_g of ~1.4 nm assuming a Gaussian P(r).[3] Assuming that hIAPP in denaturant behaves as an ideal chain, hIAPP will therefore have an end-to-end distance of 3.45 nm in 6M GdmCl.

A MatLab program was written to find the rescaling factor q_0* for the bimolecular quenching coefficient of CGRP and other Ct family peptides with similar N_loops. The program defines k_R as a function of two functions, P(r) and q(r), as shown in Eq. 2.

$$k_R = \int_{a_0}^{l_c} P(r)q(r)dr \qquad \text{Eq 2}$$

The equation for q(r) used in the MatLab program is given by Eq 1, except now the proportionality constant is taken into account:

$$q(r) = q_0^* \bullet q_0 \exp\left(b\left(r - a_0\right)\right) \qquad \text{Eq 3}$$

To find q_0* for all Ct family peptides that have an N_loop quencher, a table of values was created for q_0* between 0 and 1 (ranging from no quenching by the N_loop to the N_loop having the same quenching rate as a free cysteine) at 0.0001 intervals. Using a Gaussian P(r) with an end to end distance of 3.45 nm (corresponding to hIAPP in denaturant) and Eq. 3 above, a set of k_R values was calculated, one for each value of q_0*. Using a minimization search, the program finds the rescaling factor q_0* that gives a calculated value of k_R that most closely matches the experimental value for k_R of 0.32 μs^{-1} for hIAPP in 6M GdmCl pH 4.9 buffer at 20C (measured in Vaiana, et al 2009).[1] This gives a rescaling factor q_0* for the N_loop of Ct family peptides of 0.1681.

REFERENCES

[1]Vaiana, S. M., Best, R. B., Yau, W. M., Eaton, W. A., & Hofrichter, J. (2009). Evidence for a partially structured state of the amylin monomer. *Biophysical journal*, *97*(11), 2948-2957.

[2]Lapidus, L. J., Eaton, W. A., & Hofrichter, J. (2001). Dynamics of intramolecular contact formation in polypeptides: distance dependence of quenching rates in a room-temperature glass. *Physical review letters*, *87*(25), 258101.

[3]Buscaglia, M., Lapidus, L. J., Eaton, W. A., & Hofrichter, J. (2006). Effects of denaturants on the dynamics of loop formation in polypeptides. *Biophysical journal*, *91*(1), 276-288.

APPENDIX V

PUBLISHED WORK

The work in this appendix was published in PLOS One under Tsen, S.-W.D., Kingsley, D.H., Kibler, K., Jacobs, B., Sizemore. S., Vaiana, S.M., Anderson, J., Tsen, K.-T., Achilefu, S. (2014) Pathogen Reduction in Human Plasma Using an Ultrashort Pulsed Laser. PLoS ONE 9(11): e111673. doi:10.1371/journal.pone.0111673. This work was done in collaboration with Dr. Kong-Thon Tsen and expanded upon previously published work on the inactivation of viruses using ultra-short pulsed lasers. My contribution to this work consisted of the measurement and analysis of light scattering and circular dichroism measurements of fibrinogen, both before and after irradiation with an ultra-short laser, in order to check for any changes in secondary structure or aggregation after irradiation.

ABSTRACT

Pathogen reduction is a viable approach to ensure the continued safety of the blood supply against emerging pathogens. However, the currently licensed pathogen reduction techniques are ineffective against non-enveloped viruses such as hepatitis A virus, and they introduce chemicals with concerns of side effects which prevent their widespread use. In this report, we demonstrate the inactivation of both enveloped and non-enveloped viruses in human plasma using a novel chemical-free method, a visible ultrashort pulsed laser. We found that laser treatment resulted in 2-log, 1-log, and 3-log reductions in human immunodeficiency virus, hepatitis A virus, and murine cytomegalovirus in human plasma, respectively. Laser-treated plasma showed ≥70% retention for most coagulation factors tested. Furthermore, laser treatment did not alter the structure of a model

coagulation factor, fibrinogen. Ultrashort pulsed lasers are a promising new method for chemical-free, broad-spectrum pathogen reduction in human plasma.

INTRODUCTION

Pathogen reduction (PR) is an ideal strategy to combat emerging pathogens and ensure the continued safety of blood products. However, the PR techniques that are currently in use for clinical blood products have limitations that preclude their widespread use (for reviews, see [1–3]). The solvent-detergent (SD) method,[4,5] which inactivates enveloped viruses by disrupting lipid membranes, was discontinued in the United States due to an association with unexpected thromboses in some patients.[4,6] Light-activated photochemicals such as methylene blue[7,8] and amotosalen,[9,10] which inactivate pathogens through crosslinking, also involve introducing chemicals with concerns of side effects. Such side effects include allergic reactions (in the case of methylene blue) and the generation of antibodies against the treated blood product (in the case of the chemical S-303),[1] as well as the concern of unknown, unpredictable long-term effects that invariably arise with any administered compound. Furthermore, all of the above mentioned methods are ineffective against non-enveloped viruses such as hepatitis A virus (HAV).[6]

Ultrashort pulsed (USP) lasers have recently emerged as an attractive potential technique for pathogen inactivation.[11] The visible USP laser PR technology does not involve potentially toxic or carcinogenic chemicals. Visible USP lasers are non-ionizing and do not covalently modify proteins, thereby reducing concerns of neoantigen formation.

Furthermore, USP laser treatment can inactivate a broad spectrum of viruses and bacteria,[11-14] including non-enveloped viruses that are traditionally difficult to inactivate. Under these treatment conditions, the structure of bovine serum albumin protein was well preserved.[14]

In this work we demonstrate inactivation of human immunodeficiency virus (HIV), HAV, and murine cytomegalovirus (MCMV) in human plasma using a USP laser operating at a wavelength of 425 nm. These pathogens are structurally representative of a broad range of viruses including enveloped RNA virus (HIV), non-enveloped RNA virus (HAV), and enveloped DNA virus (MCMV). MCMV serves as a surrogate for human herpesviruses including HCMV. We used MCMV for this study because it is not infectious to humans, allowing us to conduct more detailed studies in a less restrictive environment. MCMV is also readily available in our lab and straightforward to analyze on the bench; more importantly, as an enveloped DNA virus, MCMV serves structurally as a model for clinically relevant enveloped DNA viruses which include Hepatitis B virus, HCMV, and poxviruses. The USP laser technology has been shown to inactivate viruses through mechanical means; in other words, inactivation by the USP laser is most dependent on the structure of a virus.

Furthermore, we assess the function of coagulation factors in treated plasma versus untreated plasma after USP laser irradiation.

MATERIALS AND METHODS

FEMTOSECOND LASER IRRADIATION

The excitation source employed in this work was a diode-pumped continuous wave mode-locked Ti-sapphire laser (Trestles-100, Del Mar Photonics, USA). The laser produced a continuous train of 60 fs pulses at a repetition rate of 80 MHz. The output of the second harmonic generation system of the Ti-sapphire laser was used to irradiate the sample. The excitation laser was chosen to operate at a wavelength of λ = 425 nm and with an average power of approximately 120 mW. This laser wavelength was chosen because we have recently demonstrated that it was capable of efficiently inactivating enveloped/non-enveloped, DNA/RNA viruses including HIV, MCMV, murine norovirus, encephalomyocarditis virus, and human papillomavirus.[11] It has a pulse width of full-width at half maximum = 100 fs. A lens was used to focus the laser beam into a spot within the sample volume. Samples were laser-irradiated for 90 min. A magnetic stirring device was used to facilitate exposure of the sample to the laser beam. Irradiation was carried out at 22°C and with the single laser beam excitation. After laser irradiation, samples were immediately stored at -80°C.

VIRUSES AND INFECTIVITY ASSAYS

HIV inactivation. HIV stock was propagated in MT-4 cells following transfection of HeLa cells with pNL4-3 plasmid (both MT-4 cells an pNL4-3 were kind gifts of Dr. Kuan-Teh Jeang). Approximately $4x10^6$ reverse transcriptase (RT) units of NL4-3 stock was added to pooled normal plasma (George King Biomedical, Inc., Overland Park, KS).

The infected plasma was placed into each of 6 glass vials for transport to the laser lab. Each of the 3 vials containing a stir bar was laser-irradiated as described above. During the treatment time, a vial serving as a room temperature control was placed in a beaker in the same room. During each treatment time, 4 of the 6 vials remained on ice. When each of 3 vials had been irradiated, all 6 vials were transported back to the HIV lab, where they were stored at -80°C until used in a Multinuclear Activation Galactosidase Indicator (MAGI) assay. For the MAGI assay, the MAGI cells (U373-MAGI-CXCR4 CEM, catalog #3596, contributed by Dr. Michael Emerman) were obtained through the NIH AIDS Research and Reference Reagent Program, Division of AIDS, NIAID, NIH, Bethesda, USA. The standard MAGI assay protocol was followed. Briefly, plasma/virus mixture was added to MAGI cells, incubated for 48 h, fixed with 4% paraformaldehyde for 2 h, and X-gal (Teknova, USA, Cat # X1205) staining was visualized. Three irradiated samples, three room temperature control samples, and the original virus stock were used in the assay. The final dilution factor for treated samples and controls was 1:2 compared to the original virus stock dilution used in the assay.

HAV inactivation. HAV stock was obtained from the American Type Culture Collection (Manassas, VA) as VR1402, a cell culture-adapted cytopathic clone of strain HM-175 that was originally designated as HM-175/18f. The virus was propagated on fetal rhesus monkey kidney (FRhK-4) cells as previously described.[15] The HAV stock was stored at -70°C in DMEM (Gibco, Grand Island NY) with 10% fetal bovine serum (FBS) (Gibco) prior to use. To partially purity HAV, the virus was pelleted at 490,000xg for 6 h, followed by resuspension of the HAV in human plasma (George King Biomedical Inc.,

Overland Park, KS) and filtration through a 0.1 μm filter. Samples of human plasma alone or human plasma spiked with HAV were laser-irradiated as described above. Plaque assay was performed by making an initial 100-fold dilution followed by 10-fold serial dilutions made in Earle's balanced salt solution (Gibco) and infecting 100-mm dishes confluent with FRhK-4 cell and infecting with 2 ml of virus dilution as described previously.[16] After 2 h, the plates were overlaid with DMEM medium with 5% FBS, and 1% agarose (Sigma-Aldrich, St. Louis, MO). At 17 days post-inoculation, HAV was inactivated by 10% formaldehyde treatment, the agarose overlay was removed, and HAV plaques were visualized by crystal violet staining (Fisher Scientific, Kalamazoo, MI).

MCMV inactivation. Murine embryonic fibroblast 10.1 (MEF 10.1) cells[17] (a generous gift from Dong Yu, Washington University School of Medicine, St Louis, MO) were cultured in Dulbecco's Modified Eagle Medium (DMEM), supplemented with 10% FBS, 1 mM sodium pyruvate, and nonessential amino acids. GFP-expressing MCMV virus (hereafter referred to as ''MCMV'') was generated as previously described.[18] To produce viral stocks, MEF 10.1 cells were infected with MCMV at a low multiplicity of infection. Cell supernatants were harvested 24 h post-infection after 100% cytopathic effect and cleared of cell debris by centrifugation. Extracellular virions were pelleted by ultracentrifugation with sorbitol cushion and resuspended in phosphate-buffered saline (PBS). Samples of human plasma alone or human plasma spiked with MCMV were laser-irradiated as described above. Viral titers were determined using a median tissue culture infectious dose (TCID50) assay, as previously described.[13] Briefly, MEF 10.1 cells were seeded into 96-well plates at a density of 1.25×10^5 cells/ml and incubated overnight.

Cells were approximately 80% confluent at the time of infection. Laser-treated or control (untreated) viruses were serially diluted and added to cells, which were incubated for 4 days. Viral titers were determined on day 4 post-infection by scoring each well for GFP-positive cells using a fluorescent microscope.

COAGULATION FACTOR ASSAYS

To evaluate the activity of coagulation factors in plasma with or without USP laser treatment, we performed standard coagulation factor assays.[19] Plasma samples derived from the same lot of pooled normal human plasma (George King Biomedical, Inc.) were kept untreated or laser-treated as described previously. Factor (F) II, FV, FVII, FVIII, FIX, FX, FXI, FXII, and fibrinogen were evaluated in Barnes-Jewish Hospital Laboratory, St. Louis, MO. Assays were completed on the IL ACL TOP 700, according to the manufacturer's protocols contained within the package inserts (Instrumentation Laboratories Company, Bedford, MA). Plasma levels of FII, FV, FVII, and FX were determined using functional assays based on the prothrombin time with human plasma immunodepleted of FII, FV, FVII, or FX. Similarly, plasma levels of FVIII, FIX, FXI, and FXII were determined using the activated partial thromboplastin time with human plasma immunodepleted of FVIII, FIX, FXI, and FXII. Plasma deficient in FII, FV, FVII, FVIII, FIX, FX, FXI, or FXII consisted of human plasma that was immunodepleted of the individual coagulation factors, and were purchased from Instrumentation Laboratories Company. HemosIL RecombiPlasTin 2G and HemosIL SynthASil (Instrumentation Laboratories Company) were additional reagents used in the assay. Fibrinogen level was

determined by a quantitative assay based on the Clauss method[20,21] using Q.F.A. Thrombin (Bovine) reagent (Instrumentation Laboratories Company).

PROTEIN GEL ELECTROPHORESIS

To evaluate protein aggregation of samples with or without USP laser treatment, we employed gel electrophoresis analysis. For SDS-PAGE, control (untreated) or laser-treated samples containing equivalent quantities of plasma were boiled in loading buffer (dH_2O (47.5%), 0.5 M Tris pH 6.8 (12.5%), glycerol (10%), SDS (20%), b-mercaptoethanol (5%), and bromophenol blue (5%)) under reducing conditions, and separated on a Mini-Protean TGX 10% precast polyacrylamide gel (Bio-Rad, Hercules, CA). For native PAGE, control (untreated) or laser-treated samples containing equivalent quantities of plasma were separated on the 10% gel under non-denaturing conditions. Protein bands were visualized with Coomassie blue staining (LabSafe Gel Blue, G-Biosciences).

FIBRINOGEN PROTEIN PREPARATION

Purified human fibrinogen was obtained from Haemtech Technologies, Inc (Essex Junction, VT). For protein structure characterization measurements, fibrinogen solutions (2.5 mg/ml) were prepared by dissolving pure, lyophilized peptide in PBS buffer which was filtered with a 0.02 mm Whatman Anotop25 filter. The actual concentration was checked by measuring the absorption of the sample with a Cary50 UV-Vis spectrophotometer (Agilent, Inc., Santa Clara, CA), using an extinction coefficient of fibrinogen at 280 nm of 5.12×10^5 M^{-1} cm^{-1}. Dynamic light scattering (DLS), circular

dichroism (CD) and absorbance measurements were carried out immediately before and after irradiation of the sample.

DYNAMIC LIGHT SCATTERING MEASUREMENTS

To determine the effect of USP laser treatment on the aggregation of fibrinogen protein, we employed dynamic light scattering analysis. Before and after irradiation, fibrinogen samples were centrifuged at 12,000xg for 15 min to clear them from dust, and 5 ml aliquots were taken to measure the DLS signal of the sample. Autocorrelation functions of the scattered intensity at 90° scattering angle were collected at 25°C with a 5 sec acquisition time, using a Wyatt Technology DynaPro NanoStar with a 658 nm, 120 mW GaAs linearly polarized laser. Measurements of fibrinogen were done in a 1 ml MicroCuvette (Wyatt Technology Corp., Santa Barbara, CA), previously calibrated with clear water. Data were analyzed using Wyatt Technology Dynamics 7 software, using a regularization fit method to determine hydrodynamic radii of fibrinogen from the autocorrelation functions.

CIRCULAR DICHROISM MEASUREMENTS

To examine laser-induced alterations in the secondary structure of fibrinogen protein, circular dichroism measurements were made. Immediately before and after irradiation, an aliquot of the fibrinogen sample was diluted (1:20 for the 2.5 mg/ml sample and 1:10 for 1.5 mg/ml and 0.6 mg/ml samples) and transferred to a 1 mm quartz cuvette (Starna Cells, Atascadero, CA, USA) and circular dichroism spectra were measured at room temperature using J-710 spectropolarimeter (Jasco Instruments, Easton, MD). Far UV

spectra from 200 nm to 250 nm were obtained by averaging over eight scans, with a 1 nm bandwidth, 0.5 nm pitch and 50 nm/min scan speed, and then buffer subtracted. Fibrinogen concentration was estimated from the absorption spectra of undiluted samples, measured before and after laser irradiation. These values were used to convert CD signals to mean residue ellipticity (MRE). We note that a slight decrease in the signal amplitude was observed each time the samples were transferred from one container to another. This was consistent with the expected loss of protein due to adsorption of fibrinogen to the surface of containers.[22]

STATISTICS

Quantitative experiments were performed in triplicate. Differences between mean titers of control and laser-treated virus were analyzed by Student's t-test using Graphpad Prism and Microsoft Excel software. $p<0.05$ was used as a threshold for statistical significance.

RESULTS

USP laser treatment inactivates viruses in human plasma

For this study, we chose HIV and HAV as medically significant enveloped and non-enveloped RNA viruses, respectively, and we chose MCMV as a representative enveloped DNA virus whose results could be extrapolated to relevant human pathogens such as cytomegalovirus and hepatitis B virus. To demonstrate that the USP laser treatment can inactivate viruses in plasma, aliquots of HIV, HAV, or MCMV were spiked into human plasma and treated with the laser. USP laser treatment of virus-spiked plasma

samples resulted in approximately 2-log, 1-log, and 3-log reductions in HIV, HAV, and MCMV titers, respectively (Figure 1A–C). The reduction in HAV titers after USP laser treatment exceeds that achieved by the currently licensed SD and amotosalen techniques.[6] It is anticipated that further optimization of laser parameters such as wavelength (i.e., operating at wavelengths where absorption by bilirubin/hemoglobin are minimal) would yield greater inactivation of viruses. These data indicate that USP laser treatment can achieve clinically meaningful reduction of viruses in human plasma.

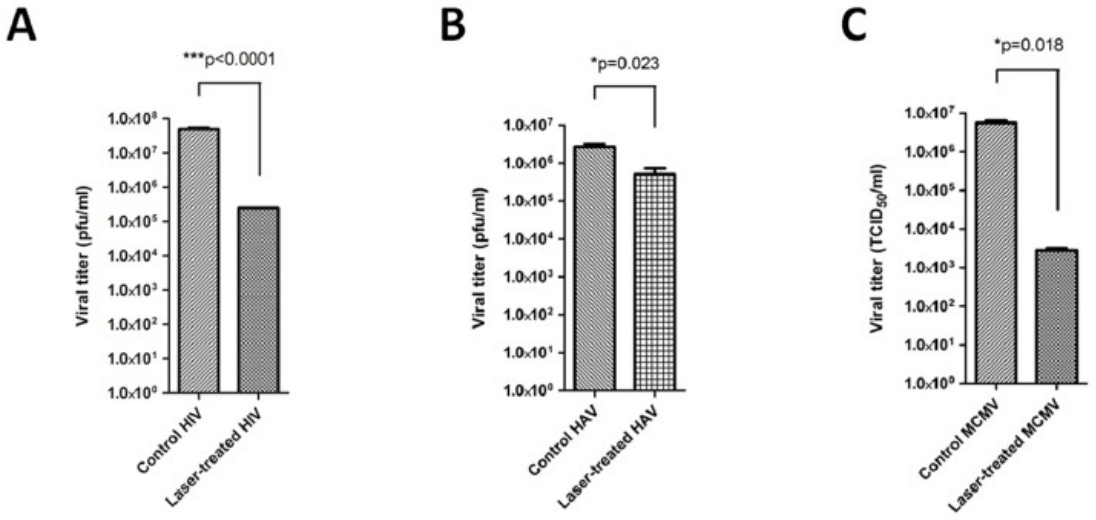

Figure 1. Inactivation of viruses in plasma using a USP laser. Human plasma containing HIV (A), HAV (B), or MCMV (C) were treated with the USP laser. For the HIV-spiked plasma, viral titer was assessed by plaque assay in MAGI cells. For the HAV-spiked plasma, viral titer was assessed by plaque assay in fetal rhesus monkey kidney cells. For the MCMV-spiked plasma, viral titer was assessed by $TCID_{50}$ assay in murine embryonic fibroblast cells. Results are representative of triplicate experiments and are shown as means ± SEM.

The function of human plasma proteins is preserved after USP laser treatment

To determine the functional integrity of human plasma after USP laser treatment, we laser-treated human plasma alone using the same conditions used to inactivate the viruses. After treatment, samples were subjected to standard coagulation assays. Human coagulation factors in laser-treated plasma showed preservation of activity comparable to that achieved with other clinically tested PR methods.[6] The percent retention of individual coagulation factors after laser treatment relative to control is shown in Table 1. With the exception of Factor VII, the activities of all the plasma proteins were near or within the normal reference range. Relative to non-irradiated sample, Factors II, V, VII, IX, and X showed ≥90% retention. Factor XII and fibrinogen showed ≥70% retention. Factors VIII and XI were the most sensitive and showed 68% and 54% retention, respectively. Although Factor II activity was increased by 20% relative to control ($p = 0.04$), the value still fell within the normal reference range, and similar small increases in the activity of certain factors after treatment using current PR methods have been reported, potentially due to the intrinsic variation in the assay.[2] As an example, riboflavin treatment was previously shown to increase the measured activity of Factor XIII to 113% the control value.[6] Therefore, we did not attribute clinical significance to the observed increase in Factor II activity. Interestingly, the USP laser treatment caused a dramatic enhancement in the measured activity of Factor VII in plasma (Table 1). This effect could either be direct (i.e., laser-induced structural changes in Factor VII protein) or indirect (i.e., laser-induced damage to factor(s) that inhibit Factor VII activity). We believe that the latter scenario is more likely, since it is difficult to envision how USP laser treatment

could directly increase the activity of Factor VII protein by altering its native structure. Therefore, a plausible explanation is that the USP laser treatment may cause damage to Factor VII inhibitor(s) that are present in human plasma (such as tissue factor pathway inhibitor, TFPI), which leads to an apparent "enhancement" in measured Factor VII activity. It is expected that further optimization of laser parameters such as wavelength (i.e., operating at wavelengths where absorption by bilirubin and/or hemoglobin are minimal) would yield greater preservation of plasma proteins. These data demonstrate that USP laser irradiation retains coagulation factor activities in an acceptable range for clinical translation.

Coagulation factor	Control plasma	Laser-irradiated plasma	Normal reference range	% retention after treatment
Fibrinogen (mg/dl)	218±4	158.5±2.5	170–400	73
Factor II (IU/ml)	0.82±0.02	0.98±0.03	0.75–1.30	120
Factor V (IU/ml)	0.84±0.01	0.80±0.06	0.50–1.25	95
Factor VII (IU/ml)	0.92±0.01	2.22±0.23	0.50–1.75	241
Factor VIII (IU/ml)	0.72±0.01	0.49±0.01	0.50–1.60	68
Factor IX (IU/ml)	1.01±0.01	0.96±0.09	0.55–1.60	95
Factor X (IU/ml)	1.02±0.03	1.04±0.03	0.60–1.60	102
Factor XI (IU/ml)	1.01±0.01	0.55±0.09	0.60–1.40	54
Factor XII (IU/ml)	0.90±0.00	0.69±0.02	0.45–1.70	77

Table 1. Retention of coagulation factor activity for USP laser-treated plasma. The function of individual coagulation factors in control (untreated) or USP laser-treated plasma was assessed using standard coagulation assays.

USP laser treatment does not induce detergent-resistant aggregation in human plasma proteins

To determine the effects of laser treatment on human plasma proteins, we analyzed control (untreated) and laser-treated plasma by SDS-PAGE (Figure 2A, left panel). Both

control and laser-treated plasma contained some intrinsic level of detergent-resistant aggregates as evidenced by the presence of low-mobility protein complexes that are unable to migrate through the gel. However, USP laser treatment of plasma did not cause any significant qualitative increase in these aggregates. We were also unable to find evidence for any laser-induced increase in detergent-resistant aggregates in plasma by native PAGE (Figure 2B). These data suggest that USP laser treatment does not induce detergent-resistant aggregation among plasma proteins.

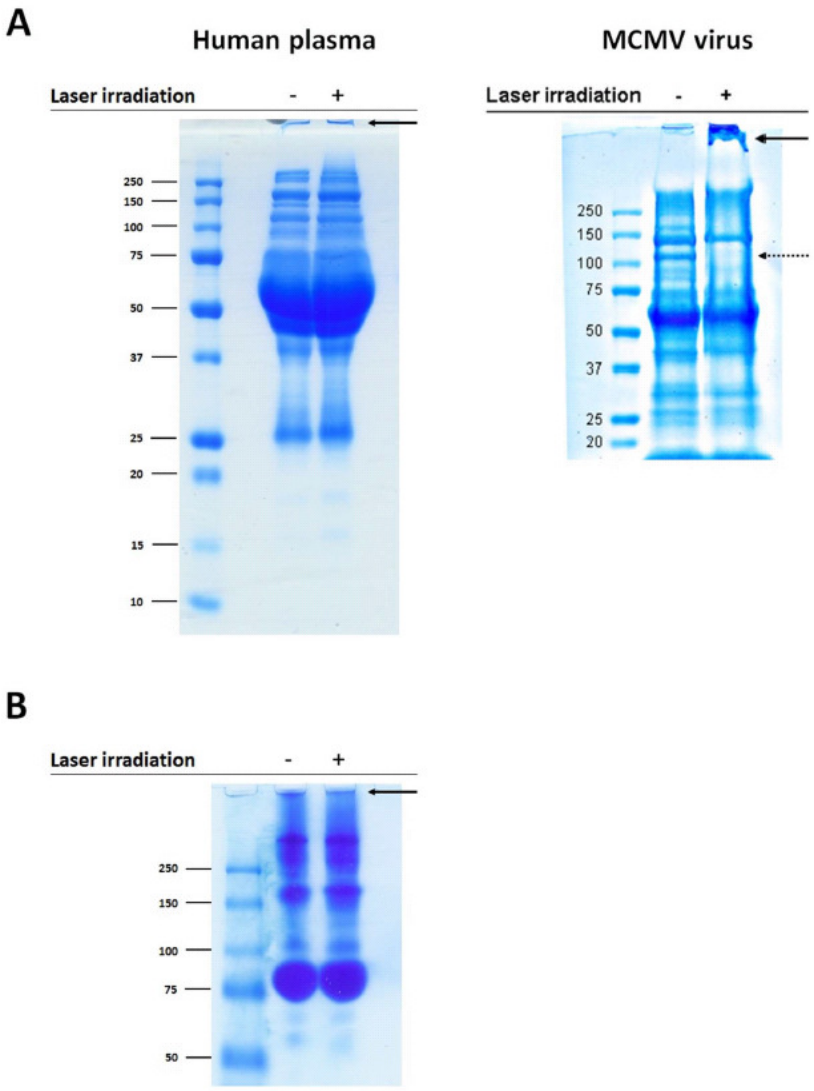

Figure 2. SDS-PAGE and native PAGE analysis of control and USP laser-treated plasma proteins. (A) On the left is shown the SDS-PAGE of control and laser-treated plasma; on the right, for comparison, is shown the SDS-PAGE of laser-treated MCMV virus adapted from Tsen et al [13] (reprinted with permission from the Society of Photo-Optical Instrumentation Engineers). Control (untreated) or USP laser-treated plasma were boiled in reducing buffer and separated on a 10% gel. Proteins were visualized by Coomassie blue stain. The solid arrow indicates the location of low mobility detergent-resistant aggregates; the dotted arrow indicates missing band(s) corresponding to aggregated proteins. (B) Native PAGE of control and laser-treated plasma. Control (untreated) or USP laser-treated plasma were separated on a 10% gel. Proteins were visualized by Coomassie blue stain. Arrows indicate location of low mobility detergent-resistant aggregates.

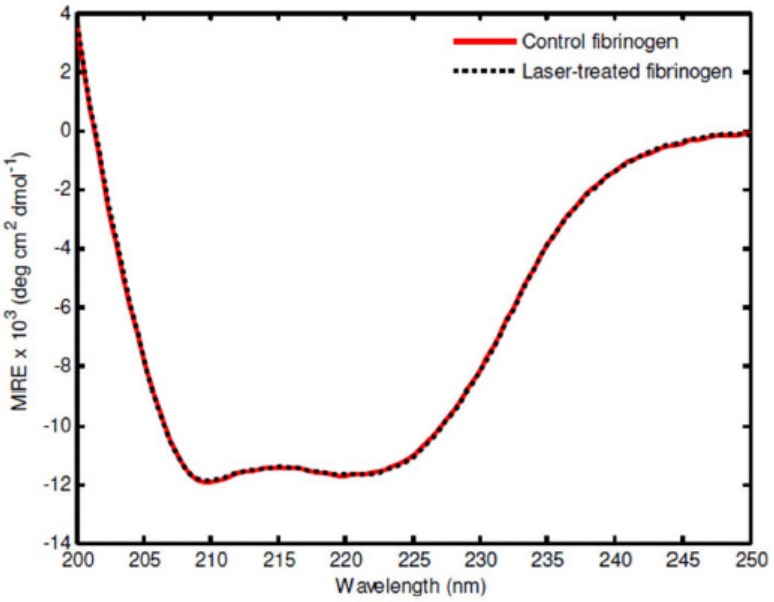

Figure 3. Structural analysis of control and laser-treated fibrinogen protein. Control (untreated) or laser-treated fibrinogen protein was analyzed by circular dichroism. The red line indicates the CD spectrum of control fibrinogen, while the dotted black line indicates laser treated fibrinogen. The spectra (in Mean Residue Ellipticity, rescaled for concentration) show virtually complete overlap.

The secondary structure and aggregation state of purified human fibrinogen are unaltered after USP laser treatment

As shown in Table 1, the function of some coagulation factors was reduced after laser treatment. In particular, the function of fibrinogen, which is the coagulation factor that occurs at the highest concentration in plasma (~2–4 mg/ml) among the factors tested, was reduced to 73% of control. To determine if direct, laser-induced change in protein structure and/or aggregation state of the protein itself was responsible for this reduction in function, we analyzed the structure and aggregation state of purified human fibrinogen

protein at physiological concentration (2.5 mg/ml) after USP laser treatment using circular dichroism and dynamic light scattering analysis, respectively.

We found no evidence for laser-induced alterations in the secondary structure of fibrinogen by circular dichroism measurements (Figure 3). Furthermore, we did not observe any significant laser-induced aggregation of fibrinogen protein by dynamic light scattering, as evidenced by near-identical proportions of monomer in both control and laser-treated groups (Table 2). We note that these values represent the percentage of scattered intensity from monomers (i.e. species with hydrodynamic radius of 12 nm). In both the controls and the irradiated samples, the remaining 40% of intensity came from a much larger species, with a hydrodynamic radius around 100 nm. Because large aggregates scatter much more than monomers, these values indicate that roughly 90% of the protein mass was monomeric (assuming that the aggregates are spherical). Similar results were obtained with fibrinogen at lower concentrations (1.5 mg/ml and 0.6 mg/ml). These findings indicate that USP laser treatment does not directly cause alterations in the secondary structure or aggregation state of purified fibrinogen protein itself when the protein is treated at physiological or sub-physiological concentrations.

Fibrinogen concentration	Sample	% monomer
2.5 mg/ml	Control fibrinogen	60+/−3
	Laser-treated fibrinogen	61+/−7
1.5 mg/ml	Control fibrinogen	63+/−4
	Laser-treated fibrinogen	56+/−9
0.6 mg/ml	Control fibrinogen	65+/−7
	Laser-treated fibrinogen	57+/−10

Table 2. Aggregation state of control and laser-treated fibrinogen protein. Control (untreated) or laser-treated purified fibrinogen protein was analyzed for aggregation state by dynamic light scattering. Values corresponding to the percentage of scattered intensity from Fibrinogen monomers are shown.

DISCUSSION

In this report we demonstrate inactivation of representative viruses in plasma using a visible USP laser, with preservation of plasma proteins. Although we achieved significant reductions in virus, we note that the laser inactivation efficiency for viruses in plasma is decreased relative to that for viruses in phosphate buffered saline (PBS).[13,23] This is likely due to the reduced penetration of light through plasma, which is less transparent than PBS. This can be remedied by designing a laser treatment chamber that is sufficiently thin (<1 mm depth) to maximize light transmission. For example, in a continuous-flow treatment scenario (for example using a syringe pump), a tube or capillary with a small depth would ensure more complete exposure of the sample to the laser light. In future studies, we estimate that the use of more powerful commercially available lasers would enable focused spot sizes on the order of millimeters. Coupled with continuous flow

systems, this could provide a plasma treatment efficiency on the order of ~100 ml per minute which would bring the technology closer to clinical plausibility.

After USP laser treatment, most coagulation factor activities were retained in the range of 70–100% control. Typically, in the field of blood transfusion the acceptable retention percentage of protein activities for PR methods in human plasma is about 70%.[6] For example, methylene blue (MB)-treated plasma has been used extensively in the clinic, and this method reduces the activity of several proteins to this threshold (fibrinogen, 65%; FVIII, 67%).[6] Other clinically employed methods such as amotosalen have similar damage profiles. The proteins (except Factor XI) in human plasma treated with our USP laser technology were retained at around 70% activity or above (Table 1); therefore, it should be considered to be meeting this requirement. We believe that this non-invasive USP laser technology will have minimal side effects partly because of the nature of the inactivation mechanism by the USP laser irradiation, and partly because no chemicals are introduced in the treatment process. Therefore, using human plasma treated with the USP laser irradiation would be safer compared with other PR methods. Although the level of preservation is in the range of other established PR methods, there is potential for improvement. Human plasma contains bilirubin, a molecule that absorbs light at the 425 nm wavelength we used for laser PR.[24] This absorption leads to intermolecular energy transfers that may negatively affect the structure of bilirubin-associated proteins in plasma. Since viruses in PBS alone are efficiently inactivated by USP laser treatment,[12-14,23,25-27] bilirubin is clearly not required for laser PR. Thus it is possible that by selecting a different wavelength where absorption by bilirubin is minimized, the detrimental effects

of the USP laser treatment on plasma proteins can be mitigated. For example, use of near-infrared excitation wavelengths above 700 nm will improve the penetration depth of light and minimize absorption of light by plasma proteins for effective pathogen inactivation.

Previous data supported a model whereby the USP laser inactivates enveloped viruses such as MCMV by laser-driven excitation of vibrational modes within viral capsids, resulting in aggregation of densely-packed tegument and capsid proteins.[13,28] The laser treatment caused the formation of large, strongly bound aggregates of viral capsid/matrix proteins that did not readily dissociate under denaturing or reducing conditions, which we term "detergent-resistant aggregates".[13] Figs. 2A and 2B demonstrate that USP laser treatment does not induce detergent-resistant aggregates in human plasma. On the other hand, our previous gel results on the control and USP laser-treated MCMV in buffered solution, which is shown in the right panel of Fig. 2A, indicated that USP laser irradiation caused detergent resistant aggregates, leading to the inactivation of MCMV.

Ideally, it is the gel analysis for the MCMV in human plasma that needs to be made. However, we have found that the signature signal of MCMV was overwhelmed by the tremendously large background contributions from the various components present in the human plasma in the gel analysis of the MCMV spiked in human plasma. As a result, the analysis is too complicated to be reliably made. Therefore, we chose to analyze the best possible experiments next to the ideal one, namely purified MCMV in buffered solution. Because the analysis of the gel results on the purified MCMV is not the ideal one, as a compromise, we make a reasonable assumption that the effects of USP laser treatment on

enveloped viruses such as MCMV are the same in the buffered solution as in the human plasma. This assumption is reasonable because it is supported by our observations that MCMV is efficiently inactivated by the USP laser irradiation both in the buffered solution and in human plasma. Under this assumption, it can be shown that the protein aggregation induced by the USP laser irradiation is a plausible mechanism for our experimental observations that the USP laser efficiently inactivates viruses while retaining protein activities in the human plasma. The protein aggregation induced by the USP laser irradiation has been demonstrated to be density-dependent;[13] namely, the more closely the proteins are packed, the larger the probability of protein aggregation. Because the protein density is significantly higher within the MCMV virion than in human plasma, it is expected that protein aggregation by the USP laser irradiation would be much more probable within the MCMV than in the human plasma, leading to the efficient inactivation of MCMV but retention of the majority of coagulation factor activities in human plasma.

We also note that that ideally, it is the fibrinogen within human plasma that needs to be analyzed. However, we have found that the CD and DLS analyses for fibrinogen in human plasma are too complicated to be reliably made due to the presence of background contributions from other components present in the human plasma. Therefore, we chose to analyze the best possible experiments next to the ideal one, namely the CD and DLS of purified fibrinogen. Because the CD and DLS analysis of purified fibrinogen is not the ideal one, as a compromise, we choose not to make a definitive conclusion based on the CD and DLS results on purified fibrinogen. Instead, we conclude that the CD and DLS

results on purified fibrinogen provide a possible clue to explain why the USP laser irradiation preserves the majority (73%) of the fibrinogen activity in human plasma.

We were unable to correlate the observed reduction in plasma protein function with any changes in the secondary structure or aggregation state of the proteins. There are two potential explanations for this observation. Firstly, the USP laser may cause only minimal structural damage to these proteins at a level undetectable by circular dichroism, dynamic light scattering, and SDS-PAGE. In this case, more sensitive methods such as nuclear magnetic resonance may be required to elucidate these changes. Alternatively, the function of plasma proteins might be indirectly inhibited by laser-induced damage to other factors in plasma that promote the coagulation activity of these proteins. Indeed, the absorption of laser light by other molecule(s) present in plasma, such as bilirubin, might lead to energy transfer from these molecule(s) to closely bound/closely associated proteins. Studies on the effect of bilirubin on plasma protein preservation after USP laser treatment are currently underway.

Visible USP laser treatment provides important advantages in the field of PR. The USP laser technology does not involve introducing potentially toxic or carcinogenic chemicals, and thus avoids possible side effects from such additives. Unlike the SD and amotosalen methods, which have seen significant clinical use in Europe, USP laser treatment can inactivate non-enveloped viruses. In addition, USP lasers are non-ionizing and do not disrupt covalent bonds, thereby reducing the potential to generate immunogenic neoantigens in blood products. Furthermore, USP lasers are environmentally friendly,

circumventing the need to incorporate undesirable compounds such as mercury which is used in UV lamps.

Such qualities make USP lasers a promising potential method for sterilization not only of blood products, but of pharmaceuticals, biologicals, and cell culture as well. As described above, the ISRS inactivation mechanism of USP lasers is very likely to leave small molecule pharmaceuticals and soluble recombinant proteins structurally undamaged. In addition, we have previously shown that a therapeutic window exists for which viruses and bacteria can be inactivated without causing death in human cells.[12] Studies are currently ongoing to conclusively demonstrate these applications.

CONCLUSION

We have performed PR experiments on three representative viruses in human plasma by using a visible USP laser. Our experimental results demonstrate that it is feasible to use this novel USP laser technology to inactivate viruses while retaining the function of coagulation factors in human plasma at a clinically acceptable level. This is the first proof-of-concept study of PR in human plasma using USP lasers. This chemical-free USP laser technology has potential advantages over current PR techniques.

REFERENCES

[1]AuBuchon, J. P. (2011). Update on the status of pathogen inactivation methods. *ISBT Science Series*, *6*(1), 181-188.

[2]Allain, J. P., Bianco, C., Blajchman, M. A., Brecher, M. E., Busch, M., Leiby, D., Lily, L., & Stramer, S. (2005). Protecting the blood supply from emerging pathogens: the role of pathogen inactivation. *Transfusion medicine reviews*, *19*(2), 110-126.

[3]Bryant, B. J., & Klein, H. G. (2007). Pathogen inactivation: the definitive safeguard for the blood supply. *Archives of pathology & laboratory medicine*, *131*(5), 719-733.

[4]Hellstern, P. (2004). Solvent/detergent-treated plasma: composition, efficacy, and safety. *Current opinion in hematology*, *11*(5), 346-350.

[5]Hellstern, P., & Solheim, B. G. (2011). The use of solvent/detergent treatment in pathogen reduction of plasma. *Transfus Med Hemother*, *38*(1), 65-70.

[6]Rock, G. (2011). A comparison of methods of pathogen inactivation of FFP. *Vox sanguinis*, *100*(2), 169-178.

[7]Zeiler, T., Riess, H., Wittmann, G., Hintz, G., Zimmermann, R., Müller, C., Heuft, H. G., & Huhn, D. (1994). The effect of methylene blue phototreatment on plasma proteins and in vitro coagulation capability of single - donor fresh - frozen plasma. *Transfusion*, *34*(8), 685-689.

[8]Garwood, M., Cardigan, R. A., Drummond, O., Hornsey, V., Turner, C. P., Young, D., Williamson, L. M., & Prowse, C. V. (2003). The effect of methylene blue photoinactivation and methylene blue removal on the quality of fresh frozen plasma. *Transfusion*, *43*(9), 1238-1247.

[9]Musso, D., Richard, V., Broult, J., & Cao‐Lormeau, V. M. (2014). Inactivation of dengue virus in plasma with amotosalen and ultraviolet A illumination. *Transfusion*, *54*(11), 2924-2930.

[10]Singh, Y., Sawyer, L. S., Pinkoski, L. S., Dupuis, K. W., Hsu, J. C., Lin, L., & Corash, L. (2006). Photochemical treatment of plasma with amotosalen and long - wavelength ultraviolet light inactivates pathogens while retaining coagulation function. *Transfusion*, *46*(7), 1168-1177.

[11]Tsen, S. W., Wu, T. C., Kiang, J. G., & Tsen, K. T. (2012). Prospects for a novel ultrashort pulsed laser technology for pathogen inactivation. *J Biomed Sci*, *19*, 62.

[12]Tsen, K. T., Tsen, S. W. D., Sankey, O. F., & Kiang, J. G. (2007). Selective inactivation of micro-organisms with near-infrared femtosecond laser pulses. *Journal of Physics: Condensed Matter*, *19*(47), 472201.

[13]Tsen, S. W. D., Chapa, T., Beatty, W., Tsen, K. T., Yu, D., & Achilefu, S. (2012). Inactivation of enveloped virus by laser-driven protein aggregation. *Journal of biomedical optics*, *17*(12), 128002-128002.

[14]Tsen, K. T., Tsen, S. W. D., Fu, Q., Lindsay, S. M., Li, Z., Cope, S., Vaiana, S., & Kiang, J. G. (2011). Studies of inactivation of encephalomyocarditis virus, M13 bacteriophage, and Salmonella typhimurium by using a visible femtosecond laser: insight into the possible inactivation mechanisms. *Journal of biomedical optics*, *16*(7), 078003-078003.

[15]Lemon, S. M., Murphy, P. C., Shields, P. A., Ping, L. H., Feinstone, S. M., Cromeans, T., & Jansen, R. W. (1991). Antigenic and genetic variation in cytopathic hepatitis A virus variants arising during persistent infection: evidence for genetic recombination. *Journal of virology*, *65*(4), 2056-2065.

[16]Kingsley, D. H., & Chen, H. (2009). Influence of pH, salt, and temperature on pressure inactivation of hepatitis A virus. *International journal of food microbiology*, *130*(1), 61-64.

[17]Harvey, D. M., & Levine, A. J. (1991). p53 alteration is a common event in the spontaneous immortalization of primary BALB/c murine embryo fibroblasts. *Genes & development*, *5*(12b), 2375-2385.

[18]Qian, Z., Xuan, B., Chapa, T. J., Gualberto, N., & Yu, D. (2012). Murine cytomegalovirus targets transcription factor ATF4 to exploit the unfolded-protein response. *Journal of virology*, *86*(12), 6712-6723.

[19]Schmaier AH (2012) Hematology: Basic Principles and Practice. Philadelphia, PA: Elsevier.

[20]Clauss, A. (1957). Rapid physiological coagulation method in determination of fibrinogen. *Acta haematologica*, *17*(4), 237.

[21]Rossi, E., Mondonico, P., Lombardi, A., & Preda, L. (1988). Method for the determination of functional (clottable) fibrinogen by the new family of ACL coagulometers. *Thrombosis research*, *52*(5), 453-468.

[22]Feng L, Andrade JD (1995) Structure and adsorption properties of fibrinogen. In: Brash JL, Horbett TA, editors. *Proteins at Interfaces II: Fundamentals and Applications*. Washington, D. C.: American Chemical Society. 66–79.

[23]Tsen, K. T., Tsen, S. W. D., Hung, C. F., Wu, T. C., & Kiang, J. G. (2008). Selective inactivation of human immunodeficiency virus with subpicosecond near-infrared laser pulses. *Journal of Physics: Condensed Matter*, *20*(25), 252205.

[24]Bhadri, P. R., Kumar, S. A., Salgaonkar, V. A., Beyette Jr, F. R., & Clark, J. F. (2008). Development of an integrated hardware and software platform for the rapid detection of cerebral aneurysm rupture. *Analog Integrated Circuits and Signal Processing*, *56*(1-2), 127-134.

[25]Tsen, K. T., Tsen, S. W. D., Chang, C. L., Hung, C. F., Wu, T. C., & Kiang, J. G. (2007). Inactivation of viruses with a very low power visible femtosecond laser. *Journal of Physics: Condensed Matter*, *19*(32), 322102.

[26]Tsen, K. T., Tsen, S. W. D., Chang, C. L., Hung, C. F., Wu, T. C., & Kiang, J. G. (2007). Inactivation of viruses by laser-driven coherent excitations via impulsive stimulated Raman scattering process. *Journal of biomedical optics*, *12*(6), 064030-064030.

[27]Tsen, K. T., Tsen, S. W. D., Fu, Q., Lindsay, S. M., Kibler, K., Jacobs, B., Wu, T. C., Karanam, B., Jagu, S., Roden, R. B. S., Hung, C. F., Sankey, O. F., Ramakrishna, B., & Kiang, J. G. (2009). Photonic approach to the selective inactivation of viruses with a near-infrared subpicosecond fiber laser. *Journal of biomedical optics*, *14*(6), 064042-064042.

[28]Tsen, S. W., Kingsley, D. H., Poweleit, C., Achilefu, S., Soroka, D. S., Wu, T. C., & Tsen, K. T. (2014) Studies of inactivation mechanism of non-enveloped icosahedral virus by a visible ultrashort pulsed laser. *Virol J, 11,* 20.